INVESTIGATING THE EFFECT OF DYNAMIC COVALENT BONDS ON THE CRYSTALLIZATION, RHEOLOGY AND MOLECULAR RELAXATION IN ETHYLENE VITRIMERS

BY

BHASKAR SOMAN

DISSERTATION

Submitted in partial fulfillment of the requirements
for the degree of Doctor of Philosophy in Materials Science and Engineering
in the Graduate College of the
University of Illinois Urbana-Champaign, 2022

Urbana, Illinois

Doctoral Committee:

Associate Professor Christopher M. Evans, Chair
Professor Kenneth S. Schweizer, Director of Research
Associate Professor Cecilia Leal
Associate Professor Charles E. Sing

ABSTRACT

Vitrimers, dynamic polymer networks with topology conserving exchange reactions, have emerged as a promising platform for sustainable and reprocessable materials. Vitrimers are a class of polymer networks with properties intermediate to thermosets and thermoplastics. Their properties are a consequence of the dynamic crosslinks which undergo reversible exchange reactions and allow for local rearrangements in network structure resulting in stress relaxation and flow. This thesis aims to investigate properties that will be critical to the design, processing, and use of vitrimers as sustainable commodity polymers and functional materials. A series of precise ethylene based vitrimers were synthesized and investigated for their (i) rheological response, (ii) dielectric relaxation behavior, (iii) crystallization and crystal evolution, and (iv) the effect of topological defects on shear modulus and crystallization kinetics. The ethylene vitrimers are also shown to be easy to recycle. Networks are dissolved in water and alcohol-based solvents and can be recovered by repolymerization while preserving their material properties.

Over a broad temperature window, the viscosity of the vitrimer shows a positive deviation from its characteristic Arrhenius trend, indicating an increasing role of segmental dynamics on the flow. From dielectric spectroscopy, three distinct relaxation modes are identified - the alpha process, the beta process, and a normal mode relaxation that is interpreted as the time taken for the exchange of network strands between crosslink junctions. At high temperatures, a strong correlation between the rheological flow timescale and the normal mode relaxation shows that flow is controlled by bond exchange, while at lower temperatures an increase in alpha relaxation time correlates with the positive deviation from Arrhenius behavior

in the networks. While prior work has documented how dynamic bonds impact stress relaxation and viscosity, their role in crystallization has not been systematically explored. In this report, a comparison between permanent and dynamic networks with the same linker length, suggests that the incorporation of dynamic junctions allows for local rearrangement of the network structure which facilitates crystallization. The ethylene vitrimers also show an unexpected evolution in melting temperature, crystal structure, and morphology over time that is also attributed to the dynamic bond exchange. The incorporation of dangling chain defects into the ethylene vitrimers results in a decrease in shear modulus that can be modeled by the rubbery network theory. X-ray scattering patterns reveal that increasing defect concentration results in the formation of imperfect crystals. A counterintuitive trend in crystallization kinetics is observed in the defected networks and is speculated to be a consequence of an increase in the entropic barrier to crystallization coming from the dangling chains.

ACKNOWLEDGEMENTS

A Ph.D. is like a marathon, a long and arduous journey that tests your mental and physical stamina. It has its share of ups and downs, and the most valuable lesson you learn over the years is to take things in stride. A Ph.D. is just as much yours as it is of the many people who have supported you along the way. This acknowledgment is my humble attempt at expressing gratitude to the many who have been by my side through this marathon.

First and foremost, I could not have undertaken this journey without my advisor Christopher Evans. Thank you for accepting me into the Evan's research group. Apart from the subject matter knowledge that I have acquired from you, there are many other intangibles that I have picked up from you. "It doesn't matter if you don't get the perfect result, as long as you are honest about the data, there's nothing you have to worry about", I've heard you say this many times over the years and it's always made me feel more confident about my work. You have given me the best possible combination of freedom and guidance any graduate student can ask for and I'm extremely grateful for it.

I would like to thank all my committee members for their collaboration and scientific insight, making me dig deeper and improving the quality of my research. Thanks to Prof. Kenneth Schweizer for lending his expertise in polymer physics which has been crucial to the ethylene dielectrics project. Thanks to Prof. Cecilia Leal for her contributions and support in the vitrimer crystallization project and Prof. Charles Sing for his insight on vitrimer self-assembly and his support through simulation and theory.

Thanks should also go to Dr. Chengtian (John) Shen, Yookyung Go, Dr. Brian Jing, Dr. Ellie Porath, Dr. Guangxin Lyu, and Seongon Jang for collaborating and bringing their broad knowledge and insight into various projects and boosting the impact of my research.

I cannot overstate the importance of the inclusive, collaborative, and joyful work environment I was welcomed into when I joined the group. I want to wholeheartedly thank Dr. Chengtian (John) Shen, Dr. Qiujie Zhao, Dr. Brian Jing, Dr. Ellie Porath, Dr. Grant Sheridan, and Seongon Jang for making the lab such a happy and wonderful place to work. John, Qiujie, Brian, Ellie, and Grant, thank you so much for teaching me what it means to work as a team. Ellie and Grant, thank you for being great friends and for making our conference visits so enjoyable.

A special thanks to Dr. Roddel Remy and Dr. Juan Lopez at MRL for all the technical support and guidance they have provided over the years. My research would not have gone as smoothly as it has without your help. Roddel, thank you for being patient with me and taking the time out for numerous hour long discussions on polymer characterization. The knowledge you've shared with me has been extremely valuable to my growth as a researcher.

I would also like to acknowledge my friends at UIUC who helped me navigate the ups and downs of graduate life: Ganesh Ananthakrishnan, Mitisha Surana, Shraddha Shirguppe, Kaustubh Panse, and Iswarya Alex. You are the reason Urbana-Champaign feels like home. Iswarya Alex, thank you for holding us together through the years, despite my many mistakes you didn't let go. I couldn't have asked for a better companion.

To my best friends, Ishan Vyas and Gokul T Anandan. Thank you for being a part of my life. I believe the true meaning of the words "best friend" can only be understood when one has friends like you.

And finally, to my family, thank you for your unconditional love and support, it is because of your upbringing and sacrifices that I have reached this stage in life.

To my family and friends

TABLE OF CONTENTS

CHAPTER 1: INTRODUCTION

1.1. Vitrimers

The development of sustainable and recyclable plastics is a major challenge to handle the massive volume of products that end up in landfills.[1] Polymer networks, either elastomers or thermosets, are not processesable with traditional chemistries but can be made recyclable via the incorporation of dynamic covalent bonds into the polymer. Polymer networks containing dynamic covalent bonds are a promising platform for reconfigurable, recyclable, self-healing, and dissolvable polymers.[2-7] Such systems are called covalent adaptable networks (CANs) regardless of the bond exchange mechanism, while the subclass of CANs containing associative dynamic covalent bonds are commonly called vitrimers. Notably, Leibler and coworkers described dynamic polyester networks which exhibit glass-like processability due to conserved ester exchange reactions, now commonly called vitrimers.[8, 9] This concept has been widely applied to a range of dynamic bonds including esters,[9-18] boronic esters/boroxine,[19-27] urethanes,[28] vinylogous urethanes,[29-36] oxime-esters,[37, 38] olefin metathesis,[8, 39] triazolium transalkylation,[40] silyl ether metathesis[41-43] and Meldrum's acid.[44, 45] The ever growing toolbox of dynamic covalent bonds which conserve the network topology is described in review articles.[3, 6] A major focus thus far has been to understand how the exchange kinetics, crosslink density, and polymer backbone chemistry control the stress relaxation and reprocessability of vitrimers. The crosslink density in vitrimers has been investigated showing how the stress relaxation times and creep are impacted.[32, 46-48] The glass transition temperature (T_g) and a hypothetical topology freezing temperature (T_v) have been discussed to understand the interplay with bond exchange processes which governs the

temperature dependent viscoelasticity. Vitrimers pose a plethora of fundamental questions about the role of molecular scale chemistry on the complex, temperature-dependent, viscoelastic response of dynamic polymer networks. The viscosity profile of vitrimers is distinct from both thermoplastics (sharp non-Arrhenius drop on heating above the glass temperature) and thermosets (no flow),[49] while less is has been investigated regarding their temperature dependent moduli. Dynamic networks are a potentially transformative way to independently control modulus (via crosslink density) and viscosity (through bond exchange kinetics), as well as their temperature dependences, without changing polymer chemistry, using copolymerization strategies, or adding plasticizer/anti-plasticizers or other fillers. Dynamic bonds also have the potential to impart functionality into polymers and can affect the ability of materials to self-assemble and crystallize. Vitrimers can serve as a model platform to advance our understanding of viscoelastic design, self-assembly and functional polymers (**Figure 1**).

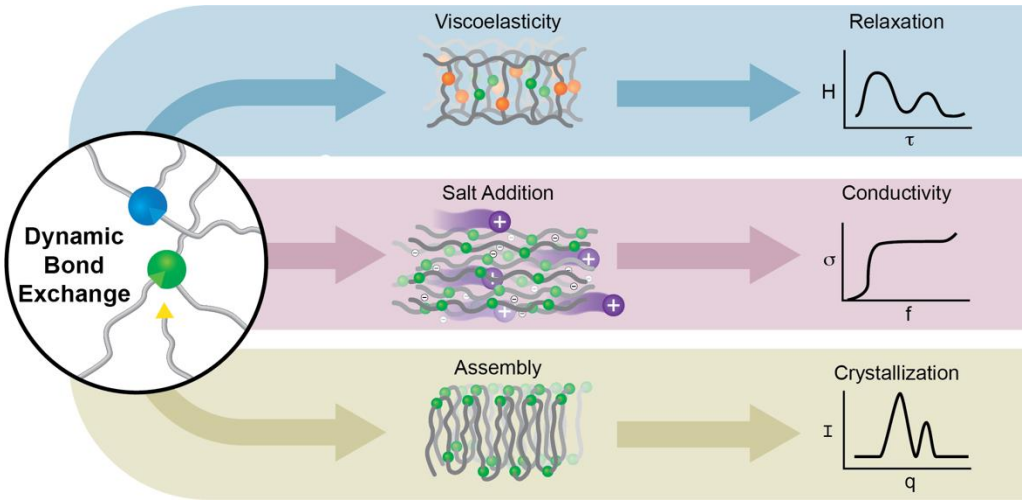

Figure 1.1: Dynamic bond exchange can impart functionality into polymer networks and control of both static and dynamic properties. Viscoelastic properties are tunable in vitrimers via control of the polymer backbone and crosslinker chemistry, density, and kinetically distinct crosslinkers (illustrated as orange and green spheres). Adding salt to vitrimers yields networks that are both conductive and self-healing (cations shown as purple spheres), which can improve battery electrolytes and actuators. In polymer networks that can self-assemble, the dynamic bond can facilitate assembly in otherwise trapped structures.

1.2 Synthesis of Ethylene Vitrimer

Polyethylene (PE) and its derivatives have been extensively studied for more than half a century and it is the largest volume plastic in the world[1]. Despite attractive properties such as low cost, high strength to weight ratio and chemical stability, PE poses a challenge when it comes to disposal and recycling. The development of sustainable and recyclable alternatives is a major challenge that is being explored from a variety of angles. Recent works have showed that incorporation of dynamic bonds into commodity plastics allows closed-loop recycling of otherwise unusable polymers with minimum loss in mechanical properties.[50, 51]

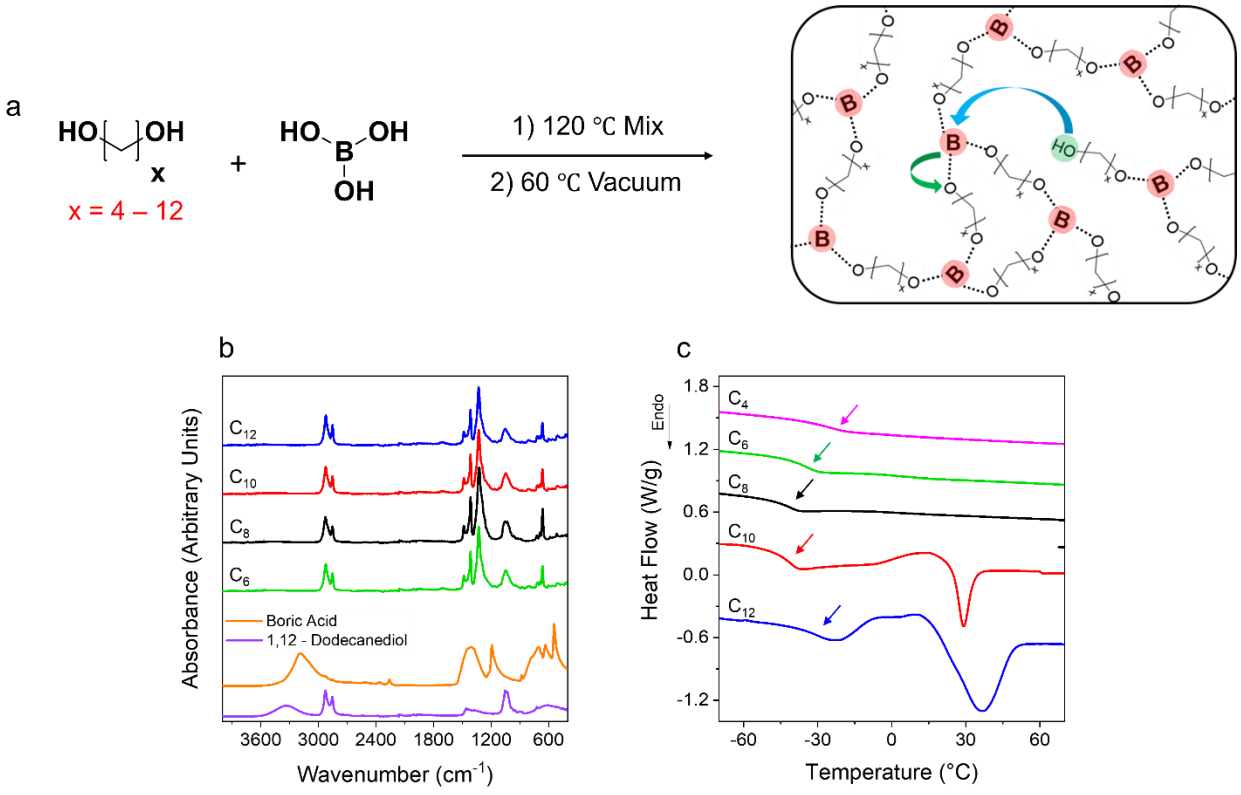

Figure 1.2. (Continued)

Figure 1.2. (a) Step growth polymerization of telechelic alkane diols and boric acid to make PE vitrimers. By controlling the length of the diols, networks with precise spacing between crosslinks were synthesized. The arrows in the schematic represent boronic transesterification reactions that result in local rearrangement of network strands and gives the network its dynamic properties. (b) ATR-FTIR spectra of the vitrimers show no free OH peak (3000 cm-1 - 3500 cm-1) indicating a high reaction conversation as there are no detectable unreacted diols. (c) Heating of the networks after quenching to -80 °C reveals a non - monotonic increase in Tg (arrows) with increasing linker length or decreasing crosslink density. Following the Tg, cold crystallization and melting transition were observed in C10 and C12 networks.

Precise ethylene vitrimers were synthesized by the step growth polymerization of telechelic alkane diols and boric acid. Networks with exactly 4, 6, 8, 10 or 12 carbons (C_4, C_6, C_8, C_{10}, C_{12}) between boronic ester crosslinking junctions were prepared by mixing the diol and acid, followed by heating to melt the diol and then application of vacuum to drive off water condensate (**Figure 1.2a**). Fourier transform infrared spectroscopy (FTIR) of the networks was performed at 80 °C to confirm the absence of the broad OH peak in the 3000 cm^{-1} to 3500 cm^{-1} range corresponding to unreacted species on the diols, boric acid, and water. Within the sensitivity of the instrument, no OH peak is detected indicating that the network formation reached high conversion (**Figure 1.2b**). This should not be taken as an indicator of 100 % conversion, and defects in the network are expected. The emergence of a sharp peak at 1300 cm^{-1} corresponds to the asymmetric B-O stretch[52] indicating the formation of the boronic ester crosslinks.

Thermal properties of the networks were investigated using differential scanning calorimetry (DSC) by first rapidly quenching from 150 °C to -80 °C and then heating at 20 °C/min. The C_6 and C_8 networks show no melting transitions while the C_{10} and C_{12} networks show cold crystallization followed by a melting transition with peak melting temperatures (T_m) in the 25-30 °C range. The glass transition temperatures (T_g) of the networks are -27 °C (C_4), -36 °C (C_6), -43 °C (C_8), -41 °C (C_{10}) and -32 °C (C_{12}) (**Fig 1.2c**). The increase in crosslink density is expected to

lead to a monotonic increase in T_g,[53] but a reproducible non-monotonic trend is observed. This is correlated with the appearance of crystallization during quenching and cold crystallization on heating in the C_{10} and C_{12} networks (**Supplementary Fig 2.1**). No crystallization is observed in the heating or cooling cycles for C_4, C_6 and C_8 networks.

1.3. *References*

1. Geyer, R.; Jambeck, J. R.; Law, K. L., Production, use, and fate of all plastics ever made. *Science Advances* **2017,** *3* (7), e1700782.

2. Kloxin, C. J.; Bowman, C. N., Covalent adaptable networks: smart, reconfigurable and responsive network systems. *Chem. Soc. Rev.* **2013,** *42* (17), 7161-7173.

3. Denissen, W.; Winne, J. M.; Du Prez, F. E., Vitrimers: Permanent organic networks with glass-like fluidity. *Chemical Science* **2016,** *7* (1), 30-38.

4. Yang, Y.; Xu, Y.; Ji, Y.; Wei, Y., Functional epoxy vitrimers and composites. *Progress in Materials Science* **2021,** *120*, 100710.

5. Zheng, J.; Png, Z. M.; Ng, S. H.; Tham, G. X.; Ye, E.; Goh, S. S.; Loh, X. J.; Li, Z., Vitrimers: Current research trends and their emerging applications. *Materials Today* **2021,** *51*, 586-625.

6. Van Zee, N. J.; Nicolaÿ, R., Vitrimers: Permanently crosslinked polymers with dynamic network topology. *Progress in Polymer Science* **2020,** *104*, 101233-101233.

7. Guerre, M.; Taplan, C.; Winne, J. M.; Du Prez, F. E., Vitrimers: directing chemical reactivity to control material properties. *Chemical Science* **2020,** *11* (19), 4855-4870.

8. Lu, Y.-X.; Tournilhac, F.; Leibler, L.; Guan, Z., Making Insoluble Polymer Networks Malleable via Olefin Metathesis. *Journal of the American Chemical Society* **2012,** *134* (20), 8424-8427.

9. Montarnal, D.; Capelot, M.; Tournilhac, F.; Leibler, L., Silica-Like Malleable Materials from Permanent Organic Networks. *Science* **2011,** *334* (6058), 965.

10. Demongeot, A.; Groote, R.; Goossens, H.; Hoeks, T.; Tournilhac, F.; Leibler, L., Cross-Linking of Poly(butylene terephthalate) by Reactive Extrusion Using Zn(II) Epoxy-Vitrimer Chemistry. *Macromolecules* **2017,** *50* (16), 6117-6127.

11. Brutman, J. P.; Delgado, P. A.; Hillmyer, M. A., Polylactide Vitrimers. *ACS Macro Letters* **2014,** *3* (7), 607-610.

12. Zhou, Y.; Goossens, J. G. P.; Sijbesma, R. P.; Heuts, J. P. A., Poly(butylene terephthalate)/Glycerol-based Vitrimers via Solid-State Polymerization. *Macromolecules* **2017,** *50* (17), 6742-6751.

13. Yang, Z.; Wang, Q.; Wang, T., Dual-Triggered and Thermally Reconfigurable Shape Memory Graphene-Vitrimer Composites. *ACS Applied Materials & Interfaces* **2016,** *8* (33), 21691-21699.

14. Yang, Y.; Zhang, S.; Zhang, X.; Gao, L.; Wei, Y.; Ji, Y., Detecting topology freezing transition temperature of vitrimers by AIE luminogens. *Nature Communications* **2019,** *10* (1), 3165.

15. Lossada, F.; Jiao, D.; Yao, X.; Walther, A., Waterborne Methacrylate-Based Vitrimers. *ACS Macro Letters* **2020,** *9* (1), 70-76.

16. Self, J. L.; Sample, C. S.; Levi, A. E.; Li, K.; Xie, R.; de Alaniz, J. R.; Bates, C. M., Dynamic Bottlebrush Polymer Networks: Self-Healing in Super-Soft Materials. *Journal of the American Chemical Society* **2020,** *142* (16), 7567-7573.

17. Yang, Y.; Pei, Z.; Li, Z.; Wei, Y.; Ji, Y., Making and Remaking Dynamic 3D Structures by Shining Light on Flat Liquid Crystalline Vitrimer Films without a Mold. *Journal of the American Chemical Society* **2016,** *138* (7), 2118-2121.

18. Capelot, M.; Montarnal, D.; Tournilhac, F.; Leibler, L., Metal-Catalyzed Transesterification for Healing and Assembling of Thermosets. *Journal of the American Chemical Society* **2012,** *134* (18), 7664-7667.

19. Jing, B. B.; Evans, C. M., Catalyst-Free Dynamic Networks for Recyclable, Self-Healing Solid Polymer Electrolytes. *Journal of the American Chemical Society* **2019,** *141* (48), 18932-18937.

20. Cash, J. J.; Kubo, T.; Bapat, A. P.; Sumerlin, B. S., Room-Temperature Self-Healing Polymers Based on Dynamic-Covalent Boronic Esters. *Macromolecules* **2015,** *48* (7), 2098-2106.

21. Cromwell, O. R.; Chung, J.; Guan, Z., Malleable and Self-Healing Covalent Polymer Networks through Tunable Dynamic Boronic Ester Bonds. *Journal of the American Chemical Society* **2015,** *137* (20), 6492-6495.

22. Ricarte, R. G.; Tournilhac, F.; Cloître, M.; Leibler, L., Linear Viscoelasticity and Flow of Self-Assembled Vitrimers: The Case of a Polyethylene/Dioxaborolane System. *Macromolecules* **2020,** *53* (5), 1852-1866.

23. Ricarte, R. G.; Tournilhac, F.; Leibler, L., Phase Separation and Self-Assembly in Vitrimers: Hierarchical Morphology of Molten and Semicrystalline Polyethylene/Dioxaborolane Maleimide Systems. *Macromolecules* **2019,** *52* (2), 432-443.

24. Caffy, F.; Nicolaÿ, R., Transformation of polyethylene into a vitrimer by nitroxide radical coupling of a bis-dioxaborolane. *Polymer Chemistry* **2019,** *10* (23), 3107-3115.

25. Saed, M. O.; Gablier, A.; Terentejv, E. M., Liquid Crystalline Vitrimers with Full or Partial Boronic-Ester Bond Exchange. *Advanced Functional Materials* **2020,** *30* (3), 1906458.

26. Röttger, M.; Domenech, T.; van der Weegen, R.; Breuillac, A.; Nicolaÿ, R.; Leibler, L., High-performance vitrimers from commodity thermoplastics through dioxaborolane metathesis. *Science* **2017,** *356* (6333), 62-65.

27. Ogden, W. A.; Guan, Z., Recyclable, Strong, and Highly Malleable Thermosets Based on Boroxine Networks. *Journal of the American Chemical Society* **2018,** *140* (20), 6217-6220.

28. Fortman, D. J.; Brutman, J. P.; Cramer, C. J.; Hillmyer, M. A.; Dichtel, W. R., Mechanically Activated, Catalyst-Free Polyhydroxyurethane Vitrimers. *Journal of the American Chemical Society* **2015,** *137* (44), 14019-14022.

29. Denissen, W.; Droesbeke, M.; Nicolaÿ, R.; Leibler, L.; Winne, J. M.; Du Prez, F. E., Chemical control of the viscoelastic properties of vinylogous urethane vitrimers. *Nature Communications* **2017,** *8* (1), 14857.

30. Denissen, W.; Rivero, G.; Nicolaÿ, R.; Leibler, L.; Winne, J. M.; Du Prez, F. E., Vinylogous Urethane Vitrimers. *Advanced Functional Materials* **2015,** *25* (16), 2451-2457.

31. Guerre, M.; Taplan, C.; Nicolaÿ, R.; Winne, J. M.; Du Prez, F. E., Fluorinated Vitrimer Elastomers with a Dual Temperature Response. *Journal of the American Chemical Society* **2018,** *140* (41), 13272-13284.

32. Stukenbroeker, T.; Wang, W.; Winne, J. M.; Du Prez, F. E.; Nicolaÿ, R.; Leibler, L., Polydimethylsiloxane quenchable vitrimers. *Polymer Chemistry* **2017,** *8* (43), 6590-6593.

33. Lessard, J. J.; Garcia, L. F.; Easterling, C. P.; Sims, M. B.; Bentz, K. C.; Arencibia, S.; Savin, D. A.; Sumerlin, B. S., Catalyst-Free Vitrimers from Vinyl Polymers. *Macromolecules* **2019,** *52* (5), 2105-2111.

34. Lessard, J. J.; Scheutz, G. M.; Hughes, R. W.; Sumerlin, B. S., Polystyrene-Based Vitrimers: Inexpensive and Recyclable Thermosets. *ACS Applied Polymer Materials* **2020**.

35. Lessard, J. J.; Scheutz, G. M.; Sung, S. H.; Lantz, K. A.; Epps, T. H.; Sumerlin, B. S., Block Copolymer Vitrimers. *Journal of the American Chemical Society* **2020,** *142* (1), 283-289.

36. Spiesschaert, Y.; Guerre, M.; De Baere, I.; Van Paepegem, W.; Winne, J. M.; Du Prez, F. E., Dynamic Curing Agents for Amine-Hardened Epoxy Vitrimers with Short (Re)processing Times. *Macromolecules* **2020,** *53* (7), 2485-2495.

37. Liu, W.-X.; Zhang, C.; Zhang, H.; Zhao, N.; Yu, Z.-X.; Xu, J., Oxime-Based and Catalyst-Free Dynamic Covalent Polyurethanes. *Journal of the American Chemical Society* **2017,** *139* (25), 8678-8684.

38. He, C.; Shi, S.; Wang, D.; Helms, B. A.; Russell, T. P., Poly(oxime–ester) Vitrimers with Catalyst-Free Bond Exchange. *Journal of the American Chemical Society* **2019,** *141* (35), 13753-13757.

39. Liu, H.; Nelson, A. Z.; Ren, Y.; Yang, K.; Ewoldt, R. H.; Moore, J. S., Dynamic Remodeling of Covalent Networks via Ring-Opening Metathesis Polymerization. *ACS Macro Letters* **2018,** *7* (8), 933-937.

40. Obadia, M. M.; Mudraboyina, B. P.; Serghei, A.; Montarnal, D.; Drockenmuller, E., Reprocessing and Recycling of Highly Cross-Linked Ion-Conducting Networks through Transalkylation Exchanges of C–N Bonds. *Journal of the American Chemical Society* **2015,** *137* (18), 6078-6083.

41. Nishimura, Y.; Chung, J.; Muradyan, H.; Guan, Z., Silyl Ether as a Robust and Thermally Stable Dynamic Covalent Motif for Malleable Polymer Design. *Journal of the American Chemical Society* **2017,** *139* (42), 14881-14884.

42. Tretbar, C. A.; Neal, J. A.; Guan, Z., Direct Silyl Ether Metathesis for Vitrimers with Exceptional Thermal Stability. *Journal of the American Chemical Society* **2019,** *141* (42), 16595-16599.

43. Zych, A.; Pinalli, R.; Soliman, M.; Vachon, J.; Dalcanale, E., Polyethylene vitrimers via silyl ether exchange reaction. *Polymer* **2020,** *199*, 122567.

44. El-Zaatari, B. M.; Ishibashi, J. S. A.; Kalow, J. A., Cross-linker control of vitrimer flow. *Polymer Chemistry* **2020**.

45. Ishibashi, J. S. A.; Kalow, J. A., Vitrimeric Silicone Elastomers Enabled by Dynamic Meldrum's Acid-Derived Cross-Links. *ACS Macro Letters* **2018,** *7* (4), 482-486.

46. Snyder, R. L.; Fortman, D. J.; De Hoe, G. X.; Hillmyer, M. A.; Dichtel, W. R., Reprocessable Acid-Degradable Polycarbonate Vitrimers. *Macromolecules* **2018,** *51* (2), 389-397.

47. Hayashi, M.; Yano, R., Fair Investigation of Cross-Link Density Effects on the Bond-Exchange Properties for Trans-Esterification-Based Vitrimers with Identical Concentrations of Reactive Groups. *Macromolecules* **2020,** *53* (1), 182-189.

48. Li, L.; Chen, X.; Jin, K.; Torkelson, J. M., Vitrimers Designed Both To Strongly Suppress Creep and To Recover Original Cross-Link Density after Reprocessing: Quantitative Theory and Experiments. *Macromolecules* **2018,** *51* (15), 5537-5546.

49. Ferry, J. D., *Viscoelastic properties of polymers*. John Wiley & Sons: 1980.

50. Yue, L.; Guo, H.; Kennedy, A.; Patel, A.; Gong, X.; Ju, T.; Gray, T.; Manas-Zloczower, I., Vitrimerization: Converting Thermoset Polymers into Vitrimers. *ACS Macro Letters* **2020,** *9* (6), 836-842.

51. Kar, G. P.; Saed, M. O.; Terentjev, E. M., Scalable upcycling of thermoplastic polyolefins into vitrimers through transesterification. *Journal of Materials Chemistry A* **2020,** *8* (45), 24137-24147.

52. Smith, M. K.; Northrop, B. H., Vibrational Properties of Boroxine Anhydride and Boronate Ester Materials: Model Systems for the Diagnostic Characterization of Covalent Organic Frameworks. *Chemistry of Materials* **2014,** *26* (12), 3781-3795.

53. Shen, C.; Zhao, Q.; Evans, C. M., Ion specific, odd–even glass transition temperatures and conductivities in precise network polymerized ionic liquids. *Molecular Systems Design & Engineering* **2019,** *4* (2), 332-341

CHAPTER 2: EFFECT OF PRECISE LINKER LENGTH, BOND DENSITY, AND BROAD TEMPERATURE WINDOW ON THE RHEOLOGICAL PROPERTIES OF ETHYLENE VITRIMERS

2.1. Abstract

Here, we investigate a series of precise, high crosslink density telechelic ethylene vitrimers as a function of temperature and crosslink density. The networks show a rubbery plateau at high frequencies and a terminal flow regime at lower frequencies. With increasing crosslink density, the rubbery plateau modulus shows a monotonic increase and the terminal flow shifts to lower frequencies. The plateau modulus at high frequency increases as a function of temperature, as expected for a conserved network topology. When plotted against inverse temperature, the zero shear viscosities show a characteristic Arrhenius behavior, and the activation energy monotonically increases with crosslink density. Crossover frequency and shift factors (from time temperature superposition) also show Arrhenius behavior with activation energies in good agreement with those determined from zero shear viscosity. A positive deviation from this Arrhenius trend is observed beginning as high as 100 K above the glass transition temperature for C_6 and C_8 networks. Further investigations of such networks are critical for the development of sustainable and recyclable replacements for commercial plastics.

2.2. Introduction

The term vitrimer was coined by Leibler[1] based on an Arrhenius temperature dependence of viscosity for polyester networks which is reminiscent of vitreous silica. It has been noted recently that this definition is not unique to dynamic networks with conserved exchange reactions and is also frequently observed in dissociative dynamic networks.[2] Thus, there is still

a need to understand under what conditions the mechanism of the exchange reaction will play a key role to the function or properties of dynamic networks. Two areas of vitrimer physics which have received little attention are the roles of extremely broad temperature windows and precise spacing between dynamic crosslinks. While the initial work of Leibler looked at a 180 °C temperature range,[1] subsequent works have been largely limited to a less than 50 °C window.[2] It is important to investigate wider windows because many polymer are processed well above their use temperatures, and it is unclear if the Arrhenius dependence will persist. Du Prez and coworkers found two distinct Arrhenius slopes in vinylogous urethane vitrimers[3] attributed to a change in the dominant exchange mechanism with temperature. Additionally, many polymer are tested far above T_g where bond exchange is anticipated to control the macroscopic stress relaxation. It has been suggested[4] that viscosity will show increasing deviations from Arrhenius behavior when approaching T_g, but little experimental data exists in this regime.

2.3. Results and Discussion

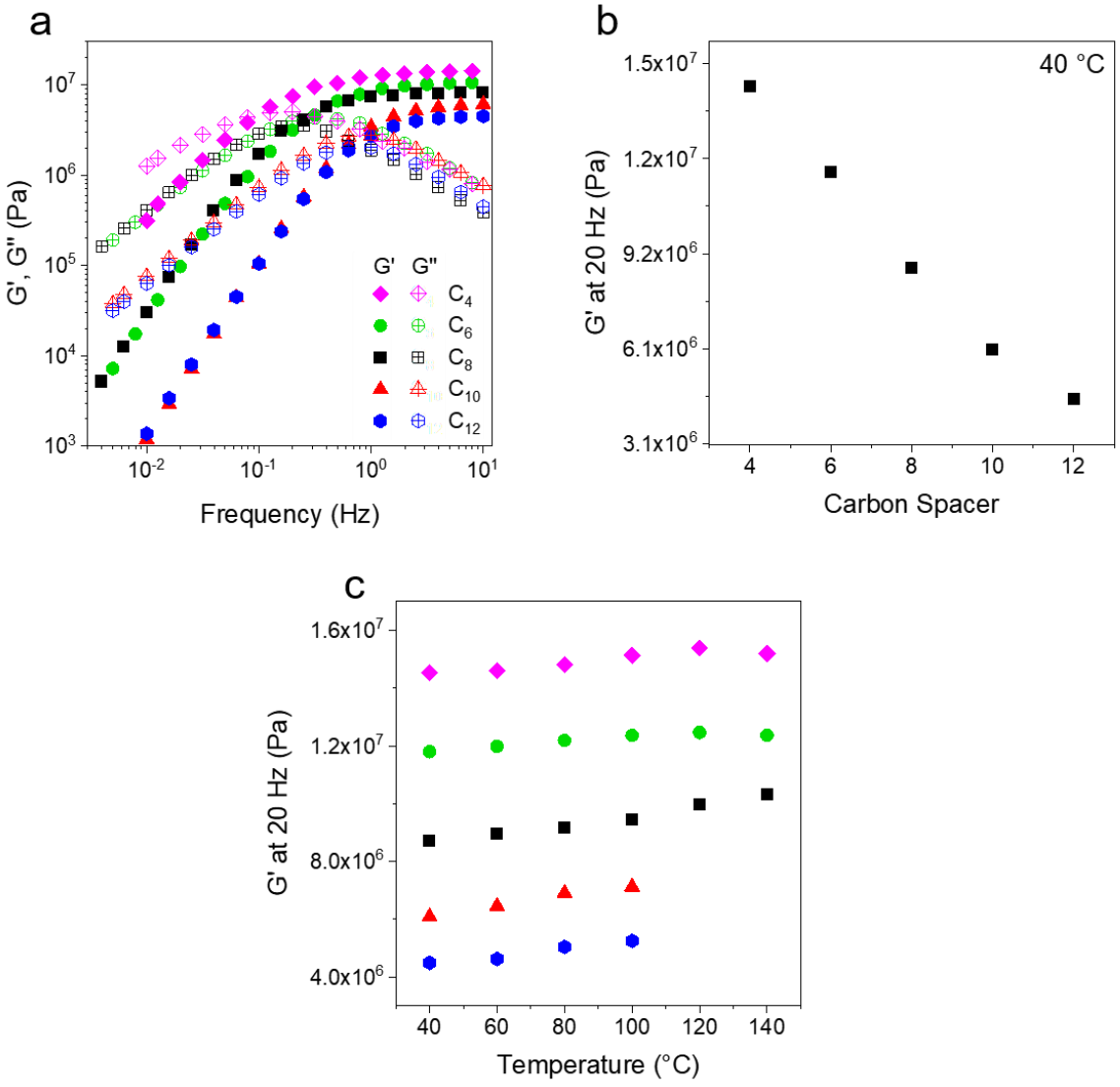

Figure 2.1. (a) Storage and loss moduli of ethylene vitrimers at 40 °C. A monotonic increase in rubbery plateau modulus at high frequency is observed with increasing crosslinking density. The terminal relaxation shifts to lower frequency as the crosslink density increases. (b) A comparison of the rubbery modulus with increasing linker length (decreasing crosslink density) shows a linear decrease as anticipated. (c) The rubbery modulus of the networks also shows a slight increase with increasing temperature as expected for networks with conserved topology. Symbols are the same as in (a).

2.3.1. Oscillatory Shear and Arrhenius Viscosity

Oscillatory shear rheology was used to probe the storage (G') and loss (G'') modulus of the PE networks. Since the C_{10} and C_{12} networks are crystalline at room temperature, all experiments were performed above 40 °C to prevent the interference of crystallization on rheological measurements. Frequency sweeps were performed at 10 °C intervals from 40 °C to 140 °C. The ethylene networks show a solid like (G' > G'') rubbery response at high frequencies and the plateau modulus at 40 °C varies from ~2 to 10 MPa depending on crosslink density (**Fig 2.1a**). This is expected of a rubbery network[5] and similar results have been shown in other experimental works on dynamic networks.[6] Although some of the data overlap at low frequency, the modulus at 20 Hz changes proportionally to the carbon spacer as expected (**Fig 2.1b**). At lower frequencies a terminal flow regime with characteristic slopes of ~ 2 for G' and ~ 1 for G'' is seen for all temperature (**Supplementary Fig 2.2**). The terminal relaxation shifts to lower frequencies with increasing crosslink density, as has been previously reported for other telechelic systems.[7, 8] The modulus measured at a constant frequency of 20 Hz also increases with temperature, as expected for systems with conserved network topology due to entropic elasticity.[52]

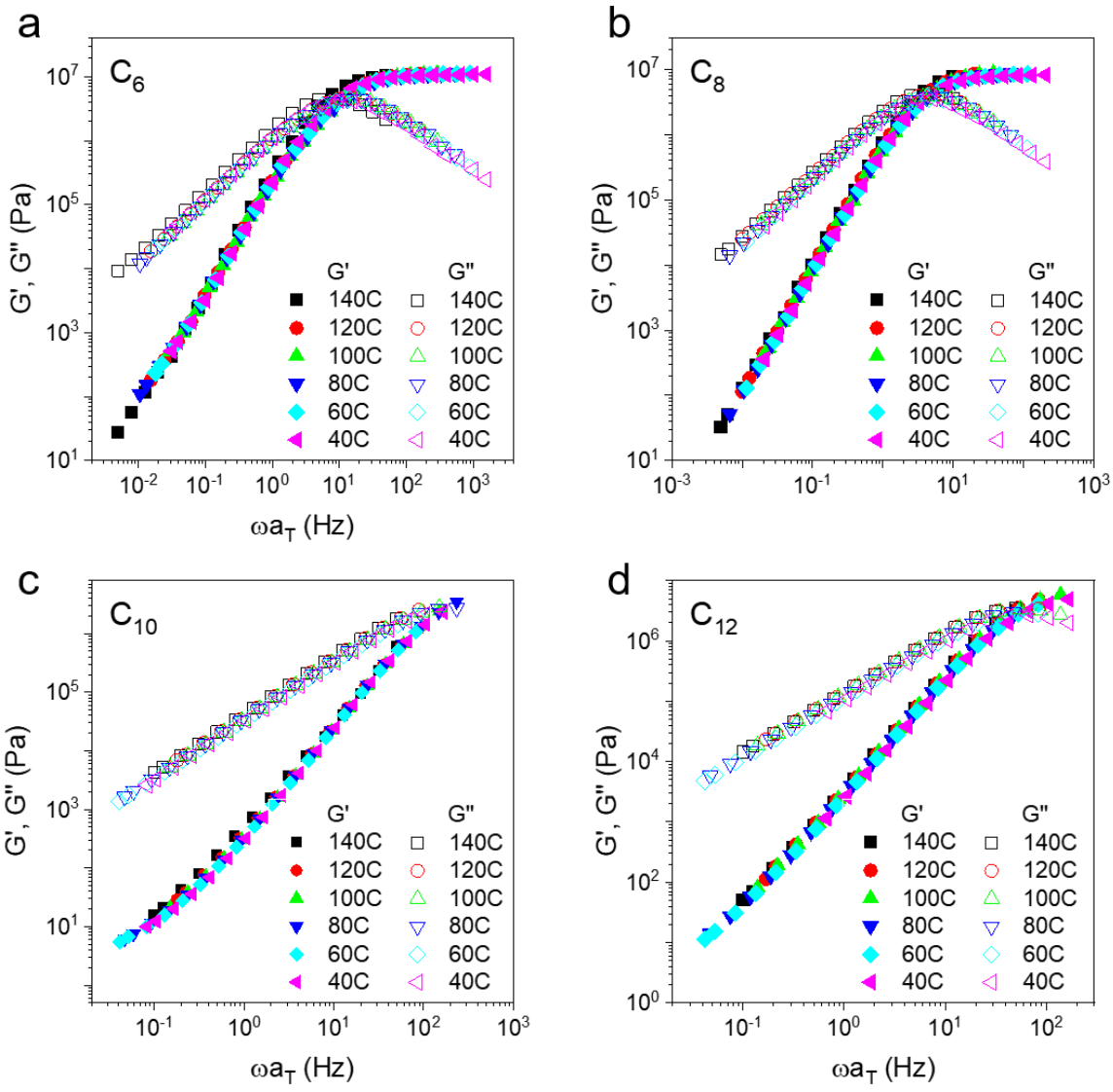

Figure 2.2. Horizontally shifted master curves (T_{ref} = 140 °C) of the networks. The high frequency rubbery modulus remains constant with increasing temperature, intermediate to expectations for permanent and dissociative dynamic networks.

Master curves of the storage and loss modulus (**Fig 2.2**) are made by horizontally shifting individual frequency sweeps onto a reference curve (T_{ref} = 140 °C) using the time temperature superposition (TTS) principle. On a seven order of magnitude log scale, the plateau appears constant; however, a closer inspection reveals that the modulus does increase with temperature, particularly at higher frequency (**Fig 2.1c and Fid S2.3**). Boronic transesterification exchange

reactions proceed in a topology conserving manner as shown by several groups[9-11] and thus this increase is expected. In prior work, polyethylene oxide dynamic networks with the same boronic ester bonds as the present work also showed an increase in modulus on heating.[12] This trend is in contrast to dissociative dynamic networks where modulus decreases with temperature.[2, 13]

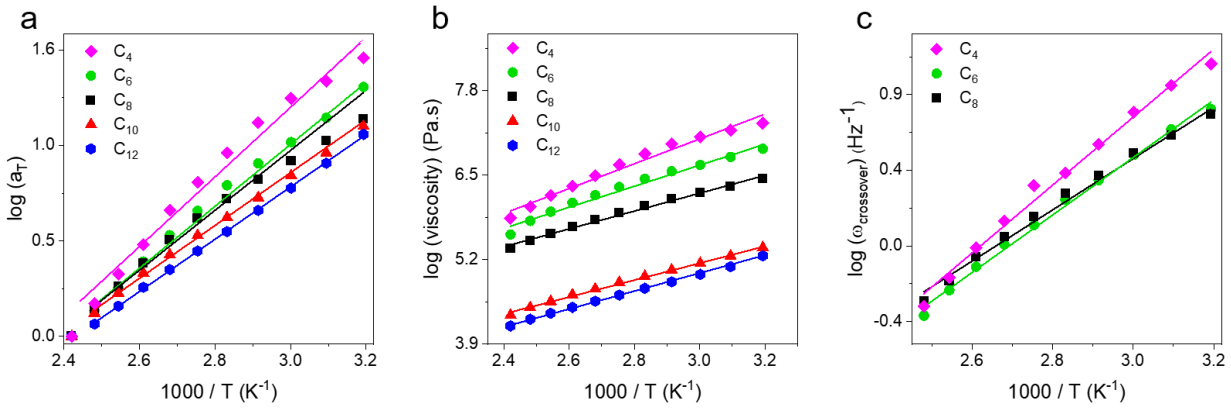

Figure 2.3. (a) Shift factors, (b) zero shear viscosity and (c) crossover frequency as a function of inverse temperature. All quantities show an Arrhenius behavior in the 100 °C temperature window.

From the horizontal shifting of frequency sweeps, shift factors (a_T) were obtained and plotted for all networks and show a systematic increase in the slope, and thus activation energy, from an Arrhenius fit (**Fig 2.3a**). Next, the zero shear viscosity of the networks was calculated from 140 to 0 °C using the low frequency slope of the loss modulus,[14] and a monotonic increase with increasing crosslink density is observed (**Fig 2.3b**). Complex viscosity was also calculated and compared to this method, with both approaches yielding identical results within error (**Supplementary Fig 2.4)**. Viscosity plotted against inverse temperature was also fit to an Arrhenius expression, and shows quantitative agreement with the values from a_T data (**Table 2.1**) indicating that they both reflect the same macroscopic flow controlled by dynamic bond

exchange. A third metric, the crossover frequency ($\omega_{crossover}$), was also examined and defined where G' = G" corresponding to the transition from a viscoelastic solid to a viscoelastic liquid. In the case of C_{10} and C_{12}, a crossover frequency could not be measured at temperatures above 60 °C because even at the highest frequencies G'' > G'. For C_4, C_6 and C_8 networks crossover frequencies were obtained as a function of temperature and are shown in **Fig 2.3c**. Although $\omega_{crossover}$ was only obtained in three networks, it is also in good agreement with zero shear viscosity and shift factor in reflecting the activation energy associated with flow. In the case of vitrimers which obey time-temperature superposition, the choice of analysis metric does not appear to matter for determining activation energies. The E_a values for our telechelic networks are all lower than what has been reported for boronic ester vitrimers with pendent dynamic bonds along the backbone by Guan and coworkers who measured E_a = 52.7 kJ/mol.[9] Sokolov and coworkers have noted that in associating polymers, telechelic structures lead to lower bond breaking energies[15] which is consistent with our findings. Additionally, we observe a major increase in E_a with increased crosslink density suggesting that exchange processes are easier in more open networks (**Table 2.1**). From the shift factor data $Ea \sim N^{-0.4}$, and it would be important to push to higher linker lengths to determine where the value becomes molecular weight independent. It is also unclear at present how polydispersity will affect these values.

Table 2.1. Activation Energy from Arrhenius fits to shift factors, zero shear viscosity and crossover frequency.

	Activation Energy, E_a (kJ/mol)		
	Shift factors	Zero shear viscosity	$\omega_{crossover}$
C_4	43.0	41.6	38.5
C_6	32.3 ± 0.12	28.9 ± 0.12	33.0 ± 0.13
C_8	32.2 ± 0.15	25.4 ± 0.08	28.9 ± 0.10
C_{10}	27.6 ± 0.06	25.6 ± 0.08	- [a]
C_{12}	27.3 ± 0.02	26.4 ± 0.03	- [a]

[a] not observable

2.3.2. Topological Freezing Temperature and Deviation from Arrhenius Behavior

In addition to T_g and T_m, a hypothetical topology freezing temperature (T_v) has been suggested for vitrimers where the bond exchange occurs on slow enough timescales that the network is frozen and $\eta = 10^{12}$ Pa s,[16] the same criterion invoked for the glass to rubber transition. The position of the T_v with respect to the T_g and T_m may provide insights regarding the relative importance of bond exchange or segmental dynamics in controlling stress relaxation in different temperature regimes.[17, 18] The T_v of our networks was obtained by extrapolating the zero shear viscosities to a value of 10^{12} Pa·s (**Fig 2.4a**). We note this massive extrapolation is not rigorous but was used to mimic protocols in the vitrimers literature.[18, 19] We do not view T_v as a particularly useful temperature as it shares the same criteria as the glass transition (viscosity = 10^{12} Pa s) leading to potential ambiguity. Additionally, depending on the modulus the T_v could correspond to timescales of relaxation spanning 10^8 to 10^3 s for networks ranging from ultrasoft (10 kPa) to glassy (1 GPa) through the Maxwell relation $\eta = G\boldsymbol{\tau}$. A topology freezing transition

based on a relaxation time would seem more informative than a temperature, but it is unclear what timescale is appropriate.

The T_v values were determined as -116 °C (C_6), -135 °C (C_8), -149 °C (C_{10}) and -143 °C (C_{12}) which are all well below T_g. Thus, upon cooling the T_g is expected to intervene and lead to an increase in viscosity above the extrapolation of an Arrhenius fit. Such a deviation is observed at ~T_g + 100 °C, and corresponds to a transition from a regime controlled by exchange reactions to a regime where segmental dynamics begin to contribute to an increased viscosity (**Fig 2.4b**). This can be clearly seen in C_6 and C_8 as their zero shear viscosities show a positive deviation from the Arrhenius trend on a 1000/T plot (**Fig 2.4c**). These networks remain amorphous on cooling while C_{10} and C_{12} crystallize and thus viscosity measurements were not made below a temperature of 40 °C. Our findings are in contrast to the initial work of Leibler who found a single Arrhenius dependence of zero-shear viscosity from T_g to T_g + 180 °C, presumably because their T_v was higher than T_g.[1] In the present work, the extrapolation based on high temperature gives a different T_v than would be determined from the lower temperature data, and emphasizes the importance of measuring relaxation over a broad temperature window. Understanding where deviations begin depending on the combination of dynamic bond and polymer chemistry will be an important direction for future research.

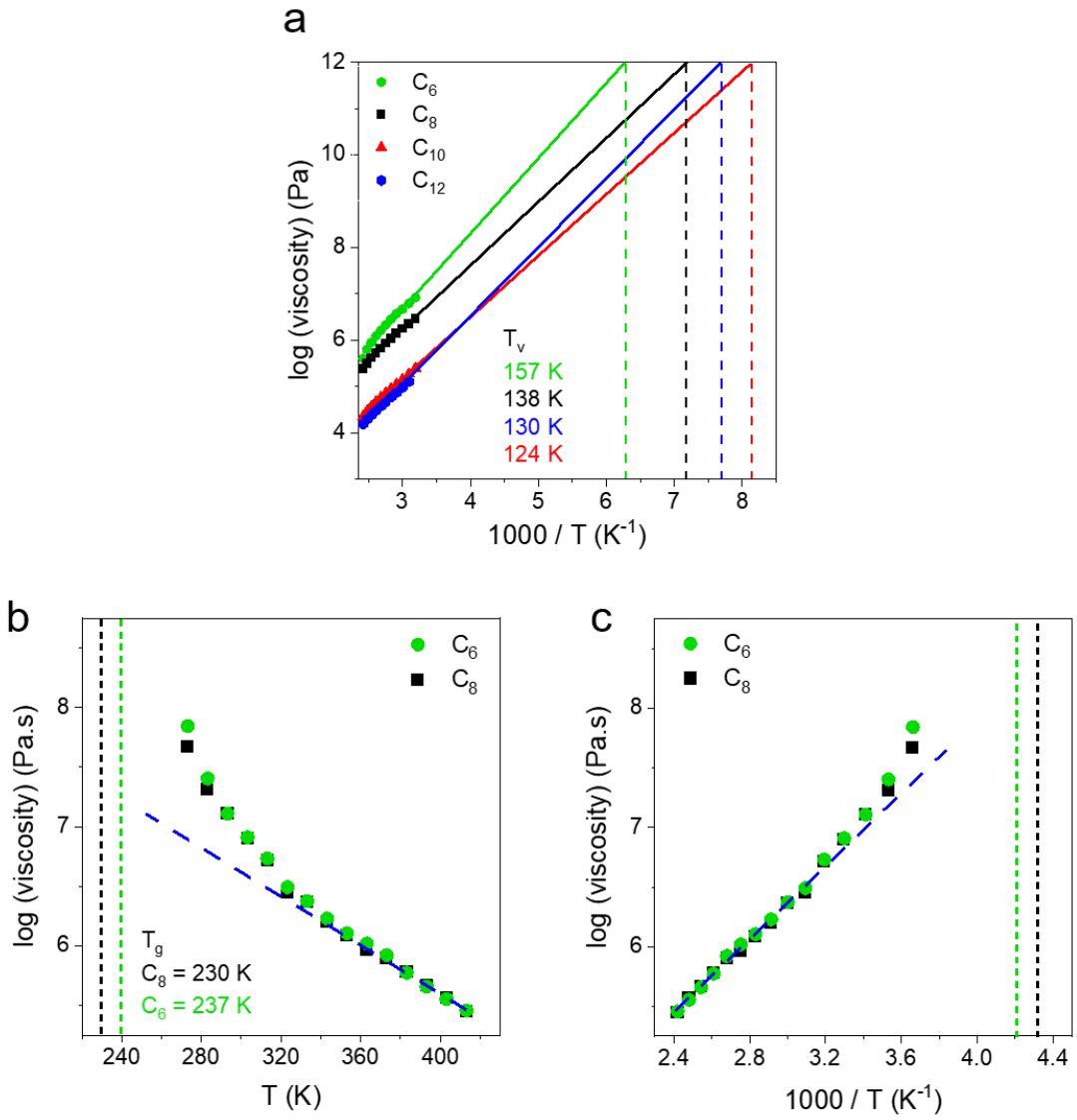

Figure 2.4. (a) The topological freezing temperature (T_v) is defined as the temperature at which the melt viscosity equals a value of 10^{12} Pa·s. We obtained the T_v by extrapolating the Arrhenius zero shear viscosity fit to a value of 10^{12} Pa·s. (b) Zero shear viscosity vs temperature and (c) inverse temperature. As the T_g is approached a positive deviation from the Arrhenius behavior is observed. The deviation indicates a transition from a regime controlled by exchange reactions to a regime where slow segmental dynamics begin to contribute to viscosity.

2.4. Conclusion

A series of precise telechelic ethylene vitrimers was investigated to understand the effect of temperature and precise crosslink density on their rheological properties. The dynamic nature of the networks manifests as a rubbery plateau at high frequencies and a low frequency terminal

relaxation. Increasing crosslink density (C_{12} to C_6) leads to a monotonic increase in the rubbery modulus and a delay of the terminal relaxation. The zero shear viscosity shows a characteristic Arrhenius temperature dependence and monotonically increases with increasing crosslink density. Similar Arrhenius fits are made for the crossover frequency and shift factors, and the activation energies calculated from all metrics are in good agreement with each other. Telechelic networks show a lower activation energy than pendant networks with boronic esters.[9] At high temperature, the rheological properties of the networks are dominated by the exchange reactions while a deviation from Arrhenius behavior is observed upon cooling. The additional increase in viscosity is attributed to the impending T_g and slowing segmental dynamics which begin to contribute as T_g + 100 K. These broad temperature window studies on model systems provide key insights to the understanding and application of vitrimers for a range of applications.

2.5. Experimental Details and Additional Plots

Materials: Boric acid ($B(OH)_3$, ≥ 99.5%), 1,4 butanediol (C_4, ≥ 99%), 1,6 hexanediol (C_6, 99%), 1,8 octanediol (C_8, 98%), 1,10 decanediol (C_{10}, 98%) and 1,12 dodecanediol (C_{12}, 99%), were purchased from Sigma-Aldrich and used without further purification.

Vitrimer Synthesis: Carefully weighed amounts of monomer were mixed together in a glass vial with stoichiometry of 1.0 mol boric acid to 1.5 mol diol. The mixture was heated and stirred continuously overnight at 120 ˚C on a hotplate. A viscous transparent gel was obtained. The vial was then transferred to a vacuum drier, held at 60˚C overnight under vacuum to drive water off

and then immediately brought into an argon glovebox maintained at < 0.5 ppm O_2 and < 0.1 ppm H_2O. No solvent was used in the synthesis.

Vitrimer Rheology: Rheological measurements were made on a TA Instruments DHR-2 rheometer using a parallel plate geometry. Samples were pressed into an 8 mm disc under ambient conditions and then loaded on to the rheometer at 40 ˚C. Samples were heated and held at 140 ˚C for 30 min to remove any water absorbed during sample loading. Sample thickness of approximately 800 µm was used for all measurements. Frequency sweeps were conducted at isothermal temperatures from 140 ˚C to -10 ˚C at 10 ˚C intervals with an applied stress of 1000 Pa. Viscosity of the networks was calculated by measuring the slope of the loss modulus vs frequency curve in the low frequency limit. Viscosity of the networks was plotted against inverse temperature and a characteristic Arrhenius behavior is observed as expected for vitrimers. Time temperature superposition master curves were generated using the TRIOS (TA Instruments) software with a reference temperature of 140 ˚C with no vertical shifting.

ATR-FTIR: IR spectra of the samples were collected using a Bruker ALPHA FTIR spectrometer with a platinum-ATR QuickSnap sampling module. All measurements were made at 80 ℃ by scanning from 400 cm^{-1} to 4000 cm^{-1} with 16 total scans. Solid samples (networks) were clamped down to the diamond ATR crystal to ensure sufficient contact, while liquid samples (monomers) were left undisturbed.

Differential Scanning Calorimetry (DSC): Samples with average weight between 3-6 mg were crimped in Tzero hermetic aluminum pans inside the glovebox. A TA Instruments DSC 25 with

a RCS 120 cooling accessory was used to take all measurements. The glass transition temperature (T_g) for each sample was obtained by first heating the samples to 150 ℃ followed by quenching to -80 ℃ and then ramping to 120 ℃ at 20 ℃ / min. The DSC quench rate is the fastest allowed by the instrument, and varies depending on the temperature range from 50 °C/min (down to -30 °C) to 5 °C/min (when approaching -75 °C). The T_g is obtained from analysis of the heating profile using the ½ ΔCp criterion.

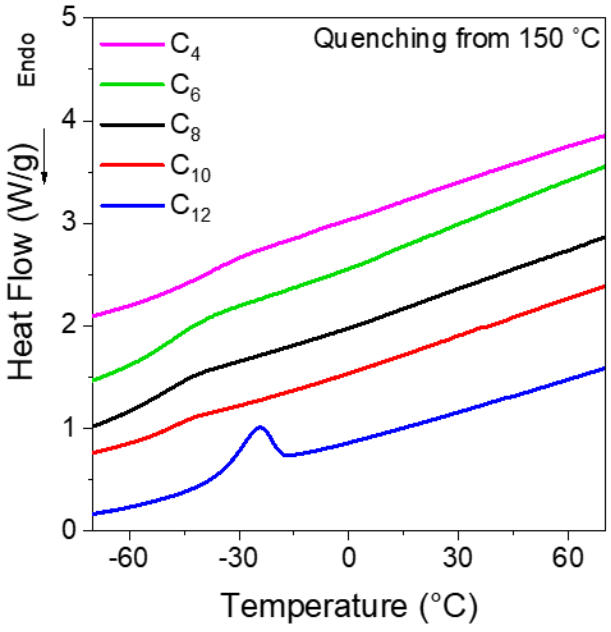

Supplementary Figure 2.1. Quenching cycle of the DSC scan. An exothermic crystallization peak can be seen for C_{12}. The other networks do not crystallize during quenching.

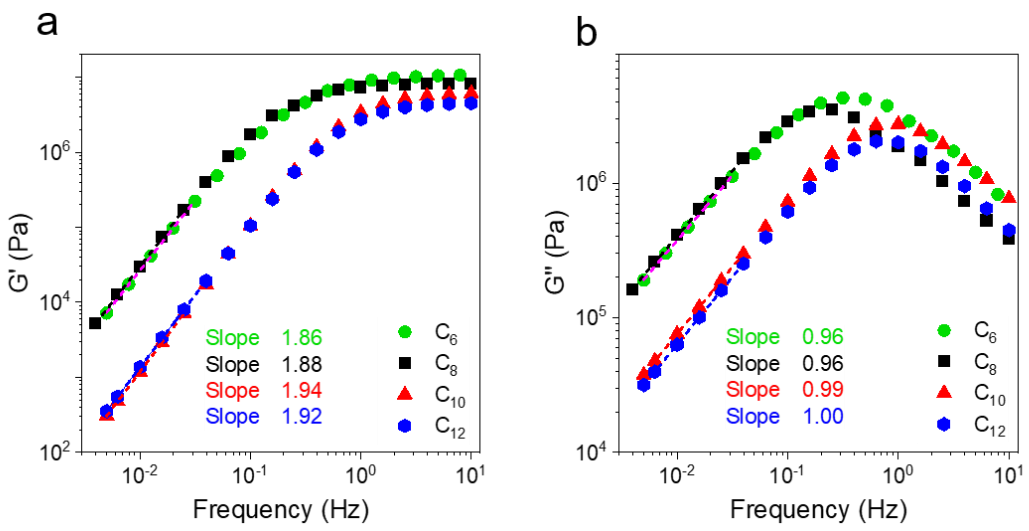

Supplementary Figure 2.2. (a) Storage - G' and (b) Loss - G'' modulus of the PE vitrimers at 40 C. A high frequency rubbery plateau modulus monotonically increasing with crosslink density observed. The terminal relaxation at low frequency is confirmed by observation of characteristic slopes of ~ 1 for G'' and ~2 for G'.

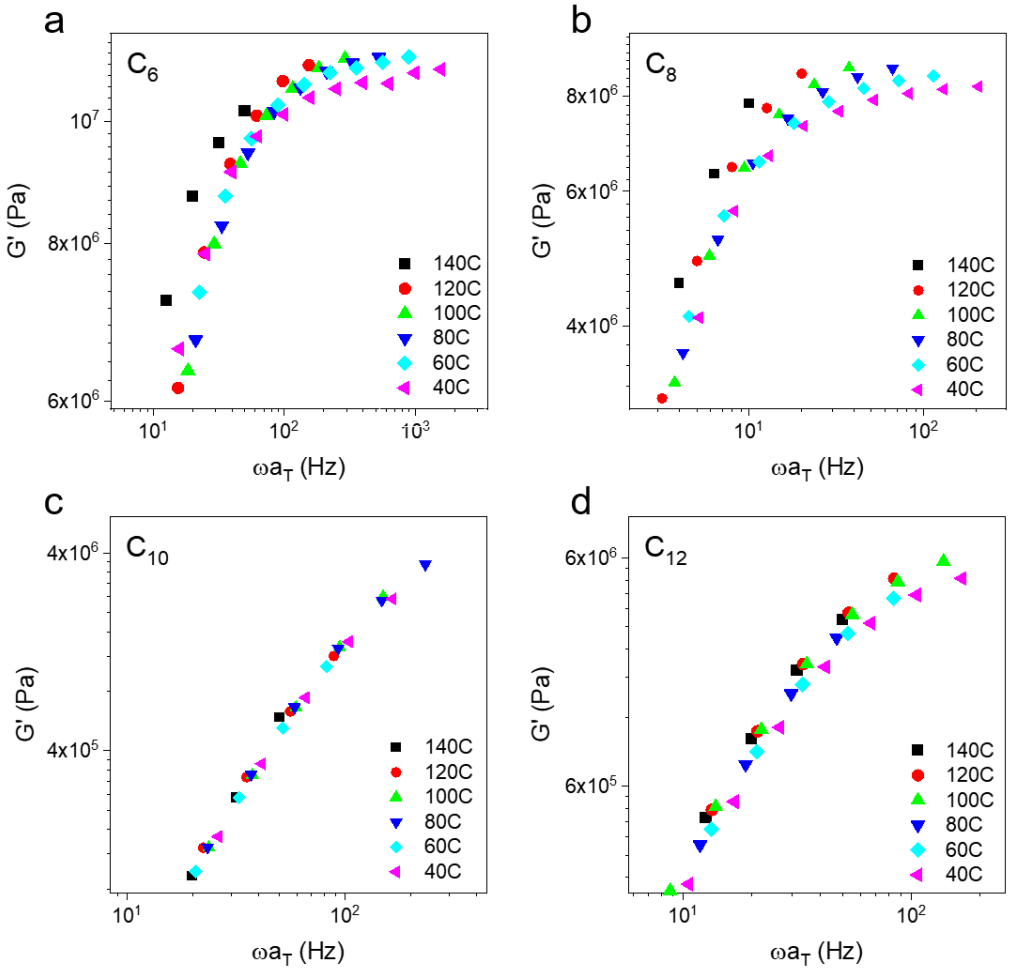

Supplementary Figure 2.3. (Continued)

Supplementary Figure 2.3. A zoomed in image of the high frequency region of the TTS plots from Figure 3. In all cases, the plateau modulus shows a slight increase with temperature.

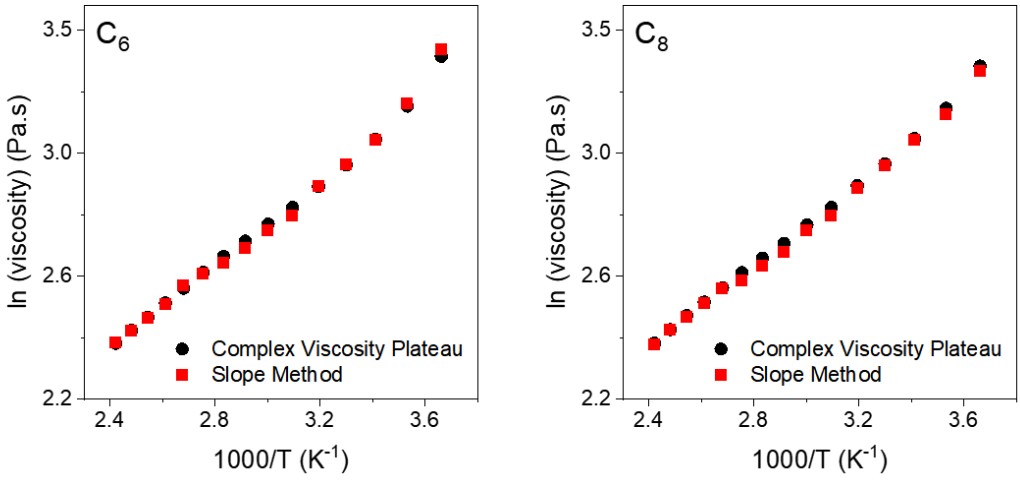

Supplementary Figure 2.4. A comparison between viscosities obtained from the low frequency slope of G" compared to the complex viscosity. The values are the same within error.

2.6. References

1. Montarnal, D.; Capelot, M.; Tournilhac, F.; Leibler, L., Silica-Like Malleable Materials from Permanent Organic Networks. *Science* **2011,** *334* (6058), 965.

2. Elling, B. R.; Dichtel, W. R., Reprocessable cross-linked polymer networks: Are associative exchange mechanisms desirable? *ACS Central Science* **2020**.

3. Guerre, M.; Taplan, C.; Nicolaÿ, R.; Winne, J. M.; Du Prez, F. E., Fluorinated Vitrimer Elastomers with a Dual Temperature Response. *Journal of the American Chemical Society* **2018,** *140* (41), 13272-13284.

4. Denissen, W.; Winne, J. M.; Du Prez, F. E., Vitrimers: Permanent organic networks with glass-like fluidity. *Chemical Science* **2016,** *7* (1), 30-38.

5. James, H. M.; Guth, E., Theory of the elastic properties of rubber. *The Journal of Chemical Physics* **1943,** *11* (10), 455-481.

6. Yan, T.; Schröter, K.; Herbst, F.; Binder, W. H.; Thurn-Albrecht, T., What Controls the Structure and the Linear and Nonlinear Rheological Properties of Dense, Dynamic Supramolecular Polymer Networks? *Macromolecules* **2017,** *50* (7), 2973-2985.

7. Breuillac, A.; Kassalias, A.; Nicolaÿ, R., Polybutadiene Vitrimers Based on Dioxaborolane Chemistry and Dual Networks with Static and Dynamic Cross-links. *Macromolecules* **2019,** *52* (18), 7102-7113.

8. Liu, Y.; Tang, Z.; Chen, J.; Xiong, J.; Wang, D.; Wang, S.; Wu, S.; Guo, B., Tuning the mechanical and dynamic properties of imine bond crosslinked elastomeric vitrimers by manipulating the crosslinking degree. *Polymer Chemistry* **2020,** *11* (7), 1348-1355.

9. Cromwell, O. R.; Chung, J.; Guan, Z., Malleable and Self-Healing Covalent Polymer Networks through Tunable Dynamic Boronic Ester Bonds. *Journal of the American Chemical Society* **2015,** *137* (20), 6492-6495.

10. Springsteen, G.; Wang, B., A detailed examination of boronic acid–diol complexation. *Tetrahedron* **2002,** *58* (26), 5291-5300.

11. Cash, J. J.; Kubo, T.; Bapat, A. P.; Sumerlin, B. S., Room-Temperature Self-Healing Polymers Based on Dynamic-Covalent Boronic Esters. *Macromolecules* **2015,** *48* (7), 2098-2106.

12. Jing, B. B.; Evans, C. M., Catalyst-Free Dynamic Networks for Recyclable, Self-Healing Solid Polymer Electrolytes. *Journal of the American Chemical Society* **2019,** *141* (48), 18932-18937.

13. Kloxin, C. J.; Bowman, C. N., Covalent adaptable networks: smart, reconfigurable and responsive network systems. *Chemical Society Reviews* **2013,** *42* (17), 7161-7173.

14. Thompson, R. L.; Alicke, A. A.; de Souza Mendes, P. R., Model-based material functions for SAOS and LAOS analyses. *Journal of Non-Newtonian Fluid Mechanics* **2015,** *215*, 19-30.

15. Xing, K.; Tress, M.; Cao, P.-F.; Fan, F.; Cheng, S.; Saito, T.; Sokolov, A. P., The Role of Chain-End Association Lifetime in Segmental and Chain Dynamics of Telechelic Polymers. *Macromolecules* **2018,** *51* (21), 8561-8573.

16. Fang, H.; Ye, W.; Ding, Y.; Winter, H. H., Rheology of the Critical Transition State of an Epoxy Vitrimer. *Macromolecules* **2020**.

17. Van Zee, N. J.; Nicolaÿ, R., Vitrimers: Permanently crosslinked polymers with dynamic network topology. *Progress in Polymer Science* **2020,** *104*, 101233-101233.

18. Gamardella, F.; Guerrero, F.; De la Flor, S.; Ramis, X.; Serra, A., A new class of vitrimers based on aliphatic poly (thiourethane) networks with shape memory and permanent shape reconfiguration. *European Polymer Journal* **2020,** *122,* 109361.

19. Lopez, G. r.; Granado, L.; Coquil, G. l.; Lárez-Sosa, A. s.; Louvain, N.; Améduri, B., Perfluoropolyether (PFPE)-based vitrimers with ionic conductivity. *Macromolecules* **2019,** *52* (5), 2148-2155.

CHAPTER 3: FRAGILE GLASS FORMATION AND NON-ARRHENIUS UPTURNS IN ETHYLENE VITRIMERS REVEALED BY COMBINING RHEOLOGY AND DIELECTRIC SPECTROSCOPY

3.1. Abstract

Vitrimers, dynamic networks with bonds that exchange without breaking, are an emerging class of reprocessable and recyclable polymer. The dynamics in such materials are complex and span from a single bond exchange or alpha relaxation event up to bulk flow. Most prior work has focused on investigations of stress relaxation times or creep experiments, but little has been pursued to investigate more local dynamics over a wide range of temperatures. A series of precise ethylene vitrimers are synthesized with four to seven carbons between dynamic bonds, and broadband dielectric spectroscopy is used to probe the segmental dynamics. Three distinct modes are identified in the dielectric spectra - an alpha process, beta process, and a normal mode assigned to strand motion in the network between dynamic bonds. The last mode corresponds within error to the rheological crossover time indicating this process is responsible for bulk flow at high temperatures. At lower temperatures, approaching the glass transition causes a positive deviation of the crossover time from Arrhenius behavior in the networks at roughly the same distance above Tg. Finally, we analyze our networks in the context of a previously developed theory for bond dissociation in associating polymers and find evidence that the non-Arrhenius behavior reflects strong decoupling of the bond exchange barrier crossing event with the segmental or alpha relaxation. This implies the bond exchange event that conserves dynamic crosslink density experiences a local frictional resistance due to the surrounding polymer matrix that is smaller and much less temperature dependent than the primary structural relaxation

process, and to a larger degree than observed in most associating copolymer melts where physical bond breaking is a dissociative process.

3.2. Introduction

Vitrimers are a subcategory of dynamic covalent networks where the polymeric backbones are crosslinked by associative exchangeable bonds.[1-9] Unlike supramolecular polymers and dissociative dynamic covalent networks that undergo breaking and reforming reactions of physical bonds, vitrimers undergo exchange reactions that do not involve bond breaking. These materials have received fast-growing interest from the recyclable polymers research community due to their unique self-healing properties, easy reprocessability and recyclability, and the numerous dynamic covalent chemistries that can be used to tailor these properties.[9-16] While a large body of work has been directed towards investigating the self-healing, recyclability, and stress relaxation behavior of these networks, focus in recent years has shifted towards investigating the effect of bond exchange on properties other than those investigated using rheology and self-healing measurements, such as crystallization[17], phase separation[18] and self-assembly[2, 19]. Vitrimers are also being investigated as functional materials with applications in solid polymer electrolytes[20], super-hydrophobic coatings[21], shape-memory materials[22, 23], and adhesives[24] to name a few. For these areas, a more comprehensive understanding of dynamics across length scales is required for materials design and optimization. Understanding how bond exchange may be impacted by glassy segmental dynamics, and if vitrimer dynamics are fundamentally different from dissociative networks in a meaningful way, requires further investigation.

A single dynamic bond exchange event occurs on a local Angstrom length scale, and is a distinct process from the segmental dynamics associated with the glass transition, which also

occur on a local scale though typically at least one nm. Nuclear magnetic resonance (NMR) spectroscopy has been used to measure the bond exchange kinetics and activation energies for the dynamic exchange reactions using small molecules which mimic the chemistry of the network,[5, 25-27] but it is difficult to directly measure single bond exchange in a dry network. The activation energy calculated from macroscopic flow properties such as viscosity can be substantially different from the values obtained in small molecule studies, even when the flow is thought to be controlled by dynamic bond exchange.[5] Thus, there is still a knowledge gap in understanding the broad range of dynamics across length and time scales ranging from very local segmental motions up to entire network flow.

Broadband dielectric spectroscopy (BDS) is a powerful tool frequently used to study molecular dynamics in linear polymers, small molecules, and associating polymers. Recent work from the Sokolov group has shown that BDS can reveal not only the segmental alpha process associated with translational and rotational dynamics of the monomers, but also the association dynamics of hydrogen-bonded supramolecular polymers.[28-32] They showed that BDS can in some cases reveal the dynamics of chain diffusion between hydrogen bonds, which is consistent with the terminal relaxation measured via shear rheology. Such measurements are lacking in the context of vitrimers, but could provide key insights on the molecular mechanisms which govern flow, self-healing, and recyclability. These samples have also been recently analyzed from a theoretical standpoint using a statistical mechanical approach to understand how the sticky groups impact the glass transition, non-sticker segmental dynamics, and sticky group relaxation.[33-35] Sticky groups with long enough lifetimes serve as permanent crosslinks on the non-sticky group segmental relaxation time, and can significantly slow down structural relaxation, modify its temperature dependence, and increase T_g. The slower or second step bond

breaking event, often called the α^* process, is associated with a local, chemically specific Arrhenius process with a well defined constant barrier. The elementary time scale is set by the friction associated with bond breaking (barrier crossing along a reaction coordinate) which can be decoupled to variable degrees from the perturbed alpha relaxation process. Many experimental systems could be well described in this picture when the two timescales are substantially different. Extension of the ideas to weakly associating telechelic melts with smaller timescale separations has very recently been formulated and successfully confronted with experimental data.[33, 34] The theory remains to be tested in vitrimers which do not break, but rather exchange, bonds with a rate that also often has an Arrhenius dependence on temperature at least over a limited range of temperatures and/or in model non-polymeric systems. The extent to which this exchange process is coupled to the alpha process and can become non-Arrhenius is not well understood, and is one focus of the present article.

In this work, ethylene vitrimers previously investigated for their flow properties and crystallization[16, 17] have been analyzed using BDS to connect the underlying segmental dynamics to the macroscopic flow as characterized by the crossover frequency, defined as the frequency at which the storage modulus (G') and loss modulus (G'') are equal. The frequency sweeps of ethylene vitrimers were previously reported,[16] and it was found that the modulus trends can be well described by affine network theory and show a proportionality with the crosslink density. They all can be described by a simple Maxwell model likely due to the simple telechelic nature of the networks.

The precise networks have an exact number of carbons between boronic ester junctions and are labeled as $C_{x,}$ where x corresponds to the number of carbons between crosslink junctions. For carbon numbers 4-7, the networks do not show any evidence of crystallization and serve as

model systems. Three modes are observed in the dielectric spectroscopy corresponding to the alpha process, a beta process, and a mode which corresponds within error to the rheological crossover time. This mode is attributed to a normal mode corresponding to linker motion within the vitrimers, and shows that the flow timescale is controlled by bond exchange at sufficiently high temperature. At lower temperatures, the glass transition leads to positive deviations from Arrhenius behavior in the networks. Normalization of relaxation times by a dynamic glass transition temperature we denote as $T_{g,\ BDS\ 0.01}$ (defined as when the alpha time is 0.01 sec) can superpose the alpha and normal mode relaxation times very well, but not the crossover time. Comparisons with a simplified version of the previously developed theory[33, 34] for associating multiblock and telechelic polymers are also discussed and used to extract activation energies from a distinct route which are in good agreement with rheological methods. For the first time, we determine decoupling exponents related to the bond exchange event experiencing a much reduced local friction compared to the alpha process, which is much lower (more decoupling) than in the analogous homopolymers with similar fragilities and smaller than in associating copolymer melts where bond breaking is a dissociative event that does not conserve crosslink density in contrast to vitrimers.

3.3. Results and Discussion

3.3.1. Identifying Relaxation Modes using Broadband Dielectric Spectroscopy

The networks were synthesized as described in our prior work via the condensation of alkane diols with boric acid.[16, 17] This leads to an exact number of carbons between crosslink points, but does not imply anything about the detailed topology or presence of loops and defects (**Scheme 3.1**). The C_4-C_7 networks were first analyzed by BDS, and **Figure 3.1** shows the

dielectric loss (ε") permittivity at four different temperatures for the networks. The source of the dipole moment is thought to be C-OH groups in the networks. While attached to the boron site, the dipoles largely cancel due to the planar symmetry of the trifunctional boron, but the exchange event breaks this symmetry and creates the signal we are observing. When a C-OH group is not attached to a boron site it is undergoing diffusive dynamics in search of a new boron partner, and thus is dielectrically active.

Data was collected from -30 ℃ to 70 ℃ at 10 ℃ intervals in a frequency window of 10^{-1} Hz to 10^{6} Hz, only four representative temperatures are shown in the plot for ease of visualization. Three distinct relaxation peaks are observed in the ethylene vitrimers over the changing temperature range: α, β, and the normal mode.

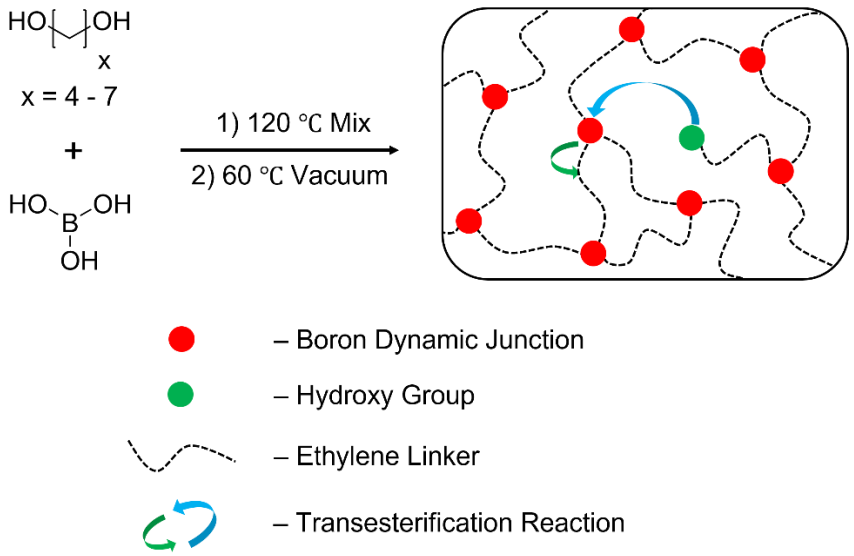

Scheme 3.1. Boronic ester ethylene vitrimers synthesized via condensation of precise alkane diols with boric acid.

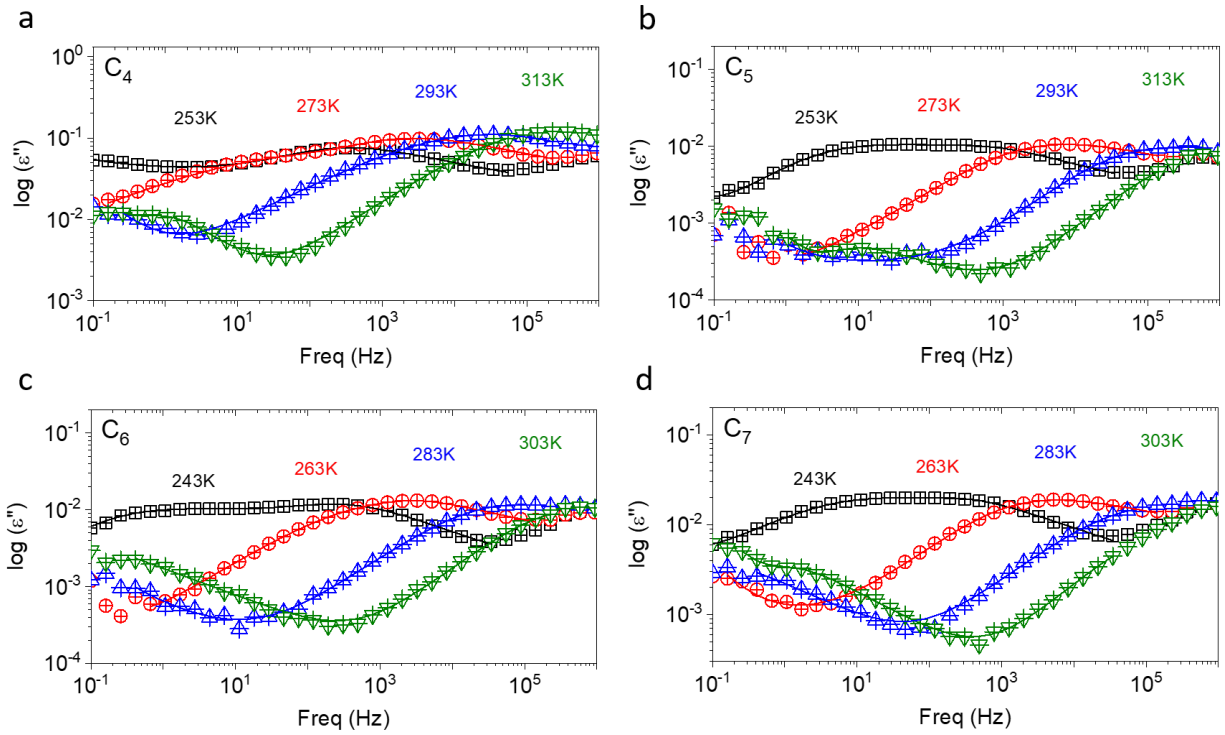

Figure 3.1. (a), (b), (c), (d) Dielectric spectroscopy of the C_4 to C_7 networks was performed in the -30 ℃ to 70 ℃ temperature window with 10 ℃ intervals. Four relaxation peaks can be distinctly identified from the loss permittivity at these representative temperatures. The solid lines through the data points are HN fits.

The relaxations observed in the dielectric loss modulus ε" were quantified by fitting the data to Havriliak−Negami (HN) functions, depending on the number of ε" peaks and a power-law function to describe the conductivity contribution:

$$\varepsilon'' = \frac{\sigma}{\omega\varepsilon_0} + \sum \frac{\Delta\varepsilon}{[1 + (i\omega\tau_{HN})^{\alpha}]^{\gamma}}$$

Here σ is the conductivity, ω is the frequency, ε_0 is the dielectric permittivity of vacuum, $\Delta\varepsilon$ is the dielectric relaxation strength, τ_{HN} is the HN relaxation time, and α and γ are HN shape parameters. The relaxation time at maximum loss was determined via:

$$\tau_p = 2\pi\tau_{HN}\left[\sin\left(\frac{\alpha\gamma\pi}{2+2\gamma}\right)\right]^{\frac{1}{\alpha}}\left[\sin\left(\frac{\alpha\pi}{2+2\gamma}\right)\right]^{-\frac{1}{\alpha}}$$

where τ_{HN} is the HN relaxation time and α and γ are the HN shape parameters. These fits are shown as lines through the experimental data in **Figure 3.1**, and the fit parameters are given in **Supplementary Table 3.1** of the SI. The shape parameters reflect some combination of the breadth and asymmetry of the peaks, and there is not a unique solution when fitting multiple modes in a spectrum. However, the values of the relaxation times are not sensitive to the precise choice of α and γ.

Each mode in BDS was plotted as a function of temperature as shown in **Figure 3.2**. At the highest temperatures, a peak can be distinctly seen in the 10^5 – 10^6 Hz range. As the temperature is decreased, this peak shifts to lower frequencies, and a second peak starts to appear. This is initially observed as a broadening of the dominant peak and then as two distinct peaks at lower temperatures. The slower of the two peaks is assigned as the α-relaxation (associated with glassy dynamics) which follows a VFT trend. The value of this process at 100 s provides a dynamic $T_{g,BDS\ 100}$ which is in excellent agreement with the calorimetric $T_{g,DSC}$ (**Table 3.1**). The faster process which splits from the alpha process on cooling is called the β-process following prior work on glass forming polymers.[36] This process may be of a Johari-Goldstein type secondary relaxation nature which is commonly observed in small molecule glass formers.

The beta process is Arrhenius with activation energies of 66.7, 69.4, 80.2, and 90.0 kJ/mole for C_4 to C_7 , respectively, consistent with prior values reported for linear polyethylene.[37] While the β process in polymers is usually attributed to side chain relaxation, there are no side chains in the present vitrimers. Even small rigid molecular glass formers can show a β relaxation believed to be associated with a bifurcation of motion of the same chemical moiety into small displacements within a confining cage (typically called the “fast beta” relaxation) and a larger scale slower activated cage escape process that defines the “alpha”

relaxation. We tentatively interpret our vitrimer results in this perspective, although the microscopic details underlying the αβ splitting or bifurcation is unclear. As a speculative comment, it perhaps is related to the localization of bond exchange within a cluster of dynamic bonding groups versus intercluster exchanges. The notion of bond exchange within a cluster is partly supported by the weak scattering peak at $q \sim 8$ nm^{-1} (**Supplementary Figure 3.1b**) and the presence of a second T_g (**Supplementary Figure 3.4**) which can imply the existence of phase separated domains. However, no large scale aggregation is seen in the SAXS data for any of the networks (**Supplementary Figure 3.1a**)

An interesting feature of the observed beta process is the modest increase of its activation energy with carbon number. A possible explanation of the latter is the increase of the characteristic ratio, a measure of local chain rigidity or Kuhn length, with number of backbone monomers for such short linkers.[38] The two modes merge at higher temperatures as is commonly observed in supercooled molecular and polymer liquids and is called the $\alpha\beta$ relaxation.[39-41] Above the splitting temperature (T_s), the $\alpha\beta$ relaxation time shows an Arrhenius behavior with a similar activation energy to the β relaxation. Zoomed in plots of the alpha and beta times are provided in **Supplementary Figure 3.1**.

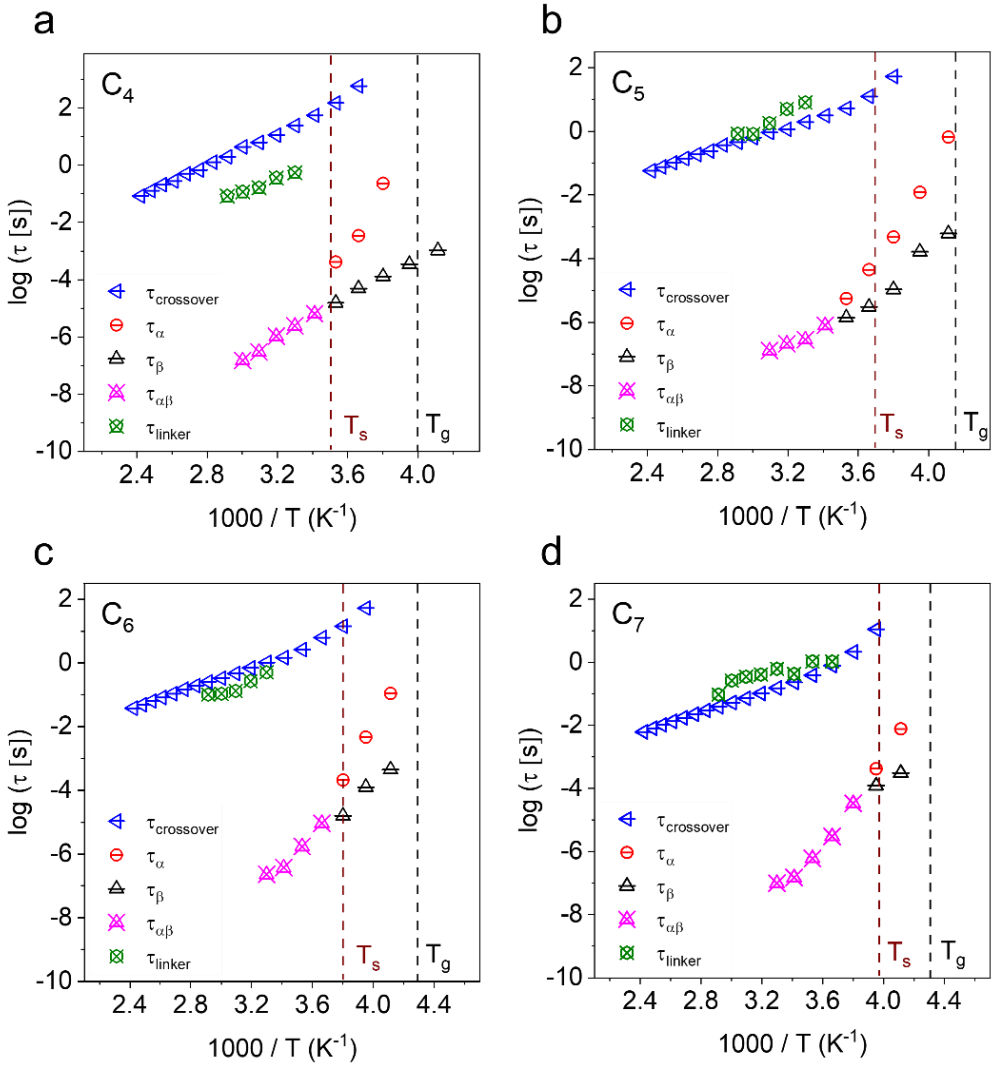

Figure 3.2. Relaxation times plotted vs inverse temperature on a semi-log plot. In all four networks, the τ_{linker} and $\tau_{crossover}$ are close in magnitude indicating a correlation between molecular-scale strand relaxation and macroscopic flow. The timescale τ_{β} shows an Arrhenius temperature dependence and merges with τ_{α} at the splitting temperature T_s, indicated by the brown vertical dasked line. The black vertical dashed line corresponds to the calorimetric $T_{g,\ DSC}$ of the networks.

To understand the lowest frequency peak in BDS, we first revisit the rheology of the ethylene dynamic networks. Oscillatory shear rheology of the networks was performed over a broad temperature window of 150 °C in 10 °C intervals following the methodology of our previous analysis of ethylene vitrimers.[16] All data appear qualitatively similar with a well-defined plateau modulus at high frequency, and a crossover frequency which is used to extract a

time scale for flow (**Figure 3.2**, blue triangles). The most common method to define a vitrimer is from the Arrhenius temperature dependence of crossover or stress relaxation times,[3, 15, 20, 25, 42, 43] and in the present system this is observed well above the T_g of each network. In the dielectric spectra, the lowest frequency peak in the 10^{-1} – 10^{1} Hz range can be observed at high temperatures. Interestingly, the relaxation time for this low-frequency peak coincides with the rheological crossover time which is assigned to the motion of linkers moving between dynamic crosslink points and called τ_{linker}. A similar low-frequency peak has been seen in numerous associating and supramolecular polymer systems, where it shows a strong coupling with mechanical relaxation.[30, 44, 45] Sokolov and coworkers attribute this relaxation to the dissociation process of the stickers in supramolecular polymers and call it the α* process. They have also observed that in certain strongly associating polymers, a normal mode relaxation is observed. The normal mode relaxation corresponds to the full chain motion (between associating groups) and thus has the longest relaxation time. In systems where both the normal mode and the α* relaxation are present, the normal mode is seen to coincide with the mechanical relaxation.[31] Thus, the bulk relaxation of the vitrimer is governed by the relaxation of the chains between boronic esters at temperatures above the upturn in crossover times. We emphasize that the ethylene vitrimers are 'associative covalent networks' and do not break or dissociate as in supramolecular studies. However, we interpret the τ_N in the present work as representing the dynamics of network strands exchanging between boronic ester junctions.

The ability to normalize the temperature dependence of the α-relaxation time of the vitrimers was examined using two measures of the glass transition temperature, one from differential scanning calorimetry (called $T_{g,\,DSC}$) and one from a dynamic criteria (called $T_{g,\,BDS}$) (alpha time of 100 sec). Both result in very good collapse of the data (**Figure 3.3**), in agreement

with what is observed in many permanent network studies where the crosslink density is generally lower and chemical crosslinks are typically random in space.[46] This non-trivial result further emphasizes that the α-process is especially well normalized by a dynamic T_g even in extremely dense networks with monodisperse strands. We note that the excellent collapse of the data may be related to the model nature of the telechelic vitrimers, where each strand is only connected at two points to the rest of the network. Similar investigations of vitrimers with many pendant dynamic crosslinks per chain are warranted to test the limits of this collapse.

In prior permanent network studies, the calorimetric T_g generally leads to poorer collapse of alpha times, and the same could be weakly argued in **Figure 3.3a**. The manner in which a dynamic T_g reflects the characteristic segmental relaxation time is more appropriate for normalizing network dynamics across different linker lengths. The dynamic fragilities of each network were calculated from the α relaxation time and range from ~70-90 (**Table 3.1**). These are typical intermediate values for many linear polymers (fragilities vary from ~40-150)[47], and indicate that the present vitrimers are fragile glass formers despite the Arrhenius viscosity dependence. However, the fragilities decrease with carbon number, typically the opposite effect found for the alpha process of homopolymer melts. On the other hand, this trend is consistent with the behavior of many homopolymer melts in the sense that a decrease of fragility is correlated with a decrease of T_g , as we find for the present vitrimers.

The crossover times from rheology were also shifted using the dynamic $T_{g,\,\mathrm{BDS}}$ and do *not* collapse, showing an apparent increase as the network crosslink density increases. The upturn from Arrhenius behavior occurs in essentially the same temperature range regardless of network once the data have been T_g-normalized. Based on crossover timescales (or viscosities), the fragility takes on a very low value of ~20 for the networks which was the initial rationale for

calling vitrimers strong glass formers. The addition of BDS data to the analysis of vitrimer dynamics reveals that the α-process is still fragile as in many linear polymers, and this is likely to be the case in most vitrimer systems.

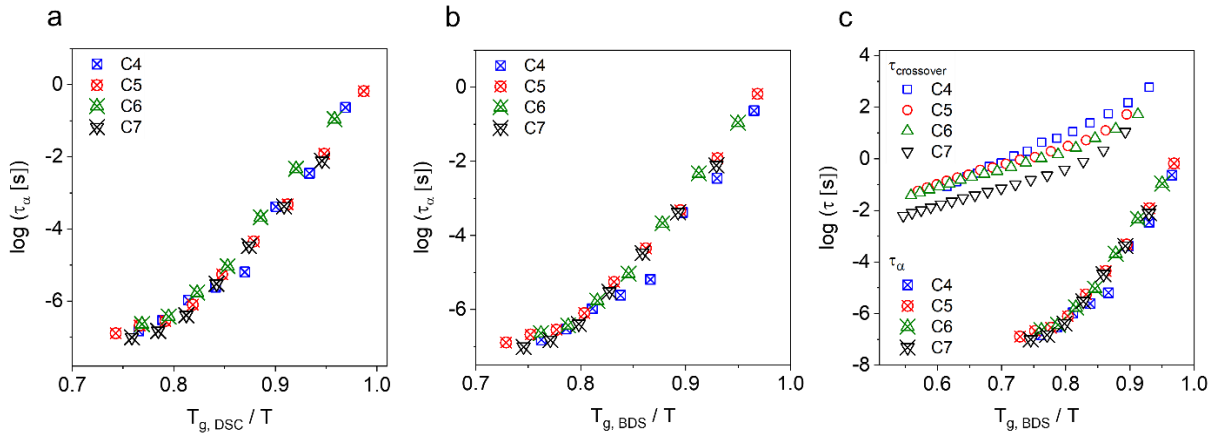

Figure 3.3. (a) The inverse temperature dependence of the α relaxation time is normalized by $T_{g, DSC}$, resulting in a reasonable collapse of the data. This is expected as the T_g is strongly coupled with the segmental dynamics. (b) Normalizing temperature by $T_{g, BDS}$ shows a better collapse of the relaxation times compared to normalization by $T_{g, DSC}$. (c) While the alpha relaxation times perfectly collapse when normalized by $T_{g, BDS}$, the crossover times clearly do not. Since macroscopic flow in vitrimers arises from an interplay of bond exchange, segmental dynamics and chain relaxation, the imperfect collapse of $\tau_{crossover}$ is expected.

Table 3.1. Glass transition temperature, activation energies and fragility of ethylene vitrimers determined from various dynamic processes.

Sample	**Glass Transition Temperatures**		**Activation Energy (kJ/mole)**		**Dynamic Fragility (m)**	
	DSC	BDS[b] (100 s)	τ_β	$\tau_{crossover}$[a]	τ_α[b]	$\tau_{crossover}$
C4	255	254	66.7	53.0	93	15.1
C5	240	236	69.4	32.8	77	25.7
C6	233	231	80.2	30.8	69	19.0
C7	230	226	90.0	29.8	73	40.9

a) Determined from high temperature data before the upturn approaching T_g
b) Determined from the VFT fit for a glass transition criterion of τ_α =100 sec using points both above and below the splitting temperature.

3.3.2. Investigating Two T_g's from Modulated Differential Scanning Calorimetry

An interesting feature of the vitrimer calorimetry is the presence of two endothermic peaks on heating (**Figure 3.4a**). The lower temperature transition is the T_g and corresponds to the alpha process observed in dielectric spectroscopy. Because the networks are made from a single polymer component and no phase separation of the linker or the boronic ester junctions is observed from wide angle X-ray scattering, it is unexpected to see two T_gs for this system. To identify the origin of the two endothermic shoulders, modulated differential scanning calorimetry (MDSC) is used to separate the reversing and non-reversing components of the heat flow. As shown in **Figures 3.4(b-e)** the first transition is identified as the traditional glass transition temperature (T_g) of the networks at -22 ℃ (C_4), -34 ℃ (C_5), -40 ℃ (C_6) and -43 ℃ (C_7). The T_g shows up as an endothermic step in the reversing heat and the enthalpic relaxation associated with physical aging shows up in the non-reversing heat flow. The second shoulder in DSC is identified as the splitting temperature (T_s) which shows an exothermic peak in the non-reversing part of the heat flow and does not show any signal in the reversing heat and is thus not a traditional glass transition. The peak temperatures of 9 ℃ (C_4), -4.5 ℃ (C_5), -10 ℃ (C_6), and -21 ℃ (C_7) are assigned as the T_s and coincide with the splitting of the $\alpha\beta$ process observed in dielectric spectroscopy. It has been previously shown that the splitting temperature can be seen in thermal spectroscopy as a change in the imaginary part of the heat capacity.[48] Future work will attempt to clarify the molecular origin of this signature, but it is reminiscent of work by Sokolov and coworkers on short, strongly phase segregating associating polymers where two T_gs have also been observed.[28]

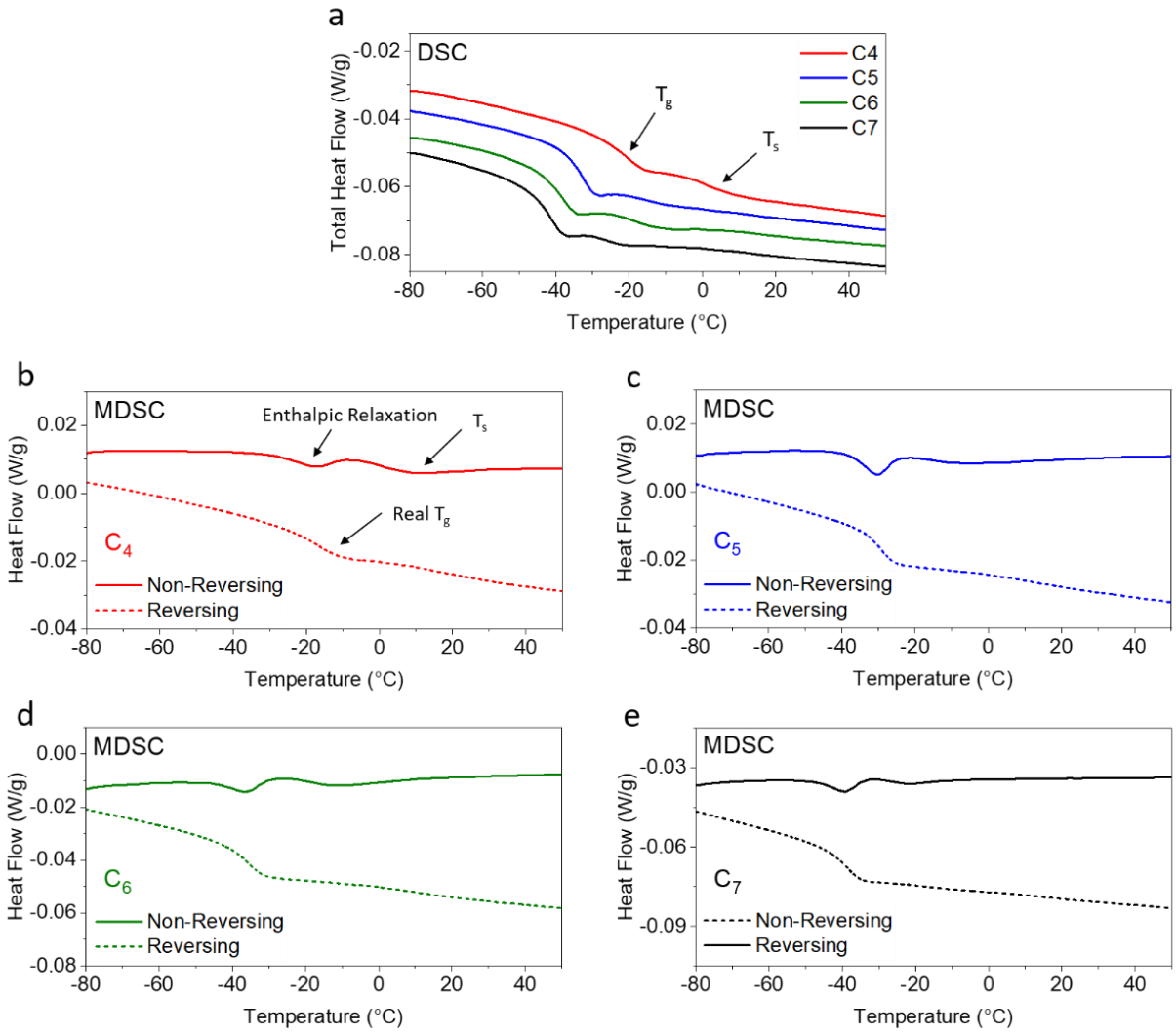

Figure 3.4. (a) Differential scanning calorimeter (DSC) of the ethylene networks show two sigmoid shoulders in the second heating cycle. The first is identified as the glass transition temperature (T_g) and the second as the splitting temperature (T_s) using modulated differential scanning calorimetry (MDSC). (b) (c) (d) (e)The T_g is seen as an endothermic shoulder in the reversing heat flow and is accompanied by an endothermic peak in the non-reversing signal. The shoulder is the glass transition while the endothermic peak corresponds to enthalpic relaxation, which is a characteristic feature of the physical aging of amorphous polymers. The T_s on the other hand is seen as an endothermic peak in the non-reversing signal and does not show a signal in the reversing heat, indicating that it is not a traditional glass transition.

3.3.3. Comparison with theory

Ghosh and Schweizer recently developed a statistical mechanical model for associating polymers that captures the interplay of the alpha relaxation with bond breaking or dissociation.[34] The basic idea is that for long lived stickers the local dynamics involves two

steps. The first faster process corresponds to the alpha relaxation of the nonsticker monomers which occurs on a timescale that associations act as permanent crosslinks which signifcantly slow down the nonsticker alpha relaxation and raises T_g, and more so as sticker concentration increases. The timescale of the slower physical bond breaking second step is related to Angstrom level chemistry of the sticker bond with a local constant activation energy for dissociation, plus an effective friction constant that impacts the bond breaking activated event timescale which includes contributions from the polymer surroundings influenced to a variable degree by the perturbed nonsticker alpha relaxation process. Since the latter is a non-Arrhenius process, the sticker bond breaking event can also acquire a non-Arrhenius form at low enough temperature. On the slower bond breaking time scale, the nonsticker segments are locally diffusive, and the relevant friction experienced by stickers is influenced by the so-called "decoupling" of relaxation and diffusion (or segmental vs chain relaxation) phenomenon that underlies the breakdown of time-temperature superposition. Embedding this physical picture phenomenologically in a dynamic model, the timescale $\tau_{\alpha*}$ for the bond breaking event was proposed as:[34]

$$\frac{\tau_{\alpha*}}{\tau_0} = \frac{\tau_\alpha}{\tau_0} + \left[\frac{\tau_{in}}{\tau_0} + \gamma\left(\frac{\tau_\alpha}{\tau_0}\right)^{\nu}\right] . e^{\left(\frac{\Delta F}{kT}\right)} \qquad \text{Equation (3.1)}$$

Here, τ_α is the average (sticker chemistry and concentration dependent) alpha relaxation time of the non-stickers, τ_0 is an elementary dynamic timescale of order 1-10 ps, and τ_{in} accounts for very local chemistry specific effects associated with the smallest scale aspects of the bonding breaking event. The second term in the square brackets reflects the frictional resistance for bond breaking due its partial viscous coupling to the segmental relaxation of the non-sticker strands. It is quantified by a numerical prefactor, γ, and a decoupling exponent, ν, less than unity. The latter is envisioned at zeroth order to be determined by the decoupling exponent for the temperature dependence of segmental and chain scale relaxation times in the analogous homopolymer melt.

Experimentally, for homopolymer melts ν ~ 0.5-1 depending on polymer chemistry and dynamic fragility. The ΔF term is the free energy cost associated with bond dissociation and consists of both enthalpic and entropic contributions.

Overall, two distinct physical issues generically arise: (i) to what extent is segmental relaxation and diffusion "decoupled", and (ii) per a chemical reaction, to what extent are the nature and amplitude of the activated local displacements of the sticker required to break an association viscously coupled with the surrounding polymer degrees of freedom that determine the structural alpha relaxation process? Eq(3.1) was confronted with an extensive set of experimental data on telechelic melts, and also some measurements on multiblock associative copolymers, for diverse sticker chemistries and a wide range of temperatures and sticker fractions, and shown to provide a unified understanding of the (often qualitative) failure of a naïve Arrhenius model, $\frac{\tau_{\alpha*}}{\tau_0} = e^{\left(\frac{\Delta F}{kT}\right)}$, and its analog based on *full* coupling of the bond breaking and alpha relaxation processes, $\frac{\tau_{\alpha*}}{\tau_\alpha(T)} = e^{\left(\frac{\Delta F}{kT}\right)}$.

With the above motivation, we consider whether similar ideas can be adapted for our vitrimer system. To minimize the number of a priori unkown parameters, we consider a more simplified model of how local friction and decoupling ideas may impact the bond exchange process. First, $\tau_{crossover}$ is identified with $\tau_{\alpha*}$ given their coincidence in **Figure 3.2**. Even without the full resolution of the linker mode in some of the dielectric spectra, these two processes close agreement within the quality of the data. The crossover has also been previously rationalized in terms of the linker diffusion between dynamic bonding sites[30, 44, 45] which further motivates our approach. Second, the timescale prefactor in an Arrhenius expression is taken to have a very local Angstrom scale component unaffected by the surrounding polymer matrix, τ_0, and a component that reflects the degree of frictional coupling of bond exchange with

the segmental dynamics of its surroundings which is quantified by a numerical factor γ and a decoupling exponent, ν. This leads to a simplified version of Eq(3.1) which we refer to as the simple friction model (SFM):

$$\tau_{crossover} = \tau_0 \left[1 + \gamma \left(\frac{\tau_\alpha}{\tau_0}\right)^{\nu}\right] . e^{\left(\frac{E_a}{kT}\right)} \quad (3.2)$$

Now, if $\gamma \sim 0$ in Eq(3.2), then the model is per a local Arrehneius process essentially unaffected by the dense polymer network. At high enough temperatures where segmental relaxation is fast, macroscopic relaxation for vitrimers is posited to be such a simple Arrhenius process controlled by bond exchange quantified by an activation energy and an elementary timescale. The effective activation energy is then a constant defined by the local chemistry of the "reacting groups" of a bond exchange. Thus, for this minimalist model the activation energy E_a can be calculated directly from the high temperature $\tau_{crossover}$ data. The second term in square brackets in Eq(2) reflects the idea that at low enough temperature the local viscosity around the reacting groups will increase enough that it provides additional frictional resistance for the bond exchange barrier crossing event. This aspect is expected to be chemistry specific, and as the vitrimer is cooled an additional temperature dependent friction emerges that slows down bond exchange and polymer strand relaxation and flow due to the steep increase in τ_α which is affected by the presence of the dynamic bonds.

A major virtue of the SFM is that it can be tested by simply cross-plotting $\log\left[\frac{(\tau_{crossover} - \tau_{crossover\_Arrhenius})}{e^{\left(\frac{E_a}{kT}\right)}}\right] vs \log\ (\tau_\alpha)$, where $\tau_{crossover\_Arrhenius} = \tau_0 . e^{\left(\frac{E_a}{kT}\right)}$ which is the extrapolation of the experimentally observed Arrhenius $\tau_{crossover}$ behavior to lower temperatures. The quantity $\tau_{crossover} - \tau_{crossover\_Arrhenius}$ is zero at high temperatures by

construction, and is relevant only when there are non-negligible deviations of $\tau_{crossover}$ from the Arrhenius trend at lower temperatures.

Figure 3.5a shows the results of our analysis. If the model linearizes the data, then at a minimum one can claim qualitative consistency between the physical ideas underlying Eq(2) and experiment. This is what we find. The slope of this plot delivers the value of ν and is reported in **Table 3.2**. An odd-even effect is seen in the decoupling parameter with $\nu \sim 0.35$ for the even carbon number networks, and a significantly higher value of 0.57 and 0.66 for the odd networks. Prior independent measurements of this decoupling parameter for pure homopolymer melts[34] find a range of ν from 0.5-1.0, with the systematic trend of smaller exponents (more decoupling) as the segmental alpha process becomes more fragile. A value of ν~0.35 is thus very low compared to all measurements of decoupling exponents on homopolymer melts, and especially low for the modest fragility values (70-90) of our vitrimer systems. This suggests that its origin is not simply generic decoupling physics in the polymer network subsystem, but rather involves chemistry specific aspects of how the bond exchange event (which has an unknown and likely complex reaction coordinate) viscously couples to the dynamics of the network carbon strands. On the other hand, for the odd carbon number networks, the decoupling exponent falls in the range relevant to homopolymer melts, but is still on the low side of what might be a priori expected for the intermediate fragility values of 70-90 of our vitrimers based on the analysis of ref.34. More broadly, the physical origin of the trends seen in **Figure 3.5a** of (i) strong odd-even effects on the frictional decoupling exponent, (ii) the near collapse of the odd carbon number data, and (iii) the strong vertical shift of the C_4 and C_6 data, is currently unknown. These features presumably reflect detailed Angstrom scale chemistry considerations associated with the

bond exchange reaction coordinate and its coupling to the network strand relaxation dynamics, and understanding them is an open challenge for the future.

As shown in **Table 3.2**, the activation energies extracted from the application of Eq(2) to the data are in good agreement with those determined from crossover times (or the dielectric linker mode), although this may not be very surprising given our formulation of the model. Nevertheless, it buttresses the view that E_a reflects a local basic chemical process with an activation barrier set at high temperature (and essentially invariant to carbon number), and the curving up of the vitrimer relaxation times at low temperatures seen in **Figure 3.2** is a consequence of the segmental friction effects and matrix strand relaxation as enhanced by the dynamic bonds. The intercept (τ_0) obtained from the straight line fit does not show any specific trend with linker length.

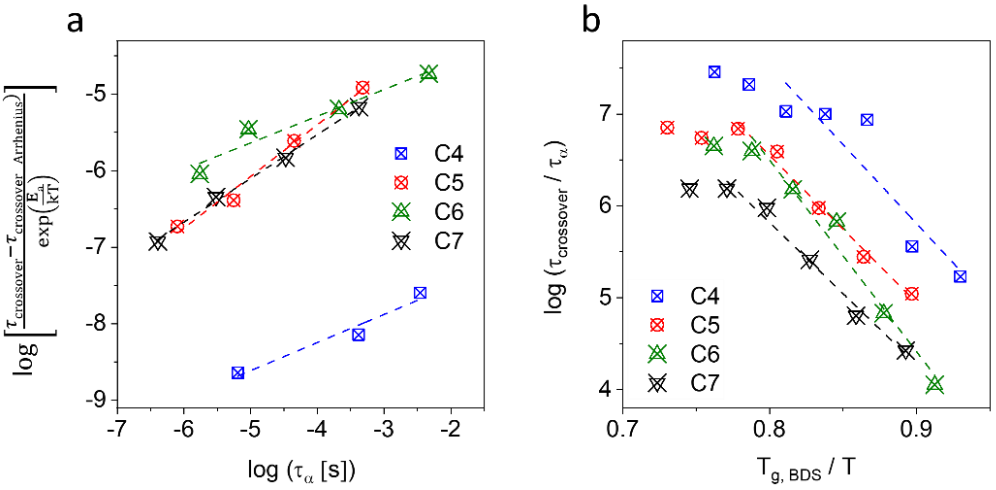

Figure 3.5. a) Log-log plot of $(\tau_{crossover} - \tau_{crossover\_Arrhenius})/e^{\left(\frac{E_a}{kT}\right)}$ vs τ_α to test the SFM of Eq (2). The straight line (power law) behavior of the data plot supports the theoretical idea that the deviation of $\tau_{crossover}$ from the Arrhenius trend is coupled with τ_α with a decoupling exponent ν. b) Log of the ratio of the crossover to α times on an Arrehnius plot which shows a strongly negative slope at lower temperatures which violates the common ansatz, $\tau_{crossover}(T) = \tau_\alpha(T).e^{\left(\frac{E_a}{kT}\right)}$, that the segmental relaxation timescale perturbed by dynamic bonds sets the elementary timescale for the slower activated bond exchange.

Table 3.2. Decoupling exponent and Arrhenius activation energy for the SFM of Eq(3.2).

Simple Friction Model		Arrhenius E_a (40°C – 140°C) calculated from $\tau_{crossover}$ (kJ/mole)
ν	τ_0 (s)	
0.36	1.7×10^{-7}	53.0
0.66	2.0×10^{-3}	32.8
0.34	1.3×10^{-4}	30.8
0.57	5.8×10^{-4}	29.8

The dielectric data was also used to analyze the ratio of the ratio of the crossover to α times following (Figure 3.5b). This ratio should have a positive slope on a log-linear Arrhenius plot if the often postulated idea (encoded in the equation $\tau_{crossover}(T) = \tau_{\alpha}(T).e^{\left(\frac{E_a}{kT}\right)}$) that the dynamic bond concentration dependent segmental relaxation time sets the time scale for bond breaking in associating copolymers[31,33,34] or bond exchange in vitrimers. For the ethylene vitrimers the ratio is almost flat at high temperatures indicating no "decoupling" of the temperature dependences of the two processes. However, upon sufficient cooling, a strongly negative slope emerges that is in qualitative disagreement with the aforementioned equation and physical picture, and indicates strong decoupling in the sense that the rheological crossover time grows much more weakly with cooling than the segmental relaxation time. A negative slope was also reported for some hydrogen bonded supramolecular networks, but not others, as analyzed by Ghosh and Schweizer.[34] Hence, in associating telechaleic melts[33,34] this behavior depends on polymer and sticker group chemistry. But even if this effect is present in associating polymer melts, it is generally a weaker deviation than we find for the present vitrimers. Thus, vitrimer dynamics driven by bond exchange appears to show a significantly different thermal behavior

than observed in associating copolymer transient networks where physical bond breaking is a dissociative process that does not dynamically conserve the effective bond density and is not as strongly decoupled from the polymer matrix structural relaxation time. Finally, we note that the data in Figure 5b where temperature is normalized by the dynamic $T_{g,\ BDS}$ does not lead to the excellent collapse observed for the α relaxation times. This again illustrates the distinct changes in bond exchange dynamics across the different sngths are not fully captured by the α process.

3.4. Conclusion

A series of precise ethylene vitrimers were synthesized and analyzed using a combination of broadband dielectric spectroscopy and rheology to access nine orders of magnitude in dynamics. The dielectrics spectra shows three distant peaks corresponding to the segmental scale α and β processes as well as a normal mode that corresponds within error to the rheological crossover time related to network strand dynamics which controls macroscopic flow. The α process of all vitrimers show intermediate values of fragility in the range of 70-90 characteristic of many fragile glass formers, despite crossover times which show an Arrhenius character (at high enough temperatures) reminiscent of strong glass formers. This illustrates the importance of probing the full range of segmental and chain level dynamics when discussing fragilities. The β process splits from the α mode at a temperature T_s which can be seen calorimetrically in the non-reversing heat flow of modulated DSC. This process is nearly Arrhenius, and displays an increasing activation energy with increasing carbon number. It is tentatively assigned to a bifurcation in dynamics between exchange events within a local cage containing multiple dynamic bonds and between different cages. The normal mode is interpreted as the time taken for the exchange of network strands between boronic ester junctions. The strong correlation between the rheological crossover time and the normal mode shows that flow is controlled by the bond exchange at high

temperatures. As the temperature is lowered, approaching the glass transition leads to positive deviations from Arrhenius behavior in the networks. Normalization of temperature by a dynamic $T_{g, BDS}$ superposes the alpha times better than normalization by the calorimteric $T_{g, DSC.}$

A recently developed model for associating polymers[34] was applied to the vitrimer system to test the physical picture of dynamics being controlled by an Arrhenius exchange process at high temperature, but with a significant deviation at lower temperatures due to the growing local friction associated with segmental dynamics which is partially coupled to the exchange process. Local free energies associated with bond exchange were deduced from the theoretical analysis which agree well with those obtained from rheological crossover times. A larger degree of decoupling (smaller ν exponents) between the bond exchange event and segmental or strand relaxation is deduced for vitrimers which is stronger compared both homopolymer and associating copolymer melts of similar fragility, especially for the odd carbon number dynamic networks. This large decoupling results in the growth of the relaxation time of processes driven by bond exchange that is much weaker than the increase of the segmental relaxation time, and generally weaker than physical bond breaking in associating polymer melts. This difference presumably reflects Angstrom scale mechanistic differences between the dissociation of a physical bond in associating copolymers versus the crosslink conserving bond exchange process in vitrimers. Understanding the precise quantitative behavior will require advances in computational chemistry and statistical mechanics based simulations. Overall, the proposed theory provides a physically clear and simple qualitative picture of the interplay between segmental and bond exchange relaxation in densely dynamic crosslinked vitrimers which can be further tested in future experimental studies of a broad range of dynamic bonds and polymer chemistries.

3.5. Experimental Details and Additional Plots

Materials: Boric acid ($B(OH)_3$, ≥ 99.5%), 1,4 butanediol (C_4, 98%), 1,5 pentanediol (C_5, 98%), 1,6 hexanediol (C_6, 98%), 1,7 heptanediol (C_7, 98%) were purchased from Sigma-Aldrich used without further purification.

Ethylene vitrimer synthesis: Carefully weighed amounts of monomer were mixed together in a glass vial with stoichiometry of 1.0 mol boric acid to 1.5 mol diol. The mixture was heated and stirred continuously overnight at 120 ˚C on a hotplate. A viscous transparent gel was obtained. The vial was then transferred to a vacuum oven, held at 60˚C overnight under vacuum to drive water off and then immediately brought into an argon glovebox maintained at < 0.5 ppm O_2 and < 0.1 ppm H_2O. No solvent was used in the synthesis.

Rheology of polymer networks: Oscillatory shear measurements were made on a TA Instruments DHR-2 rheometer using a parallel plate geometry. Samples were pressed into an 8 mm disc under ambient conditions and then loaded on to the rheometer at 40 ˚C. The dynamic networks were heated and held at 140 ˚C for 30 min to remove any water absorbed during sample loading. Sample thickness of approximately 800 - 1000 μm was used for all measurements. Frequency sweeps were conducted at isothermal temperatures from 140 ˚C to -20 ˚C at 10 ˚C intervals with an applied stress of 1000 Pa. The crossover frequency of the networks was measured as the frequency at which the loss modulus equals the storage modulus (G'' = G').

Differential Scanning Calorimetry (DSC): Samples with a mass between 3-6 mg were crimped in Tzero hermetic aluminum pans inside a glovebox. A TA Instruments DSC 25 was used to take all measurements. The glass transition temperature for each sample was measured by rapidly quenching from 150 °C to -80 °C and then heating at 20 °C/min. T_g is obtained from analysis of the heating profile using the ½ ΔC_p criterion. For measurement of the melting temperature after room temperature crystallization, samples were equilibrated to 20 °C and ramped at 20 °C /min to 120 °C. (All graphs are plotted with "endothermic down" convention.)

Modulated Differential Scanning Calorimetry (MDSC): The same samples used for DSC measurements were used for MDSC. The heat flow was modulated by a sinusoid with a period of 60 s and an amplitude of 1 K. The experiments were carried out under a nitrogen environment at a heating rate of 3 °C/min from -90 °C to 60 °C. At the beginning and end of each heating run, the samples were held at 150 °C for 1 min before being quenched to -90 °C.

Broadband Dielectric Spectroscopy (BDS): Broadband dielectric spectroscopy (BDS) was performed on a Novocontrol Concept 47 Analyzer with a PHECOS Lite temperature control system. Samples approximately 100 - 150 μm thick were sandwiched between two circular 15.5 mm stainless steel electrodes and then crimped into a coin cell. All steps of the sample preparation were performed inside the glovebox. Temperature sweeps from -30 °C to 70 °C were conducted in a frequency range of 10^{-1} Hz to 10^{6} Hz. The loss permittivity was fit to Havriliak−Negami (HN) functions in Origin software.

Small / Wide Angel Xray Scattering (SAXS): Samples were analyzed with a Xenocs GeniX3D Cu Kα X-ray source (1.54 Å) and a Pilatus 2D detector (1M pixels). The sample-to-detector distance was calibrated with silver behenate powder, and scattering patterns were collected with a 60-minute exposure. The 2D diffraction data were radially averaged using FIT2D software and the intensity was plotted as a function of scattering vector *q*. Samples were sealed between Kapton prior to being taken to the beamline.

Supplementary Table 3.1. HN fit parameters (α, γ and τ_{HN}) for different relaxation modes of the ethylene vitrimers.

Alpha Relaxation												
Sample	C4			C5			C6			C7		
Temp (C)	α	γ	□$_{HN}$	α	γ	□$_{HN}$	α	γ	□$_{HN}$	α	γ	□$_{HN}$
-30				0.41	0.93	7.9E-01	0.62	0.26	8.4E-01	0.53	0.37	4.5E-02
-20				0.56	0.78	1.8E-02	0.56	1.00	4.7E-03	0.62	0.29	2.7E-03
-10	1.00	0.34	2.3E-01	1.00	0.05	1.5E-04	0.60	1.00	2.1E-04			
0	1.00	0.02	1.1E-01	0.45	10.98	3.0E-06						
10	0.99	0.13	2.1E-02	0.75	0.39	1.7E-05						

Beta Relaxation												
Sample	C4			C5			C6			C7		
Temp (C)	α	γ	t_{HN}	α	γ	t_{HN}	α	γ	t_{HN}	α	γ	t_{HN}
-30	0.57	1.00	1.1E-03	0.68	0.36	2.3E-03	0.64	1.00	4.5E-04	0.83	1.00	3.1E-04
-20	0.61	1.00	3.4E-04	0.73	0.32	6.7E-04	0.56	1.00	3.6E-04	0.87	1.00	1.2E-04
-10	0.39	1.00	1.3E-04	0.58	1.00	4.8E-04	1.00	0.13	8.5E-05			
0	0.55	1.00	4.9E-05	0.67	1.00	4.5E-05						
10	0.46	1.00	1.5E-05	0.50	1.00	1.4E-06						

Alpha-Beta Relaxation												
Sample	C4			C5			C6			C7		
Temp (C)	α	γ	t_{HN}	α	γ	t_{HN}	α	γ	t_{HN}	α	γ	t_{HN}
-10										0.57	1.00	3.4E-05
0							0.66	0.33	4.2E-05	0.58	1.00	5.8E-06
10							0.66	0.38	6.7E-06	0.50	1.00	4.2E-07
20	0.55	1.00	6.4E-06	0.69	0.37	3.0E-06	0.64	0.43	1.3E-06	0.55	1.00	1.5E-07
30	0.54	1.00	2.4E-06	0.65	0.83	2.8E-07	0.68	1.00	2.3E-07	0.61	1.00	9.3E-08
40	0.64	1.00	1.1E-06	0.76	0.86	2.5E-07						
50	0.62	1.00	3.0E-07	0.79	1.00	1.3E-07						
60	0.66	1.00	1.5E-07									

Supplementary Table 3.1. (Continued)

Linker Mode Relaxation												
Sample	C4			C5			C6			C7		
Temp (C)	α	γ	t_{HN}	α	γ	t_{HN}	α	γ	t_{HN}	α	γ	t_{HN}
0										0.62	1.00	1.0E+00
10										0.49	1.00	1.1E+00
20										0.53	1.00	4.2E-01
30	0.65	1.00	7.4E-05	0.28	1.00	8.1E+00	0.57	0.87	1.0E+00	0.47	1.00	6.2E-01
40	0.64	1.00	3.6E-01	0.28	1.00	5.2E+00	0.50	0.95	5.5E-01	0.47	1.00	4.1E-01
50	0.63	1.00	1.6E-01	0.21	1.00	1.8E+00	0.49	0.99	2.4E-01	0.47	1.00	3.5E-01
60	0.60	1.00	1.2E-01	0.26	1.00	8.2E-01	0.46	1.00	1.1E-01	0.45	1.00	2.6E-01
70	0.56	1.00	8.3E-02	0.27	1.00	8.4E-01	0.43	1.00	1.0E-01	0.46	1.00	9.5E-02

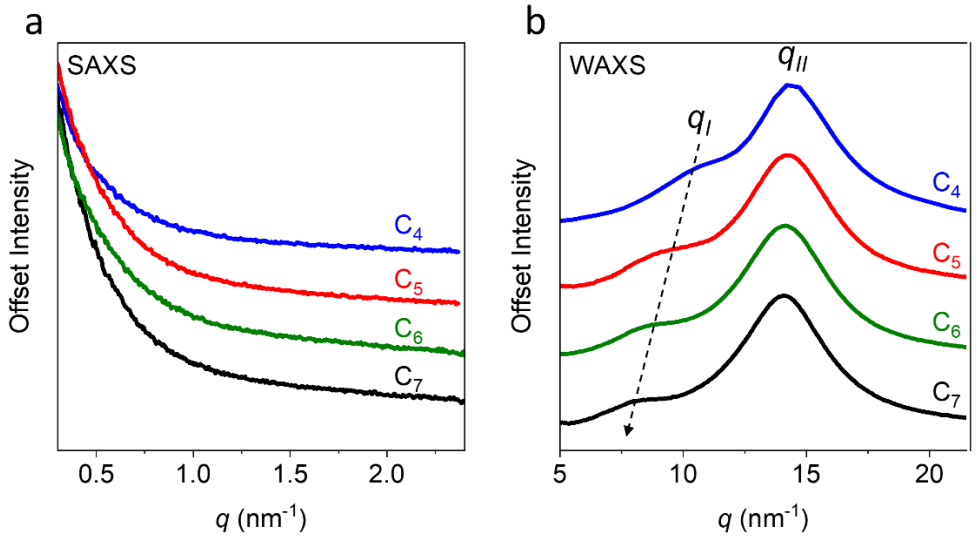

Supplementary Figure 3.1. (a) Small angle x-ray scattering shows to no prominent features indicating the absence of any self-assembly or macroscopic phase separation of the ethylene monomers or boronic crosslinkers. (b) The low q peak (q_I) is attributed to boron-boron correlations which increase in d spacing with increasing linker length, while peak q_{II} is the amorphous halo.

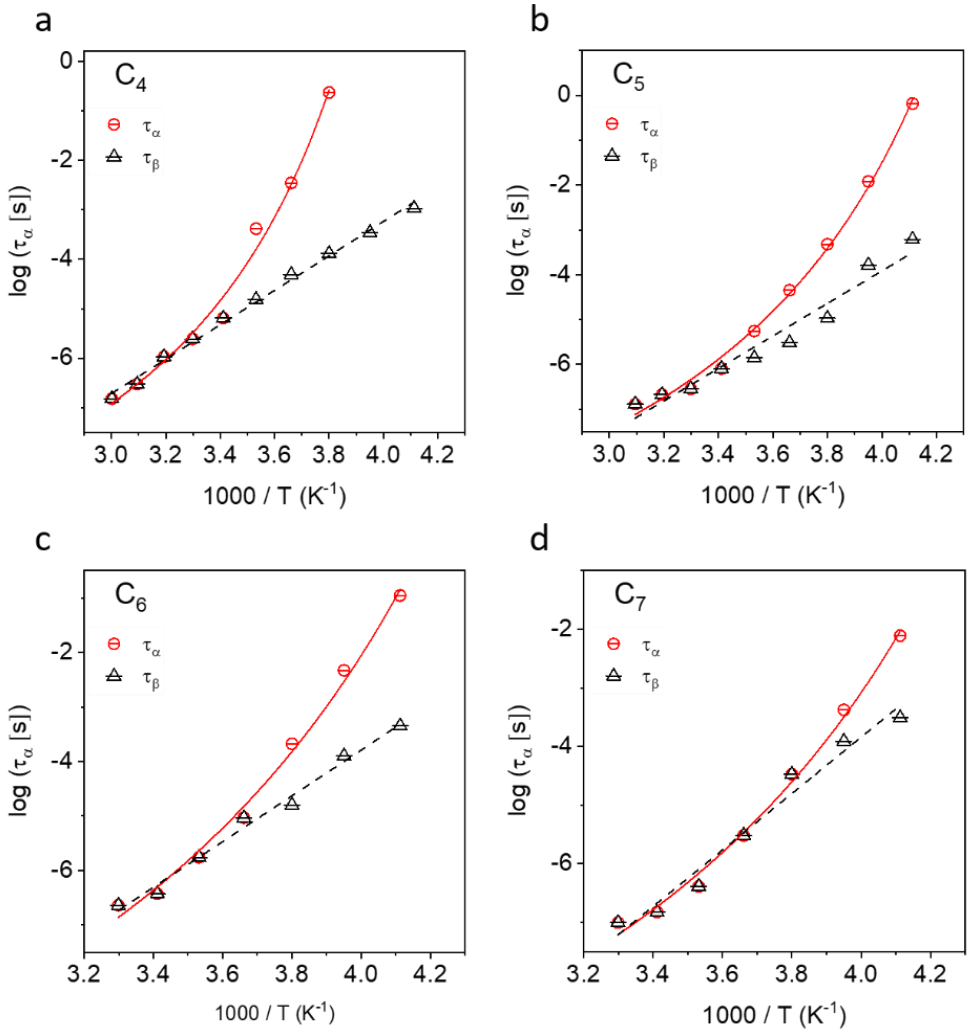

Supplementary Figure 3.2. (a), (b), (c), (d) A zoomed-in graph of the α and β relaxation. At temperature above T_s, α and β relaxation merge to give the αβ relaxation which follows the same Arrhenius trend as the low-temperature β relaxation, with an activation energy of 66.7 kJ/mole, 69.4 kJ/mole, 80.2 kJ/mole, 90.0 kJ/mole, for C_4 to C_7 respectively. Below T_s, the α relaxation splits and follows the VFT trend.

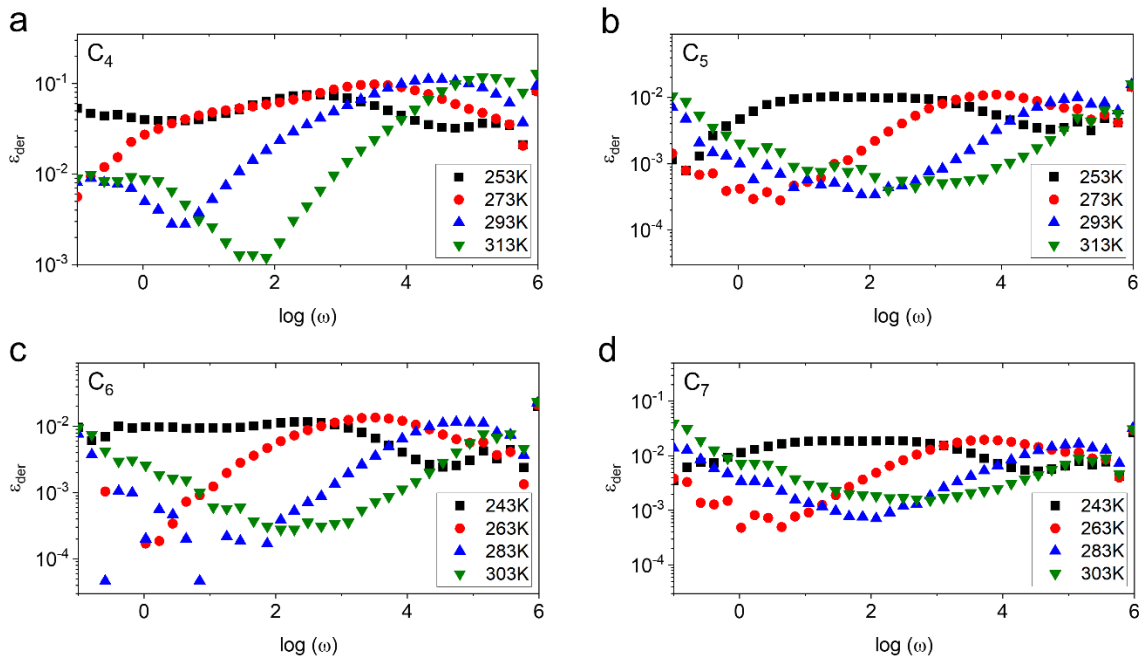

Supplementary Figure 3.2. (a) Derivative analysis of the ε'. The derivative (ε_{der}) is calculated using equation S3.1.

$$\varepsilon_{der}(\omega) = \frac{-2}{\pi}\frac{\partial \varepsilon'(\omega)}{\partial log(\omega)} \quad \text{(S3.1)}$$

3.6. References

1. Luo, J.; Demchuk, Z.; Zhao, X.; Saito, T.; Tian, M.; Sokolov, A. P.; Cao, P.-F., Elastic vitrimers: Beyond thermoplastic and thermoset elastomers. *Matter* **2022,** *5* (5), 1391-1422.

2. Porath, L.; Soman, B.; Jing, B. B.; Evans, C. M., Vitrimers: Using Dynamic Associative Bonds to Control Viscoelasticity, Assembly, and Functionality in Polymer Networks. *ACS Macro Letters* **2022,** *11* (4), 475-483.

3. Denissen, W.; Winne, J. M.; Du Prez, F. E., Vitrimers: permanent organic networks with glass-like fluidity. *Chemical science* **2016,** *7* (1), 30-38.

4. Brutman, J. P.; Delgado, P. A.; Hillmyer, M. A., Polylactide vitrimers. *ACS Macro letters* **2014,** *3* (7), 607-610.

5. Röttger, M.; Domenech, T.; van der Weegen, R.; Breuillac, A.; Nicolaÿ, R.; Leibler, L., High-performance vitrimers from commodity thermoplastics through dioxaborolane metathesis. *Science* **2017,** *356* (6333), 62-65.

6. Montarnal, D.; Capelot, M.; Tournilhac, F.; Leibler, L., Silica-like malleable materials from permanent organic networks. *Science* **2011,** *334* (6058), 965-968.

7. Van Lijsebetten, F.; De Bruycker, K.; Spiesschaert, Y.; Winne, J. M.; Du Prez, F. E., Suppressing Creep and Promoting Fast Reprocessing of Vitrimers with Reversibly Trapped Amines. *Angewandte Chemie International Edition* **2022,** *61* (9), e202113872.

8. Li, L.; Chen, X.; Jin, K.; Torkelson, J. M., Vitrimers designed both to strongly suppress creep and to recover original cross-link density after reprocessing: Quantitative theory and experiments. *Macromolecules* **2018,** *51* (15), 5537-5546.

9. Guerre, M.; Taplan, C.; Winne, J. M.; Du Prez, F. E., Vitrimers: directing chemical reactivity to control material properties. *Chemical science* **2020,** *11* (19), 4855-4870.

10. Van Zee, N. J.; Nicolaÿ, R., Vitrimer Chemistry and Applications. *Macromolecular Engineering: From Precise Synthesis to Macroscopic Materials and Applications* **2022**, 1-38.

11. Krishnakumar, B.; Sanka, R. P.; Binder, W. H.; Parthasarthy, V.; Rana, S.; Karak, N., Vitrimers: Associative dynamic covalent adaptive networks in thermoset polymers. *Chemical Engineering Journal* **2020,** *385*, 123820.

12. Wang, M.; Gao, H.; Wang, Z.; Mao, Y.; Yang, J.; Wu, B.; Jin, L.; Zhang, C.; Xia, Y.; Zhang, K., Rapid self-healed vitrimers via tailored hydroxyl esters and disulfide bonds. *Polymer* **2022,** *248*, 124801.

13. Li, H.; Zhang, B.; Wang, R.; Yang, X.; He, X.; Ye, H.; Cheng, J.; Yuan, C.; Zhang, Y. F.; Ge, Q., Solvent-Free Upcycling Vitrimers through Digital Light Processing-Based 3D Printing and Bond Exchange Reaction. *Advanced Functional Materials* **2022**, 2111030.

14. Lucherelli, M. A.; Duval, A.; Avérous, L., Biobased vitrimers: towards sustainable and adaptable performing polymer materials. *Progress in Polymer Science* **2022**, 101515.

15. Porath, L. E.; Evans, C. M., Importance of broad temperature windows and multiple rheological approaches for probing viscoelasticity and entropic elasticity in vitrimers. *Macromolecules* **2021,** *54* (10), 4782-4791.

16. Soman, B.; Evans, C. M., Effect of precise linker length, bond density, and broad temperature window on the rheological properties of ethylene vitrimers. *Soft Matter* **2021,** *17* (13), 3569-3577.

17. Soman, B.; Go, Y. K.; Shen, C.; Leal, C.; Evans, C. M., Impact of dynamic covalent chemistry and precise linker length on crystallization kinetics and morphology in ethylene vitrimers. *Soft Matter* **2022,** *18* (2), 293-303.

18. Ricarte, R. G.; Tournilhac, F.; Leibler, L., Phase separation and self-assembly in vitrimers: Hierarchical morphology of molten and semicrystalline polyethylene/dioxaborolane maleimide systems. *Macromolecules* **2018,** *52* (2), 432-443.

19. Lessard, J. J.; Scheutz, G. M.; Sung, S. H.; Lantz, K. A.; Epps III, T. H.; Sumerlin, B. S., Block copolymer vitrimers. *Journal of the American Chemical Society* **2019,** *142* (1), 283-289.

20. Jing, B. B.; Evans, C. M., Catalyst-free dynamic networks for recyclable, self-healing solid polymer electrolytes. *Journal of the American Chemical Society* **2019,** *141* (48), 18932-18937.

21. Ma, J.; Porath, L. E.; Haque, M. F.; Sett, S.; Rabbi, K. F.; Nam, S.; Miljkovic, N.; Evans, C. M., Ultra-thin self-healing vitrimer coatings for durable hydrophobicity. *Nature communications* **2021,** *12* (1), 1-10.

22. Debnath, S.; Tiwary, S. K.; Ojha, U., Dynamic carboxylate linkage based reprocessable and self-healable segmented polyurethane vitrimers displaying creep resistance behavior and triple shape memory ability. *ACS Applied Polymer Materials* **2021,** *3* (4), 2166-2177.

23. Chen, F.; Cheng, Q.; Gao, F.; Zhong, J.; Shen, L.; Lin, C.; Lin, Y., The effect of latent plasticity on the shape recovery of a shape memory vitrimer. *European Polymer Journal* **2021,** *147*, 110304.

24. Moreno, A.; Morsali, M.; Sipponen, M. H., Catalyst-Free Synthesis of Lignin Vitrimers with Tunable Mechanical Properties: Circular Polymers and Recoverable Adhesives. *ACS applied materials & interfaces* **2021,** *13* (48), 57952-57961.

25. Tretbar, C. A.; Neal, J. A.; Guan, Z., Direct silyl ether metathesis for vitrimers with exceptional thermal stability. *Journal of the American Chemical Society* **2019,** *141* (42), 16595-16599.

26. Cromwell, O. R.; Chung, J.; Guan, Z., Malleable and self-healing covalent polymer networks through tunable dynamic boronic ester bonds. *Journal of the American Chemical Society* **2015,** *137* (20), 6492-6495.

27. Roettger, M. Associative exchange reactions of boron or nitrogen containing bonds and design of vitrimers. Paris 6, 2016.

28. Xing, K.; Tress, M.; Cao, P.; Cheng, S.; Saito, T.; Novikov, V. N.; Sokolov, A. P., Hydrogen-bond strength changes network dynamics in associating telechelic PDMS. *Soft Matter* **2018,** *14* (7), 1235-1246.

29. Ge, S.; Samanta, S.; Li, B.; Carden, G. P.; Cao, P.-F.; Sokolov, A. P., Unravelling the Mechanism of Viscoelasticity in Polymers with Phase-Separated Dynamic Bonds. *ACS nano* **2022,** *16* (3), 4746-4755.

30. Xing, K.; Tress, M.; Cao, P.-F.; Fan, F.; Cheng, S.; Saito, T.; Sokolov, A. P., The role of chain-end association lifetime in segmental and chain dynamics of telechelic polymers. *Macromolecules* **2018,** *51* (21), 8561-8573.

31. Ge, S.; Tress, M.; Xing, K.; Cao, P.-F.; Saito, T.; Sokolov, A. P., Viscoelasticity in associating oligomers and polymers: experimental test of the bond lifetime renormalization model. *Soft Matter* **2020,** *16* (2), 390-401.

32. Ge, S.; Samanta, S.; Tress, M.; Li, B.; Xing, K.; Dieudonné-George, P.; Genix, A.-C.; Cao, P.-F.; Dadmun, M.; Sokolov, A. P., Critical role of the interfacial layer in associating polymers with microphase separation. *Macromolecules* **2021,** *54* (9), 4246-4256.

33. Ghosh, A.; Samanta, S.; Ge, S.; Sokolov, A. P.; Schweizer, K. S., Influence of Attractive Functional Groups on the Segmental Dynamics and Glass Transition in Associating Polymers. *Macromolecules* **2022,** *55* (6), 2345-2357.

34. Ghosh, A.; Schweizer, K. S., Physical bond breaking in associating copolymer liquids. *ACS Macro Letters* **2020,** *10* (1), 122-128.

35. Ghosh, A.; Schweizer, K. S., Microscopic Theory of the Effect of Caging and Physical Bonding on Segmental Relaxation in Associating Copolymer Liquids. *Macromolecules* **2020,** *53* (11), 4366-4380.

36. Berticat, P.; Ai, B.; Giam, H. T.; Chatain, D.; Lacabanne, C., Depolarization thermocurrent and dielectric study in polyethylene. *Die Makromolekulare Chemie: Macromolecular Chemistry and Physics* **1976,** *177* (5), 1583-1596.

37. Graff, M. S.; Boyd, R. H., A dielectric study of molecular relaxation in linear polyethylene. *Polymer* **1994,** *35* (9), 1797-1801.

38. Mattice, W. L.; Helfer, C. A.; Sokolov, A. P., On the Relationship between the Characteristic Ratio of a Finite Chain, C n, and the Asymptotic Limit, C∞. *Macromolecules* **2003,** *36* (26), 9924-9928.

39. Garwe, F.; Schönhals, A.; Lockwenz, H.; Beiner, M.; Schröter, K.; Donth, E., Influence of cooperative α dynamics on local β relaxation during the development of the dynamic glass transition in poly (n-alkyl methacrylate) s. *Macromolecules* **1996,** *29* (1), 247-253.

40. Kahle, S.; Korus, J.; Hempel, E.; Unger, R.; Höring, S.; Schröter, K.; Donth, E., Glass-transition cooperativity onset in a series of random copolymers poly (n-butyl methacrylate-stat-styrene). *Macromolecules* **1997,** *30* (23), 7214-7223.

41. Rault, J., Origin of the Vogel–Fulcher–Tammann law in glass-forming materials: the α–β bifurcation. *Journal of Non-Crystalline Solids* **2000,** *271* (3), 177-217.

42. Taplan, C.; Guerre, M.; Winne, J. M.; Du Prez, F. E., Fast processing of highly crosslinked, low-viscosity vitrimers. *Materials Horizons* **2020,** *7* (1), 104-110.

43. Ricarte, R. G.; Tournilhac, F.; Cloître, M.; Leibler, L., Linear viscoelasticity and flow of self-assembled vitrimers: the case of a polyethylene/dioxaborolane system. *Macromolecules* **2020,** *53* (5), 1852-1866.

44. Lou, N.; Wang, Y.; Li, X.; Li, H.; Wang, P.; Wesdemiotis, C.; Sokolov, A. P.; Xiong, H., Dielectric relaxation and rheological behavior of supramolecular polymeric liquid. *Macromolecules* **2013,** *46* (8), 3160-3166.

45. Tress, M.; Xing, K.; Ge, S.; Cao, P.; Saito, T.; Sokolov, A., What dielectric spectroscopy can tell us about supramolecular networks⋆. *The European Physical Journal E* **2019,** *42* (10), 1-12.

46. Mei, B.; Lin, T.-W.; Sheridan, G. S.; Evans, C. M.; Sing, C. E.; Schweizer, K. S., Structural Relaxation and Vitrification in Dense Cross-Linked Polymer Networks: Simulation, Theory, and Experiment. *Macromolecules* **2022**.

47. Qin, Q.; McKenna, G. B., Correlation between dynamic fragility and glass transition temperature for different classes of glass forming liquids. *Journal of Non-Crystalline Solids* **2006,** *352* (28-29), 2977-2985.

48. Beiner, M.; Kahle, S.; Hempel, E.; Schröter, K.; Donth, E., Two calorimetrically distinct parts of the dynamic glass transition. *EPL (Europhysics Letters)* **1998,** *44* (3), 321.

CHAPTER 4: IMPACT OF DYNAMIC COVALENT CHEMISTRY AND PRECISE LINKER LENGTH ON CRYSTALLIZATION KINETICS AND MORPHOLOGY IN ETHYLENE VITRIMERS

4.1. Abstract

Precise ethylene vitrimers with 8, 10, or 12 methylene units between boronic ester junctions were investigated to understand the impact of bond exchange on crystallization kinetics and morphology. Compared to linear polyethylene which has been heavily investigated for decades, a long induction period for crystallization is seen in the vitrimers ultimately taking weeks in the densest networks. An increase in melting temperatures (T_m) of 25-30 K is observed with isothermal crystallization over 30 days. Both C_{10} and C_{12} networks initially form hexagonal crystals, while the C_{10} network transforms to orthorhombic over the 30 day window as observed with wide angle X-ray scattering (WAXS) and optical microscopy (OM). After 150 days of isothermal crystallization, the three linker lengths led to double diamond (C_8), orthorhombic (C_{10}), and hexagonal (C_{12}) crystals indicating the importance of precision on final morphology. Control experiments on a precise, permanent network implicate dynamic bonds as the cause of long-time rearrangements of the crystals, which is critical to understand for applications of semi-crystalline vitrimers. The dynamic bonds also allow the networks to dissolve in water and alcohol-based solvents to monomer, followed by repolymerization while preserving the mechanical properties and melting temperatures.

4.2. Introduction.

The development of sustainable and recyclable plastics is a major challenge to handle the massive volume of products that end up in landfills.[1] Polymer networks, either elastomers or

thermosets, are not processesable with traditional chemistries but can be made recyclable via the incorporation of dynamic covalent bonds into the polymer. Notably, Leibler and coworkers described dynamic polyester networks which exhibit glass-like processability due to conserved ester exchange reactions, now commonly called vitrimers.[2-5] This concept has been widely applied to a range of dynamic bonds including esters,[6-8] boronic esters/boroxine,[9-18] urethanes,[19] vinylogous urethanes,[20-23] oxime-esters,[24, 25] olefin metathesis,[2, 26] triazolium transalkylation,[27] silyl ether metathesis[28-30] and Meldrum's acid.[31, 32] This ever growing toolbox of dynamic covalent bonds which conserve the network topology is described in recent review articles.[33, 34] A major focus thus far has been to understand how the exchange kinetics, crosslink density, and polymer backbone chemistry control the stress relaxation and reprocessability of vitrimers. The glass transition temperature (T_g) and a hypothetical topology freezing temperature (T_v) have been discussed to understand the interplay with bond exchange processes which governs the temperature dependent viscoelasticity. In contrast, an understanding of crystallization phenomena and melting temperatures (T_m) in vitrimers is currently lacking. Dynamic bonds provide a mechanism for chain rearrangements within a polymer network, as well as a new timescale which can potentially facilitate crystal perfection and growth. Knowledge of how dynamic bonds impact crystallization kinetics and morphology will be critical to the development of new polymers which are easier to recycle and reprocess while still retaining desirable physical and optical properties.

The crystallinity of commodity polymers such as polyethylene (PE) and polypropylene is key to their electrical breakdown strength,[35] mechanical properties,[36-38] and thermal conductivity.[39] Electron[40, 41] and ion[42-44] conducting functional polymers also show performance which is critically related to the crystal structure and amorphous fraction. In all

cases, processing conditions can lead to vastly different material properties depending on the timescales of material relaxation and rate of deformation during pressing or extrusion. With the introduction of dynamic bonds in a network, an additional timescale is generated which may facilitate crystal formation by allowing smaller strands to rearrange rather than an entire polymer chain. An understanding of how bond exchange affects kinetics and final morphology is currently lacking. While some prior work has focused on semi-crystalline vitrimers based on polyethylene,[12-14, 16, 30, 45, 46] and poly(lactic acid),[47] they did not investigate any temporal evolution of crystallinity or morphology due to dynamic bond rearrangements within the matrix.

Another key factor in determining crystal structure and melting is the presence of precise motifs. Here the term precise refers to the exact number of carbons in the spacer following prior work on "precise" polymers.[48, 49] For example, the melting temperatures of telechelic alkanes show a pronounced odd-even effect depending on the number of carbons between functional groups.[50-52] In polymers, precise polyethylenes [53] and polyacetals[54] have been made as linear polymers, including materials with periodic ionic groups which crystallize and show enhanced conductivity.[55, 56] Precise permanent networks with alkane chain linkers have shown odd-even effects on the glass transition temperature and ionic conductivity.[57] All of these studies point to the potentially critical role of precision on crystallization, which has not been investigated in vitrimers. In addition to being important from an application point of view, understanding the fundamental roles of precision and dynamic bond exchange on semi-crystalline polymers could provide new insights into the design and application of such materials.

Here, we report the synthesis and systematic investigation of ethylene vitrimers with precise carbon spacing between dynamic boronic ester crosslinks. Boronic esters are a popular dynamic bond because of the relative easy by which they can be incorporated into conventional polymers. In addition, boronic esters tend to be a fast exchanging bond, even at ambient temperatures and without catalyst. This allows us to observe the effects of dynamic bond exchanges on relatively short time scales and moderate temperatures. This model vitrimer was chosen because linear PE has been widely studied and the crystal structure evolution is well known.[58, 59] The initial crystallization of vitrimers is inhibited due to the network architecture, and long time crystallization studies indicate that T_m grows continually over 30 days. An unexpected crystal-crystal phase transition is also observed via X-ray scattering, and is further tracked via polarized optical microscopy. This morphological transition, as well as the long time evolution of T_m, is not present in linear PE and a precise, permanent ethylene network shows no crystallization even after 1 week, implicating dynamic bonds as the origin of this phenomena. This is an extension of our previous work on the rheological investigation of ethylene vitrimers in the amorphous state.[18]

4.3. Results and Discussion

4.3.1. Crystallization of Ethylene Vitrimers and Evolution in Melting Temperature

Differential scanning calorimetry (DSC) was performed using a rapid quench from 150 to -80 °C, and only a glass transition is observed in C_8 and C_{10} networks on the cooling curve while C_{12} shows a weak crystallization peak. In contrast, a linear PE standard crystallizes instantly (**Supplementary Fig 4.1b** and **4.1c**).

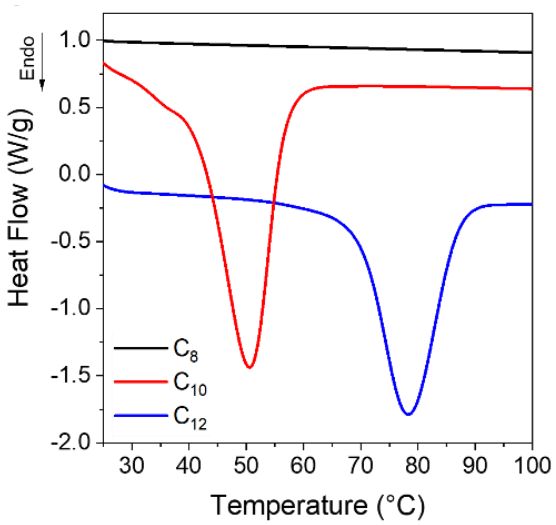

Figure 4.1. After 1-day of isothermal crystallization at room temperature, C_{10} and C_{12} show clear melting peaks whereas C_8 still has no melting transition.

The networks are termed vitrimers due to the well-known conserved exchange reaction of boronic esters in small molecules[62] and polymers.[9-17] In our prior work, oscillatory shear rheology was used to probe the storage (G') and loss (G'') modulus of the ethylene networks in their fully amorphous state to determine the characteristic timescale for flow. Frequency sweeps were performed in 10 °C intervals from 140 - 40 °C with networks showing rubbery behavior at higher frequencies and terminal relaxation at lower frequencies (**Supplementary Fig 4.1d**) due to dynamic bond exchange. As expected, the modulus tracks with crosslink density/linker length. For a constant crosslink density, the modulus should increase with temperature due to entropic elasticity,[63] which is observed in the ethylene networks supporting the presence of topology conserving exchange reactions (**Fig 4.2a**). We have previously observed that denser networks have longer relaxation times and slightly higher activation energies which is a function of both bond exchange kinetics and also the ability of dynamic bonds to find each other. A detailed discuss on the trend of the relaxation time vs the crosslink density can be found in our previous report.[18] The viscosity was calculated from the slope of G'' vs ω in the low frequency limit

and plotted against inverse temperature, which showed the anticipated Arrhenius behavior (**Fig 4.2b**). This method of zero-shear viscosity determination has been compared to the complex viscosity and gives the same values and temperature dependent trends.[18] All of these measurements are consistent with a network held together by associative dynamic covalent bonds.

The thermal transitions of the networks were next investigated using DSC by first rapidly quenching from 150 °C to -80 °C, followed by heating at 20 °C/min. The glass transition temperatures (T_g) of the networks increases monotonically from -43 °C (C_8) to -41 °C (C_{10}) to -32 °C (C_{12}) (**Fig 4.2c**), and are all well below room temperature making the networks soft and malleable prior to subsequent annealing and crystallization. This T_g trend is attributed to the presence of crystallites in the C_{12} network which can hinder mobility of the network and raise T_g. Crystallization is observed in C_{12} networks on the cooling curve (**Supplementary Fig 4.1b**), indicating that crystals will be present on first heating. Conversely, the C_8 network shows no initial crystallinity while the C_{10} and C_{12} networks have a small melting transition at 25-35 °C. A separate batch of samples was prepared and quenched directly to room temperature from 150 °C. In the C_8 network, no melting was observed on the initial heating ramp (**Supplementary Fig 4.2**) while C_{10} and C_{12} gradually develop a melting peak at room temperature over 300 min. After 1 day of isothermal crystallization at room temperature, both C_{10} and C_{12} networks show a clear melting transition with larger enthalpy and shifted to higher temperature relative to the samples directly quenched to -80 °C, whereas the C_8 vitrimer remains amorphous (**Fig 4.2d**). We attribute the latter result to the fact that this vitrimer has the highest crosslink density, which inhibits the ability of linkers to pack, as well as the highest viscosity which reduces translational mobility of network strands.

The melting transitions of C_{10} and C_{12} vitrimers were monitored with DSC as a function of isothermal crystallization time at room temperature over 30 days, and a monotonic increase in the peak melting temperature (T_m) of the networks was observed (**Fig 4.3a and 4.3b**). The C_{10} network shows a melting peak splitting around 10080 min, which eventually coalesces after 43200 min. In contrast, C_{12} vitrimers only show one peak for the entire series. Optical microscopy, to be discussed in detail subsequently, shows the growth of dendritic structures which appear only in the C_{10} networks and are assigned as the cause of peak splitting. A sigmoidal curve is typically seen for processes governed by a nucleation and growth mechanism,[64, 65] which is observed in the C_{12} networks when plotting the peak melting temperatures over 43200 min (**Fig 4.3c**). The C_{10} network has not yet plateaued even after ~10^4 min. In both cases, there is an initial induction period where T_m is flat, followed by an upturn at 100 and 1000 min for the C_{10} and C_{12} networks, respectively. The slow crystallization kinetics in C_{10} as compared to C_{12} can be rationalized because T_m is lower for C_{10} networks, thus they have a smaller thermodynamic driving force for crystallization. Additionally, a higher crosslink density in C_{10} vitrimers means that the system is more frustrated which would also impede crystallization and T_m evolution.

Over the observed period of 43200 min a ΔT_m of 25 °C for C_{12} and 30 °C for C_{10} is observed. An increase in the enthalpy of melting (and thus crystallinity) accompanies the T_m evolution, and nearly doubles for the C_{12} network (**Supplementary Fig 4.3a**). The C_{10} network shows an ~70% increase in enthalpy over the same time period. Here we only report the relative change in crystallinity and not the absolute crystallinity, as there is no reference polymer and thereby no reference enthalpy to normalize by. PE, would have been our first choice, but since we do not know the impact that periodic placement of boronic crosslinks would have on the

enthalpy of polyethylene, we did not use it's enthalpy as a reference. Ethylene vitrimer crystals undergo a polymorphic transition, discussed later, which makes an absolute degree of crystallization determination difficult. After 150 days, the T_m reaches 82 °C and 91 °C for the C_{10} and C_{12} networks, respectively (**Supplementary Fig 4.3b**). We also performed FTIR to determine if the alkane diols were being driven out of the networks due to the crystallization, and there are no free OH groups within the resolution of the instrument (**Supplementary Fig 4.3d**). Thus, we conclude that the boronic esters are incorporated into the vitrimers crystals.

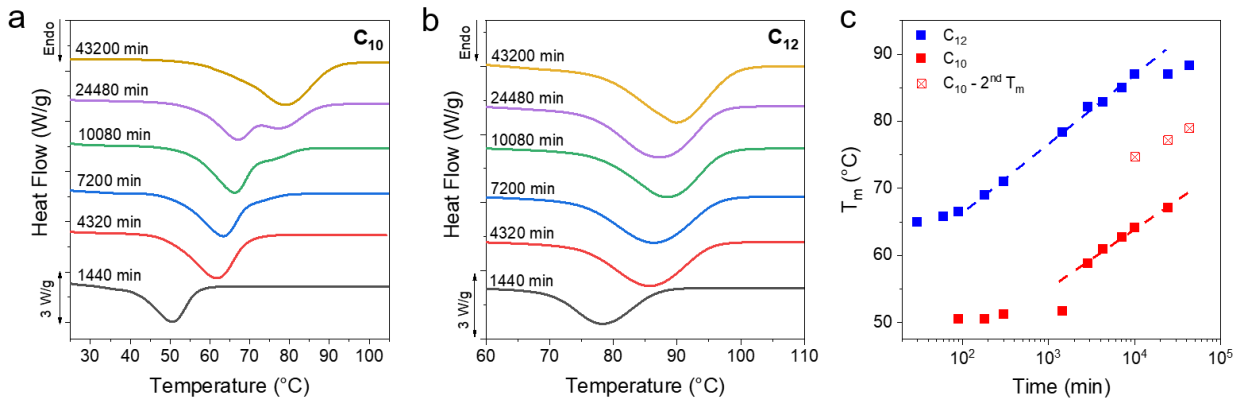

Figure 4.2. (a, b) DSC of C_{10} and C_{12} after long time crystallization at room temperature. A monotonic increase in the T_m is evident from the rightward shift of the melting curve. DSC data for less than 1 day of crystallization time can be found in **Supplementary Fig 4.2**. (c) A plot of T_m vs time shows similar slopes for the two networks. The 7, 17 and 30 day samples of C_{10} show two melting peaks, the lower one shown as solid squares and the higher peak as crossed squares.

The apparent power law dependence of T_m at intermediate times was fit to the equation $T_m(t_A) = T_0 + Dlog(t_A/t_0)$ used in prior work where t_A is annealing time and t_0 is the initial time.[66] The D values were 10.3 and 8.8 for C_{12} and C_{10} networks using only data beyond 180 and 1440 min, respectively. This is in the same range as reported for crystallization of PET at 220 °C where D varies from 7.8-12 depending on the precise processing condition.[66] The similarity in the D values is a mere coincidence as there is no reason to expect an agreement between vitrimers and linear PET. More analysis is required for a detailed molecular explanation, but we presently assign the slow evolution and emergence of crystals to dynamic

bond facilitated reorganization of strands in the amorphous region into the crystalline phase. Two key control experiments were performed, the first on linear PE (SRM 1475, 52,000 g/mol) which shows instantaneous crystallization and no substantial long-term T_m evolution (**Supplementary Fig 4.1c**). This is expected as PE exhibits fast crystallization kinetics, and T_m evolution has only been observed using flash differential scanning calorimetry with time resolution as fast as 10^{-4} s.[67] The second control involved the synthesis of a precise, permanent ethylene network with C_{10} linkers as described in the Supporting Information (**Supplementary Fig 4.4**). In the absence of dynamic bonds, this network does not crystallize even after a week while the dynamic analogue shows crystallization within the first day (**Supplementary Fig 4.5a**). A linear C_{10} polymer with the same amide linkages was also synthesized which crystallizes immediately upon cooling and indicates that the network topology, not the specific junction chemistry, are preventing crystallization (**Supplementary Fig 4.5b**). Thus, the presence of dynamic bonds is critical to the melting temperature evolution in semi-crystalline vitrimers.

The long time evolution of T_m is atypical for polymer crystals. Increases in properties like T_m, density and lamellar thickness have been previously reported for polyethylene[68, 69] and polyethylene terephthalate [66, 70-73] but only with annealing or crystallization at elevated pressure. Slow reordering would require molecular motions of the chains in the amorphous regions which can reorganize to add to the crystalline interface. Such a reorganization in local structure would be possible only if mobility is available for strands to translate. Is it noteworthy that previous reports on increasing T_m emphasize the role of an external stimuli, while the present networks sit quiescently at room temperature. In addition, these reports are on linear polymers and little is known about the role of network architectures on crystallization, particularly at such high crosslink densities.[74]

As mentioned, along with the upward shift in T_m the melting curves for C_{10} show a transition from a single peak to a double peak and then revert to a single peak (**Fig 4.3a**). The second peak is visible first as a small shoulder in the 5 day measurement and progressively increases in intensity in the 10080 min and 24480 min measurements at the expense of the first peak. This single to double peak transition is not seen in C_{12}.

4.3.2. Investigating Crystal – Crystal Transition Using Wide Angle X-ray Scattering

To probe the nature of this phenomena, wide-angle X-ray scattering (WAXS) was performed on the networks. Patterns collected over 1440 min (1 day) and 150 days of isothermal crystallization time at room temperature in an Argon glove box are shown in **Fig 4.4**. Scattering patterns were also collected more frequently on a separate benchtop XRD at room temperature for samples crystallized under ambient conditions (**Supplementary Fig 4.6**) and show the same general phenomena to be discussed. The presence of atmospheric moisture slightly modifies the kinetics of crystal evolution, while the patterns in **Fig 4.4a-c** correspond to samples crystallized in a glovebox. Prior work on PE has indicated that the semi-crystalline state at room temperature has three types of unit cells: orthorhombic, monoclinic and hexagonal.[75-77] The orthorhombic PE crystal phase is the densest and most the commonly observed phase in PE, while the monoclinic PE crystal structure may coexist with orthorhombic.[53, 56, 60] The hexagonal phase is typically seen under high pressure crystallization.[78, 79] The X-ray scattering patterns at 1 day show a single Bragg peak at 15 nm^{-1} for both C_{10} and C_{12} arising from the diffraction of planes (20), (-11), and (11) of a PE hexagonal unit cell (lattice parameters: a = 4.7 Å, b = 8.2 Å; *P6m* space group).With increasing isothermal crystallization at room temperature, a transition to a two peak pattern is observed for C_{10} (**Fig 4.4a**). The two Bragg peaks at 14.8 nm^{-1} and 16.4 nm^{-1} can be

respectively assigned to the diffraction of planes (110) and (200) of a PE orthorhombic unit cell (lattice parameters: a = 7.1 Å, b = 4.9 Å, c = 2.5 Å; in a *Pnam* space group).[80] The C_{12} network only shows one peak after 150 days in the glovebox but annealing at 65 °C for 2 days can drive a transition to the orthorhombic phase (**Fig 4.4b**). In both cases, the networks evolve from a metastable phase given sufficient time and temperature to orthorhombic with a coexistence of monoclinic. In prior work on ionic telechelic ethylenes, a hexagonal to orthorhombic transition was observed on cooling and the monoclinic phase coexisted with orthorhombic phase, which may explain the shoulder observed in the scattering result of the 150 days and annealed samples. In contrast, a linear PE standard immediately forms an orthorhombic crystal structure (**Supplementary Fig 4.7**). In the low q range the lamellar (100) and (200) reflections are observed for C_{10} and C_{12} indicating formation of lamellar stacks. The X-ray scattering patterns were also collected for C_8, which shows a single dominant peak even after 150 days of isothermal crystallization (**Fig 4.4c**). Analysis of the scattering data indicates a tetrahedral arrangement of short rods, or the C_8 alkyl chain, interconnected in a cubic crystal lattice with a lattice parameter of a = 1.55 nm and symmetry of a *Pn3m* space group. A double diamond cubic crystal structure has not been previously reported in polyethylene or in polymer networks. This network showed only a faint melting peak by DSC after 30 days (**Supplementary Fig 4.3c**) due to the extremely slow kinetics. The crystal structures and proposed packing of the linkers is illustrated in **Fig 4.4d**. The peaks for all three networks shift to higher q with annealing indicating densification of the crystalline networks, and a key finding of this work is that the crystal structure depends strongly on the choice of linker length in precise, dynamic networks.

A comparison of the scattering patterns for 150 days-crystallized networks reveals a monotonic shift of the lower q peak with increasing linker length. This is attributed to the boron-boron correlation length along the backbone based on a comparison with the calculated d-spacing ($d = 2\pi/q$) which is slightly shorter than that of an all-trans configuration of the ethylene linkers (**Table 4.1**). The correlation length of the crystals was also calculated using the Scherer equation $\varepsilon = 2\pi/\Delta q$ where Δq is the full width at half maximum of the peak corresponding to the spacer length. This length is ~ 30 nm and decreases slightly as the linker length increases.

To confirm that the network is intact after months of crystallization, FTIR spectra were collected on samples crystallized and tested inside the glovebox (**Supplementary Fig 4.3d**). The absence of free OH groups provides evidence that the boronic ester junctions do not break from the network but rather maintain the crosslink density and are incorporated into the crystal structure. Additionally, the scattering patterns of the starting alkane diols are shown in **Supplementary Fig 4.9b**, which are clearly distinct from the network patterns. Thus, the alkanes are not disengaging from the network and crystallizing separately over time.

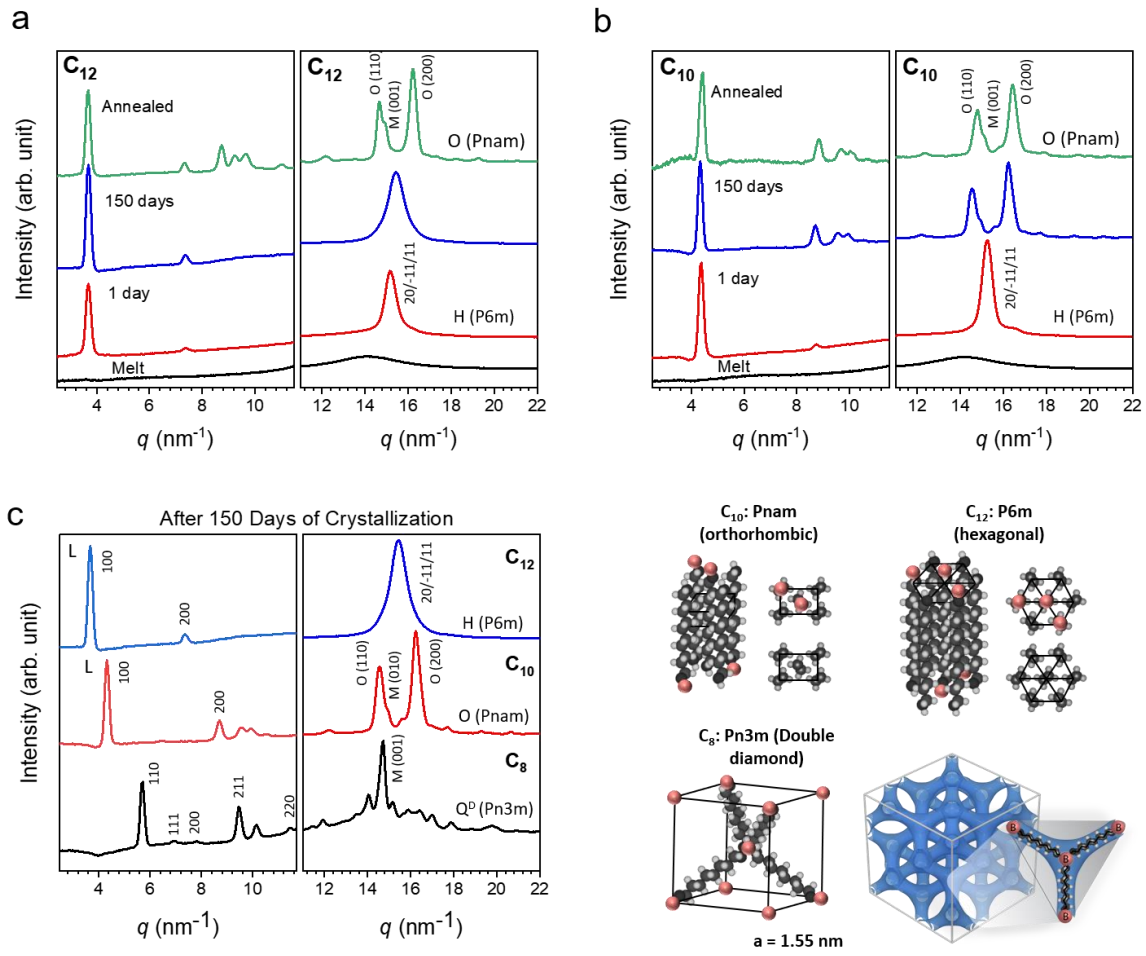

Figure 4.3. (a), (b) Room temperature WAXS patterns of C_{10} and C_{12} networks crystallized in a glove box. Samples were sandwiched and sealed between Kapton to prevent exposure to moisture. After 150 days of crystallization, samples were annealed at 50 °C (C_{10}) and 65 °C (C_{12}) for 2 days for the "annealed" data set. (c) A comparison of the WAXS patterns after 150 days of crystallization. (d) Schematic representation of the hexagonal (*P6m*), orthorhombic (*Pnam*) and double diamond (*Pn3m*) crystal lattices adopted by the C_{12}, C_{10}, and C_8 polymers, respectively.

Table 4.1. Location of low q scattering peak and analysis of peak width using the Scherrer equation

Network	q (nm^{-1})	d (nm)	All-trans linker length (nm)	Correlation length, ε (nm)
C_8	5.71	1.09	1.23	31.5
C_{10}	4.33	1.44	1.54	28.1
C_{12}	3.68	1.70	1.84	27.4

4.3.3. Emergence of New Morphology

An increase in T_m can occur for multiple reasons. First, the growth of crystallites raises the melting temperature due to the well-known Gibbs-Thomson effect and surface destabilization of a small crystal.[81-84] Second, a decreasing number of defects improves the crystal perfection[66] and decreases the free energy, leading to an increase in T_m. The long-term evolution of T_m in vitrimers is a consequence of the bond exchange reactions allowing for local rearrangements of network strands in the amorphous regions or at the crystal-amorphous interfaces which increase both the size and perfection of the crystals. To examine morphological evolution over time, cross polarization microscopy was used to observe changes in the crystal structure. The formation of uniformly distributed spherulites is observed in the C_{10} network during the initial 720 min of crystallization (**Fig 4.5a**) which is typical of linear polymers. After 1440 min of crystallization under ambient conditions, a new crystal structure emerges (**Fig 4.5b**). With time these crystals proliferate, while the growth of the spherulites is arrested (**Fig 4.5c** and **4.5d**). Eventually the new crystals dominate and the spherulites are no longer observable. We assign the initial crystals as a metastable hexagonal phase which transitions into the final orthorhombic crystal. The morphological development observed in optical microscopy is qualitatively consistent with the WAXS evolution further supporting a crystal-crystal transition in the absence of external stimuli and occurring over multiple days. Quantitatively relating these slow transformations to dynamic bond rearrangements is an important avenue for future work.

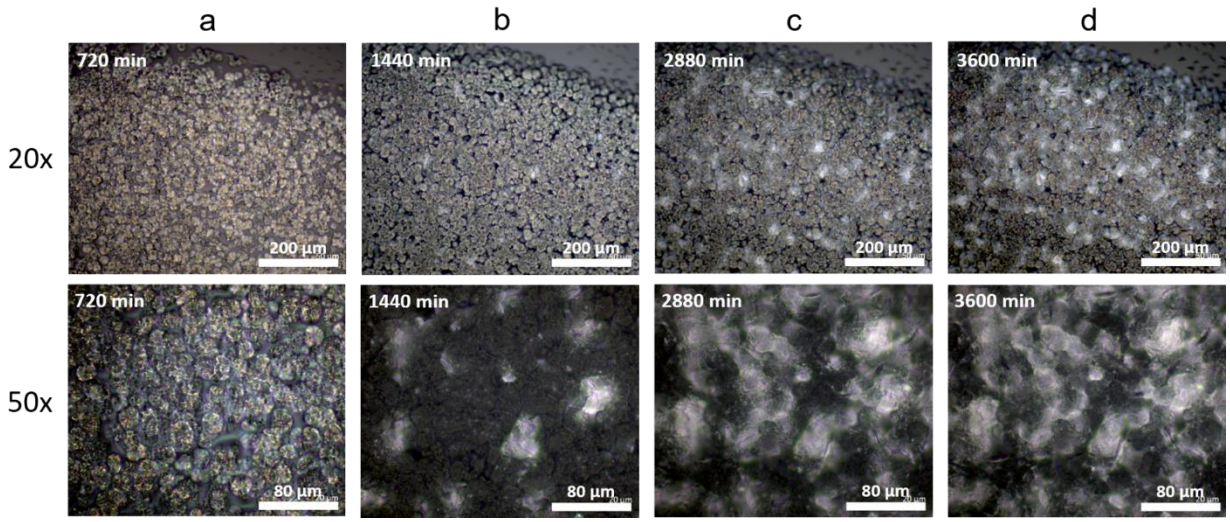

Figure 4.4. Cross polarization microscopy of C_{10}, crystallization at room temperature under ambient condition. We follow the evolution in crystal structure as a function of time (from left to right). (a) Initial formation of spherulites after 720 min of crystallization time. (b) A new crystal structure is seen alongside the spherulites at 1440 min. (c) (d) At 2400 min and 3600 min, the new crystals grow and uniformly span the image while the size of the spherulites remains constant with time.

In select regions of the initial micrographs for C_{10} networks, dendritic structures are observed alongside the spherulites (**Fig 4.6a** and **4.6b**). When annealed at 50 °C for 2880 min, the dendrites grow and eventually span the entire crystal domain (**Fig 4.6c** and **4.6d**). Comparing the morphological changes with the appearance of the second melting peak in C_{10}, we assign the second melting peak in DSC to the percolated dendritic crystal once it grows large enough to contribute to the heat flow. Compared to C_{10}, the crystal morphology of C_{12} networks is noticeably different by optical microscopy (**Supplementary Fig 4.8**). Spherulites are not resolvable in C_{12} networks indicating their size is below the resolution of our microscope. Nevertheless, WAXS confirms the presence of the same initial hexagonal crystal. Dendrites are not observed in C_{12} at any time in agreement with the absence of a second melting peak in C_{12} network DSC curves.

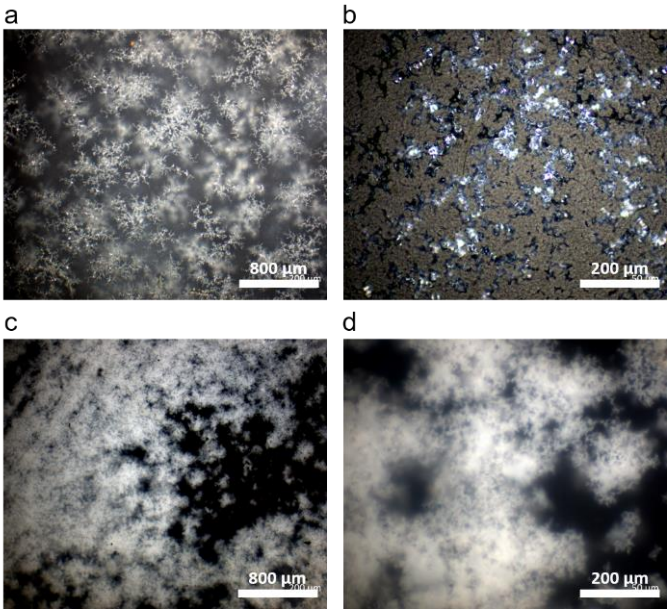

Figure 4.5. (a) and (b) Dendritic structures are seen in other locations of the same C_{10} sample along with the crystals shown in Figure 5. (c) (d) After annealing at 50 °C for 2 days the dendrites span the entire crystal domain and the spherulites are no longer visible.

One open question for the present ethylene vitrimers is how high the T_m can be with annealing protocols. Higher temperature annealing of the C_{10} and C_{12} networks at 50 °C and 65 °C, respectively, was performed after the initial isothermal crystallization for 43200 min at room temperature. Annealing for 2 days resulted in an increase of T_m to 89 °C for C_{10} and 100 °C for C_{12} (**Fig 4.7a**). Future work will investigate more complex annealing protocols for manipulating the final percent crystallinity and T_m. It is worth noting that the evolved T_m of the networks is above the T_m of their corresponding monomers and the WAXS patterns of the diols do not match those of the ethylene networks (**Supplementary Fig 4.9**). This indicates that the alkane diols are not simply being expelled from the network and crystallizing as the small molecule.

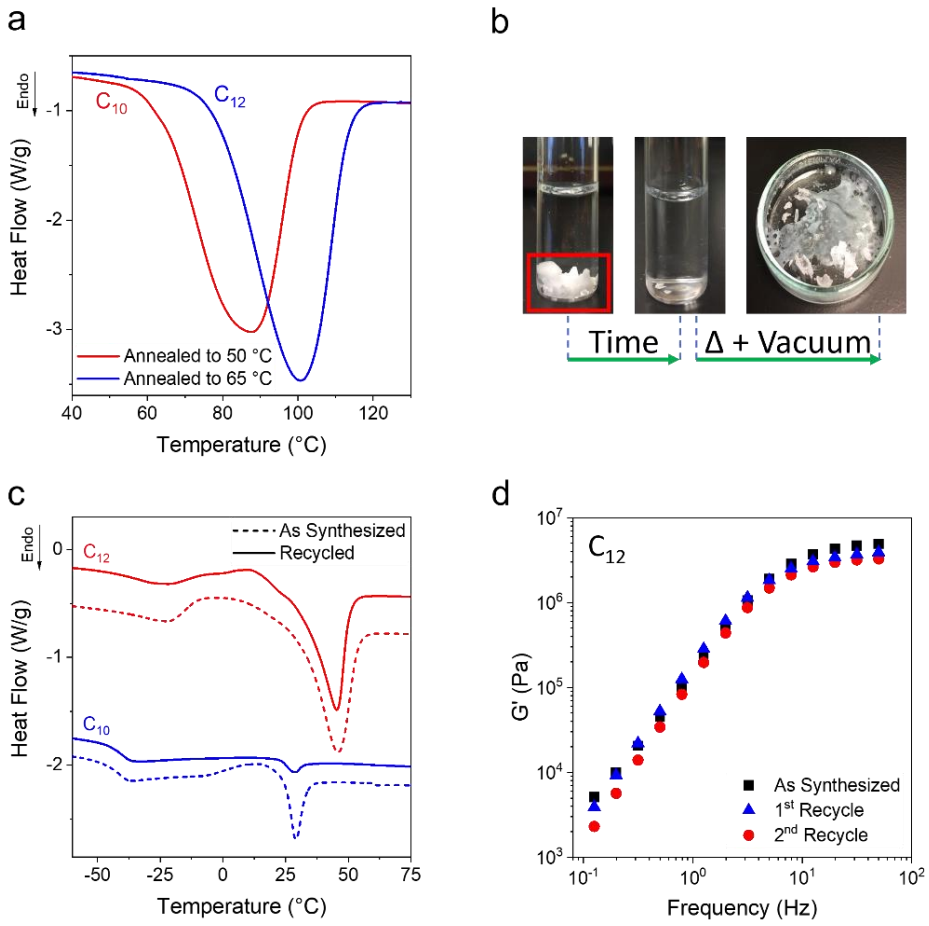

Figure 4.6. (a) DSC of the annealed samples. After annealing for 2 days an increase in T_m to 89 °C and 100 °C is observed for C_{10} and C_{12} respectively. (b) Networks were dissolved in ethanol and recovered by solvent evaporation. (c) DSC of as synthesized vs recycled C_{10} and C_{12}. The T_g and T_m of the recovered networks match the virgin networks. (d) Comparison of the rheology of recycled C_{12} and as synthesized C_{12} network indicates that there is minimal degradation in material properties.

4.3.4. Recycling and Reprocessing Vitrimers Without Degradation in Material Properties

An attractive property of vitrimers is their recyclability and the ability to recover monomer in some cases.[9, 85-89] The present ethylene vitrimers are crosslinked by boronic esters, and water or alcohol based solvent can attack the boron and dissolve the network. As a proof of concept, ethanol was used to dissolve both a C_{10} and C_{12} network, followed by removal of solvent under heat and vacuum (**Fig 4.7b**). The recovered networks were tested by DSC and oscillatory shear rheology to compare properties of freshly prepared networks ('as synthesized') to the recovered

networks. As shown in **Fig 4.7c**, the same T_g and T_m are reported for the recovered networks indicating that semi-crystalline vitrimers can be easily broken down to monomer and recovered. **Fig 4.7d** shows that the rheological properties of the networks are also retained. Future materials can incorporate bonds which are more or less sensitive to the desired solvent for recovery.

4.4. Conclusions.

Ethylene vitrimers with boronic ester bonds are shown to evolve their crystal morphology and T_m over long time periods relative to linear PE or permanent networks. With increasing crosslink density, the initial crystallization is frustrated and there is a longer induction period before T_m increases logarithmically with isothermal annealing time. In the C_{10} networks, a crystal – crystal transformation is observed by WAXS from hexagonal to orthorhombic structure which does not occur in linear PE under ambient conditions. Depending on precise linker length, either double diamond (C_8), orthorhombic (C_{10}), or hexagonal (C_{12}) crystals are formed after 150 days of isothermal room temperature crystallization in a glovebox. A C_8 network shows slow kinetics, but ultimately forms a double diamond morphology indicating the importance of linker length on the final structure. The long-time evolution of T_m, morphology transformation, and dendrite formation are all attributed to dynamic bond exchange as they are not present in linear PE or a precise, permanent ethylene network control sample. Annealing the vitrimers at higher temperatures following the initial crystallization leads to a further increase in T_m which reaches 100 °C for a C_{12} network. Vitrimer recyclability is demonstrated by dissolving the networks in common laboratory solvents and then recovered by solvent evaporation. These findings on the role of dynamic bond exchange on crystallization are critical to the design, processing, and use of vitrimers as both commodity polymers, and functional materials, which are more sustainable.

4.5. Experimental Details and Additional Plots

Materials: Boric acid ($B(OH)_3$, ≥ 99.5%), 1,8 octanediol (C_8, 98%), 1,10 decanediol (C_{10}, 98%), 1,12 dodecanediol (C_{12}, 99%), N-Hydroxysuccinimide (98%), dodecanedioyl dichloride (98%), 1,5,7-triazabicyclo[4.4.0]dec-5-ene (TBD, 98%), tris(2-aminoethyl)amine (96%), anhydrous dimethyl sulfoxide (DMSO, >99.9%) were purchased from Sigma-Aldrich without further purification. 2,2'-Diamino-N-methyldiethylamine (>98%) and dimethyl dodecanedioate (98.0+%) were purchased from TCI and was used without purification. Dichloromethane (HPLC), methanol, triethylamine was purchased from Sigma-Aldrich and stored with activated molecular sieves to remove moisture.

Ethylene dynamic network synthesis: Carefully weighed amounts of monomer were mixed together in a glass vial with stoichiometry of 1.0 mol boric acid to 1.5 mol diol. The mixture was heated and stirred continuously overnight at 120 ˚C on a hotplate. A viscous transparent gel was obtained. The vial was then transferred to a vacuum oven, held at 60˚C overnight under vacuum to drive water off and then immediately brought into an argon glovebox maintained at < 0.5 ppm O_2 and < 0.1 ppm H_2O. No solvent was used in the synthesis.

Synthesis of C_{10} diNHS linker: In a 200 mL oven dried round bottom flask charged with stir bar and N2, n-Hydroxysuccinimide (1.89 g, 16.4 mmol) and triethylamine (3.24 g, 32.0 mmol) was dissolved into 55 mL dry DCM. The reaction flask was cooled in water bath while dodecanedioyl dichloride (2.14 g, 8.0 mmol) was added dropwise via. a syringe. The reaction was then stirred overnight under N2 environment and the completion was confirmed by TLC. The reaction solution was then transferred into a separatory funnel with an additional 100 mL

DCM. The organic phase was washed with deionized (DI) water 3 times followed by saturated NaCl solution. The organic solution was then dried with NasSO4 and concentrated with rotary evaporator. A white crystalline solid (1.7g, 52% yield) was obtained after the recrystallization of the crude product with DCM. 1H NMR (500 MHz, CDCl3) □ (ppm): 2.83(s, 8H, -CH2¬¬-CON-), 2.60(t, 4H, -OCO-CH2-), 1.73(q, 4H,-CH2-CH2-), 1.43-1.27(m, 12H, -CH2-CH2-). Crystal was dried before further use.

Synthesis of C_{10} permanent amide network: A solution of triazabicyclodecene (24.6 mg, 0.17 mmol), dimethyl dodecanedioate (224.3 mg, 0.86 mmol), tris(2-aminoethyl)amine (88.2 mg, 0.58 mmol) and 109 μL CH3CN was transferred on top of a glass slide that has a layer of Kapton tape as a spacer. Another glass slide was placed on top to seal the reaction container. The reaction mixture was heated to 80 °C and allowed to cure for 24 h. The crosslinked polyamide network was then further cured at 100 °C, overnight, under vacuum (with the top glass slide removed) to push the completion of the aminolysis reaction. After the network has formed, TBD calaytst was removed by excessive washing with MeOH and water mixtures. The final network is a transparent polymer sheet.

Synthesis of C_{10} amide linear polymer: In a 15 mL oven dried round bottom flash charged with N2, 400 mg (0.94 mmol) of C_{10} diNHS was dissolved into 1.5 mL DMSO at 80 °C. Diamino-N-methyldiethylamine (112.70 mg, 0.94 mmol) was then added via a syringe. The polymerization was allowed to proceed at 80 °C for 18 hours with continuous stirring. A white precipitate is formed during the reaction. After the reaction was completed, MeOH was added to re-dissolve the reaction mixture. Polyamide was then crashed out by adding the reaction solution into 200

mL DI water dropwise with strong agitation. The polymer was collected by centrifuge and further washed in a dialysis bag for 2 days followed by drying in the vacuum oven. The final polymer was a light brown powder (yield 58 %).

ATR-FTIR: IR spectra of the samples were collected using a Bruker ALPHA FTIR spectrometer with a platinum-ATR QuickSnap sampling module. All measurements were made at 80 °C by scanning from 400 cm^{-1} to 4000 cm^{-1} with 16 total scans. Solid samples (networks) were clamped down to the diamond ATR crystal to ensure sufficient contact, while liquid samples (monomers) were left undisturbed.

Rheology of polymer networks: Oscillatory shear measurements were made on a TA Instruments DHR-2 rheometer using a parallel plate geometry. Samples were pressed into an 8 mm disc under ambient conditions and then loaded on to the rheometer at 40 ˚C. The dynamic networks were heated and held at 140 ˚C for 30 min to remove any water absorbed during sample loading. Sample thickness of approximately 800 μm was used for all measurements. Frequency sweeps were conducted at isothermal temperatures from 140 ˚C to 40 ˚C at 10 ˚C intervals with an applied stress of 1000 Pa. The viscosity of the networks was calculated by measuring the slope of the loss modulus vs frequency curve in the low frequency limit, and a characteristic Arrhenius behavior is observed as expected.

Differential Scanning Calorimetry (DSC): Samples with a mass between 3-6 mg were crimped in Tzero hermetic aluminum pans inside a glovebox. A TA Instruments DSC 25 was used to take all measurements. The glass transition temperature for each sample was measured by rapidly

quenching from 150 °C to -80 °C and then heating at 20 °C/min. T_g is obtained from analysis of the heating profile using the ½ ΔC_p criterion. For measurement of the melting temperature after room temperature crystallization, samples were equilibrated to 20 °C and ramped at 20 °C /min to 120 °C. (All graphs are plotted with "endothermic down" convention.)

X-ray scattering: Scattering patterns were first collected on a Siemens Kristalloflex (Diffractometer D5000) in the reflection geometry. Thin films of C_{10} and C_{12} were prepared by mechanical pressing at 60 °C. Films were heated at 120 °C for 12 hours to erase any thermal history and any possible effects of mechanical pressing. The films were cooled under ambient conditions and WAXS spectra were systematically collected at 12 hr time steps under ambient conditions. Next, a separate set of samples were crystallized in the glovebox and sealed between Kapton prior to being taken to the beamline. These sealed samples were analyzed with a Xenocs GeniX3D Cu Kα X-ray source (1.54 Å) and a Pilatus 2D detector (1M pixels). The sample-to-detector distance was calibrated with silver behenate powder, and scattering patterns were collected with a 10-minute exposure. The 2D diffraction data were radially averaged using FIT2D software or MATLAB-based GIXSGUI package and the intensity was plotted as a function of scattering vector q.

Optical Microscopy: Micrographs were collected using a Zeiss Axioscope A1 microscope. Thin films were prepared in a similar fashion as for X-ray diffraction and imaged under 10x, 20x and 50x magnification in reflection mode.

NMR spectroscopy**:** Solution state 1H NMR was done using a Varian UI500NB (500-MHz) at 23 degree Celsius. Solid state 13C NMR was done using Varian Unity Inova instrument (UI300WB, 300 MHz) via direct polarization magic angle spinning (DPMAS) method at 10 kHz spanning frequency with 5600 scan, and 5 s cycle delays (d1 = 5 s). A pseudo T1 measurement was done with d1 = 1, 5, 10 and 20 s to ensure 5 s is sufficient for all 13C nuclei to relax.

Recycling of ethylene dynamic networks: Approximately 0.1 g of the vitrimer network is added to 5ml of ethanol and heated to 80 °C with continuous stirring. It was observed that white crystalline chunks of the C_{10} and C_{12} networks take longer to dissolve as compared to the amorphous C_8. Ethylene vitrimers are recovered by evaporating the ethanol at 80 °C followed by vacuum drying at 60 °C to remove any residual solvent.

The networks were synthesized and characterized by FTIR which indicated high conversion of the reaction (**Supplementary Fig 4.1a**). Rapid quenching showed no crystallization in the cooling curves of C_8 or C_{10}, while a peak was observed for C_{12} and linear polyethylene (**Supplementary Fig 4.1b-c**). Rheology reveals the dynamic nature of these networks with a rubbery plateau and a flow regime (**Supplementary Fig 4.1d**).

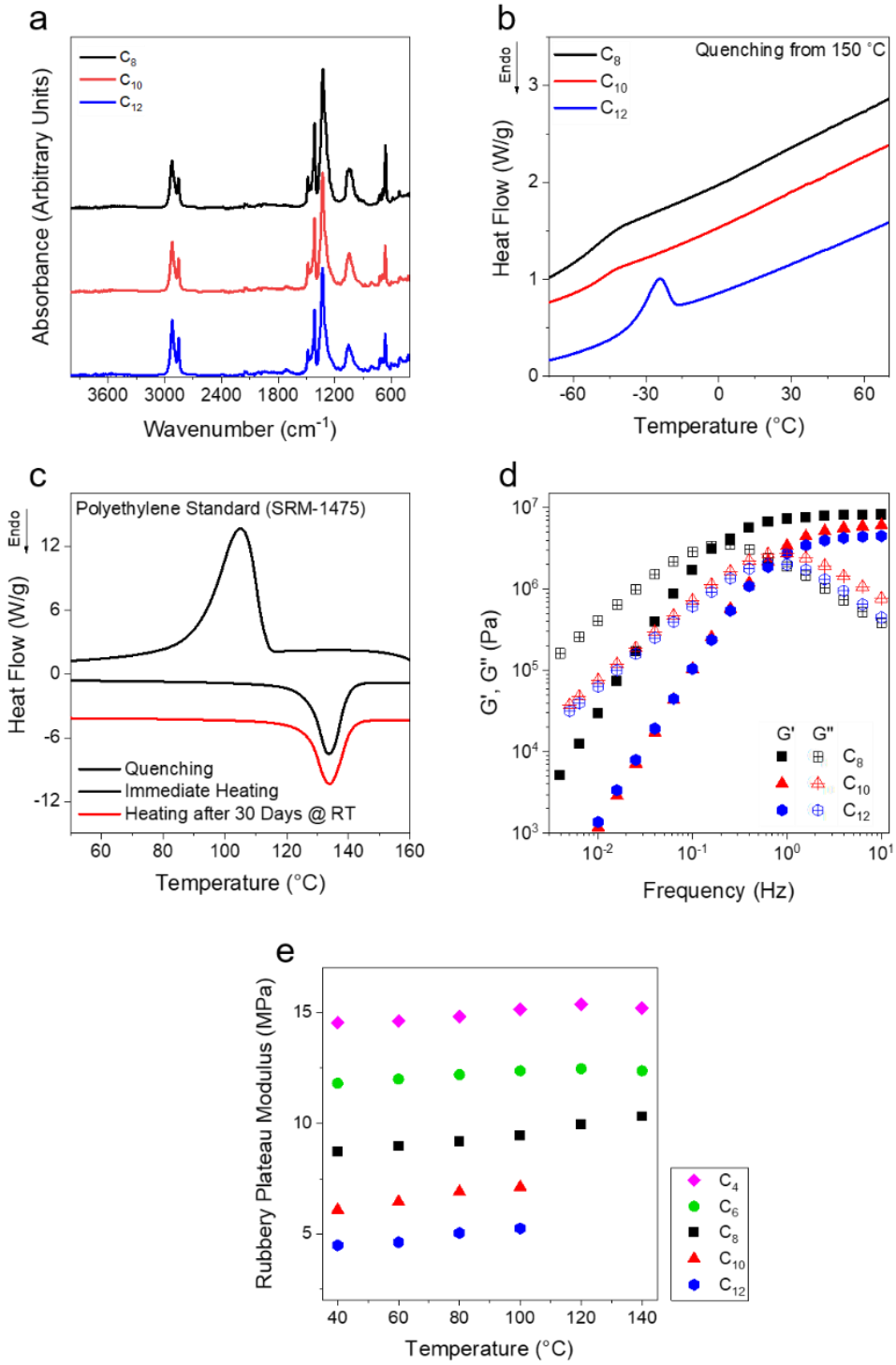

Supplementary Figure 4.1. (a) FTIR of C_8, C_{10} and C_{12} networks confirms the absence of OH peak due to unreacted diol or water. The sharp peak at ~1300 cm^{-1} is characteristic of the boronic ester bond. (b) DSC cooling curves show no crystallization for C_8 and C_{10} networks quenched from 150 °C to -80 °C, while C_{12} reveals a weak peak. (c) DSC of linear PE standard (SRM 1475) shows no change in T_m even after 43200 min at room temperature. (d) Frequency sweep of ethylene vitrimers measured at 40 °C. A high frequency rubbery plateau and a low frequency terminal relaxation are observed for all dynamic networks. (e) The rubbery plateau modulus as a function of temperature. Modulus scales systematically with crosslink density.

A separate set of samples was quenched directly to room temperature to probe the initial 300 min of crystallization (**Supplementary Fig. 4.2**).

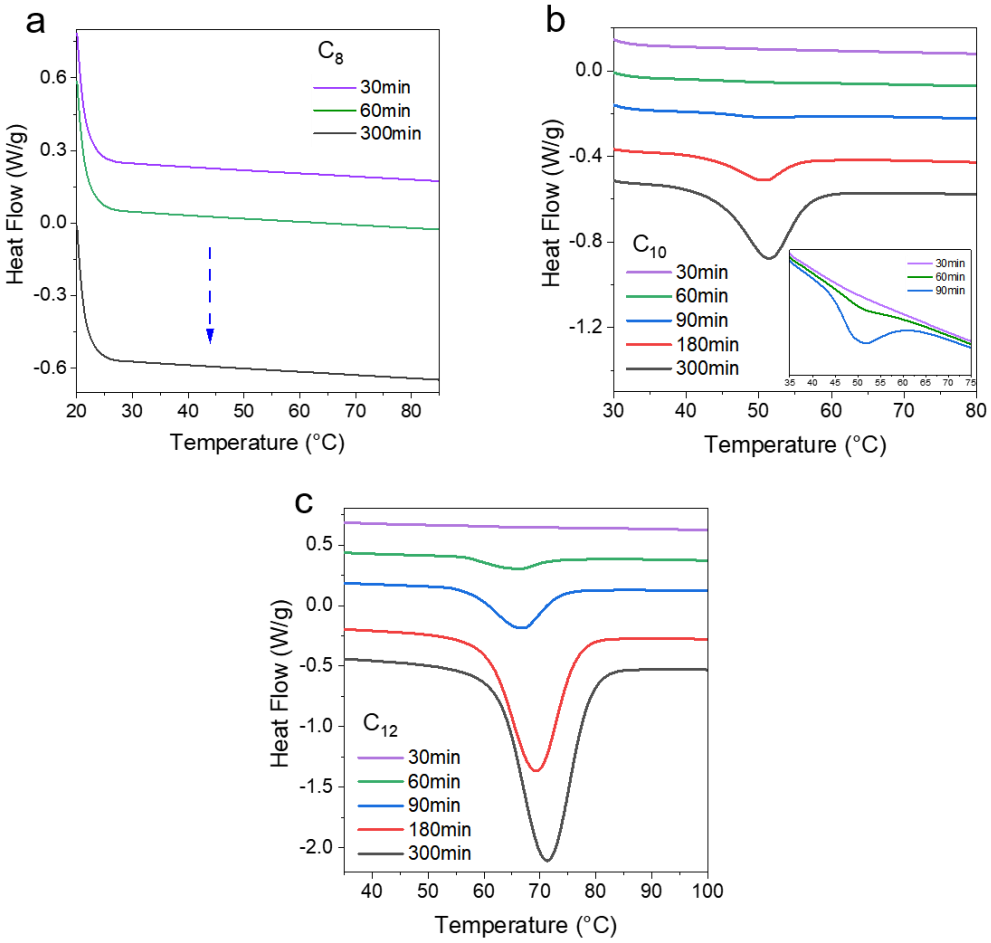

Supplementary Figure 4.2. DSC curves show the evolution of T_m following a quench to 20 °C for a 300 min isothermal crystallization (a) C_8 shows no T_m while (b) C_{10} and (c) C_{12} show a continual growth of a melting peak which shifts to higher temperature.

Over a longer time period of 30 days, the T_m continues to evolve as does the area under the DSC melting peaks (**Supplementary Fig. 4.3a**). After 150 days, the melting temperature stabilize and no free OH groups are detectable, indicating that the boronic ester is preserved and incorporated into the polymer crystal (**Supplementary Fig. 4.3b-d**).

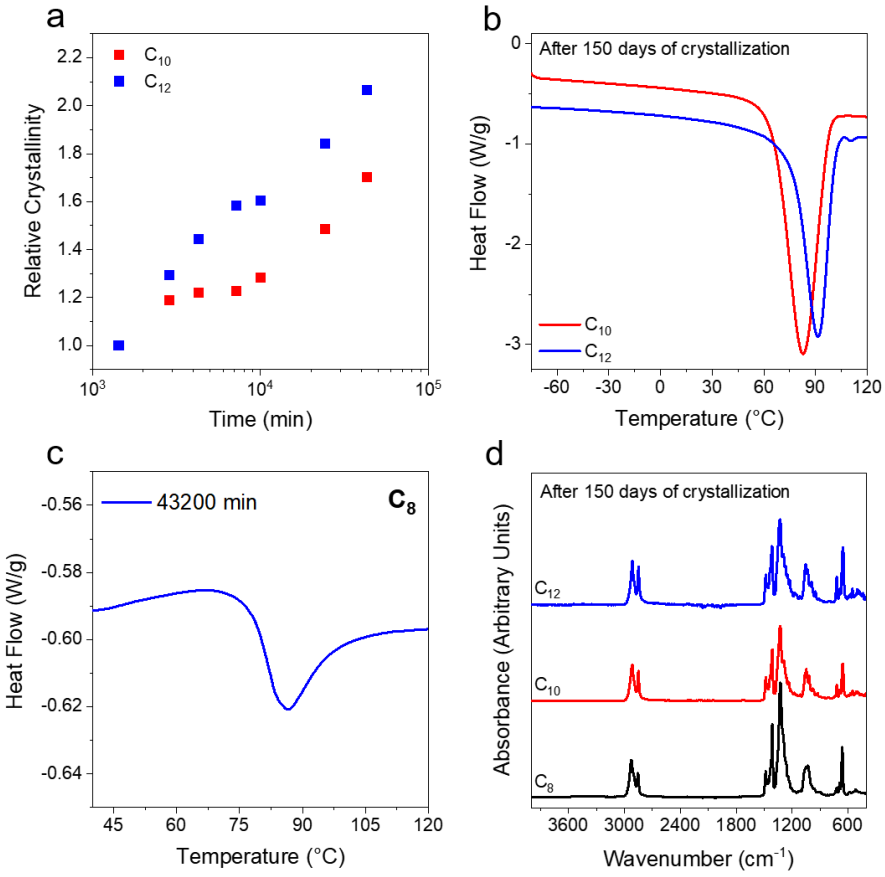

Supplementary Figure 4.3. (a) The increasing melting temperature of C_{10} and C_{12} is accompanied by an increase in the ethalpy of fusion. The relative crystallinity approximately doubles for C_{12} and increases by ~70% for C_{10} networks. Relative crystallinity of the samples was determined by normalizing to the enthalpy value at 1440 min. (b) After 150 days of isothermal crystallization, the T_g is not observed and T_m stops shifting. (c) An extremely weak melting transition is seen for C_8 networks even after 43200 min of isothermal crystallization at room temperature. (d) FTIR collected after 150 days of crystallization. Measurements were made in a glovebox, and the absence of the OH peak indicates that the crosslink density is conserved even after crystallization.

A permanent ethylene network (C_{10} amide network) and a linear permanent network (C_{10} amide polymer) were synthesized to provide a control to the dynamic system, and the synthesis is shown in **Supplementary Fig. 4.4**. DSC of the network confirms the absence of crystallization, whereas the linear amide polymer shows a distinct melting peak (**Supplementary Fig. 4.5**).

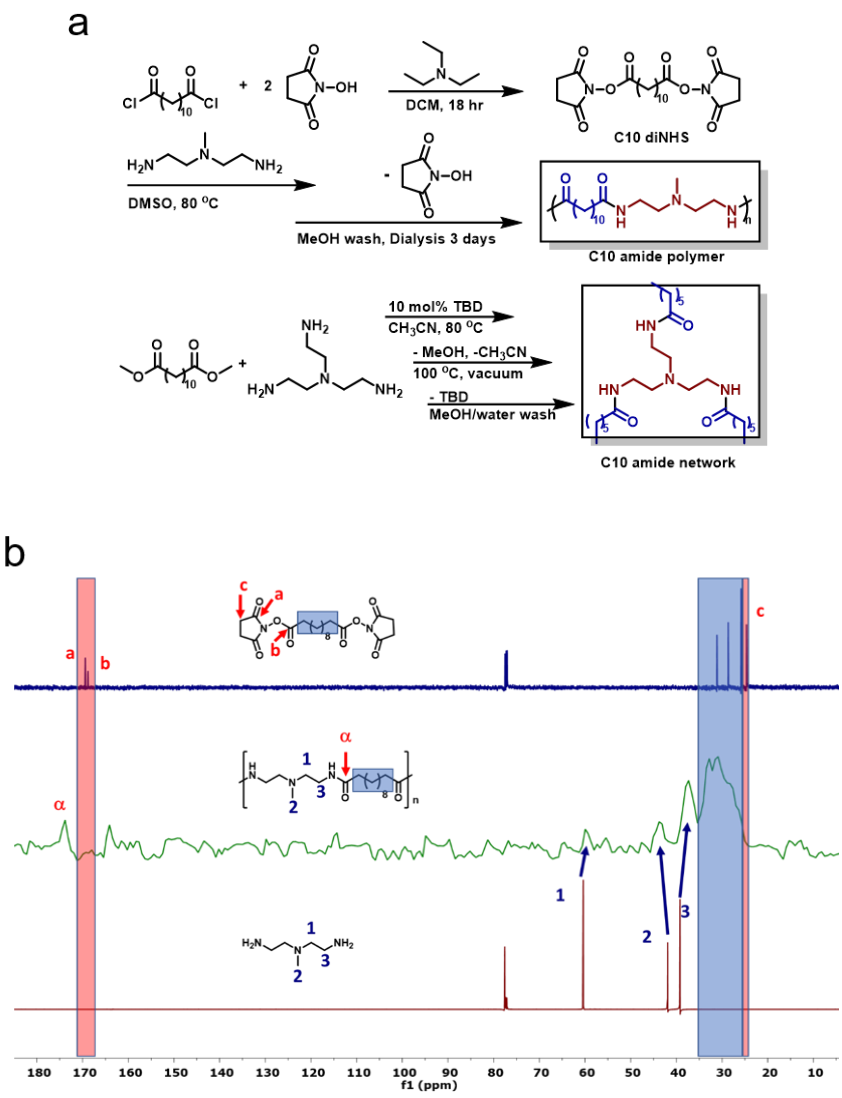

Supplementary Figure 4.4. (Continued)

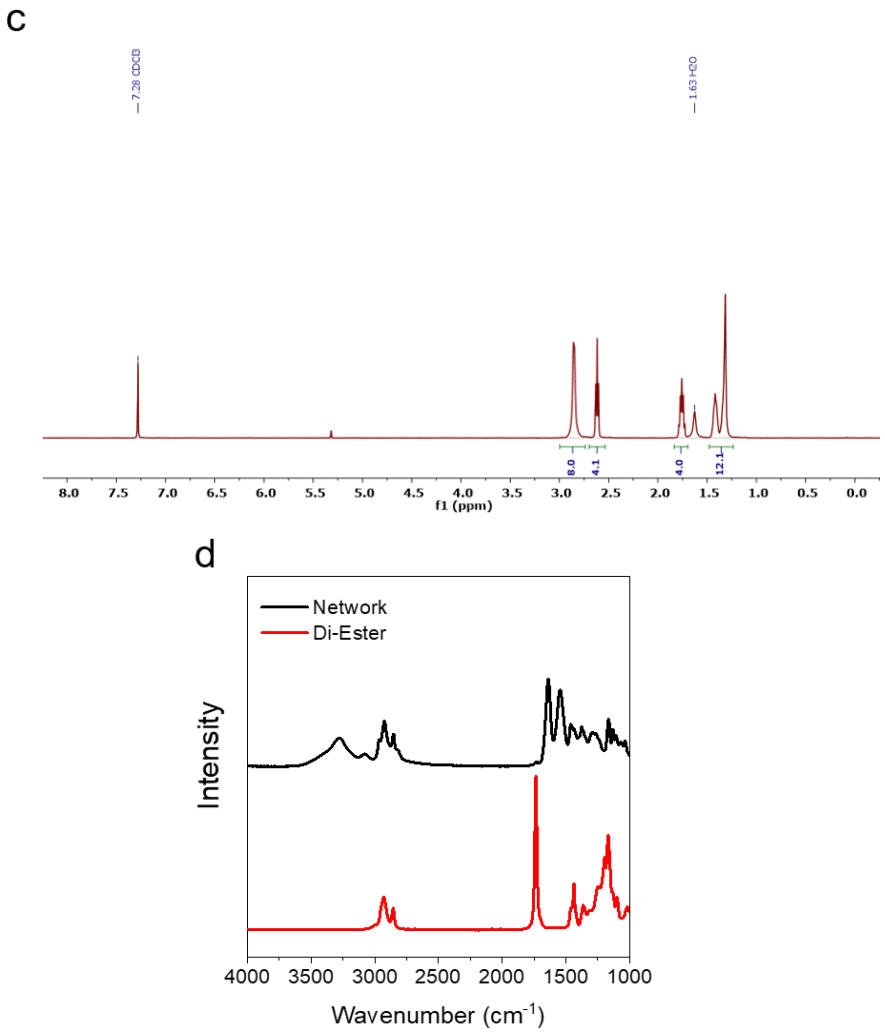

Supplementary Figure 4.4. (a) Synthesis routes for the C_{10} amide polymer and C_{10} amide network. The use of NHS functionality ensures controllable network formation as the reaction between acid chloride and amine is too fast. (b) ^{13}C Solid-state NMR (green trace) of C_{10} amide linear polymer with diNHS (blue) and diamine (red) starting materials. The disappearance of signal a,b and c from the NHS moieties of the C_{10} small molecule and the appearance of α (new amide C=O) indicates a high functional group conversion. Carbon signals from the diamine molecule (1,2 and 3) along with methylene signal from C_{10} linker (in diNHS) are also in agreement of the proposed C_{10} polyamide structure. (c) ^{1}H NMR of C_{10} diNHS linker. (d) FTIR trace of C_{10} amide network with the reference of the C_{10} di ester monomer. Ester C=O stretch (1635 and 1542 cm^{-1}) completely disappeared and new amide C=O stretch appears (1734 cm^{-1}). FTIR gives strong evidence of high reaction conversion

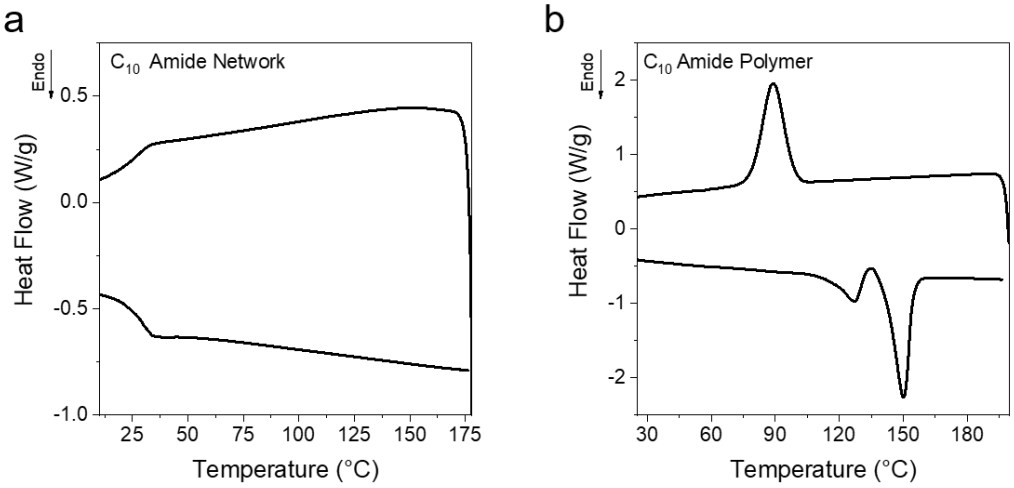

Supplementary Figure 4.5. (a) DSC of the C_{10} amide network shows a T_g of 34°C and no crystallization. (b) In comparison the DSC of the linear counterpart, the C_{10} amide polymer crystallizes and shows a broad high temperature melting peak. This provides evidence that it is the network architecture and not the chemistry of the crosslink junction that is restricting the crystallization of the permanent network.

Wide-angle diffraction was measured on a benchtop system under ambient conditions (**Supplementary Fig. 4.6**). This is in support of the patterns collected using sealed samples which crystallized entirely in a glove box (**Fig. 4.5**). Both samples show the transition from 1 to 2 dominant peaks in the C_{10} system, while the C_{12} system showed 2 peaks after higher temperature annealing.

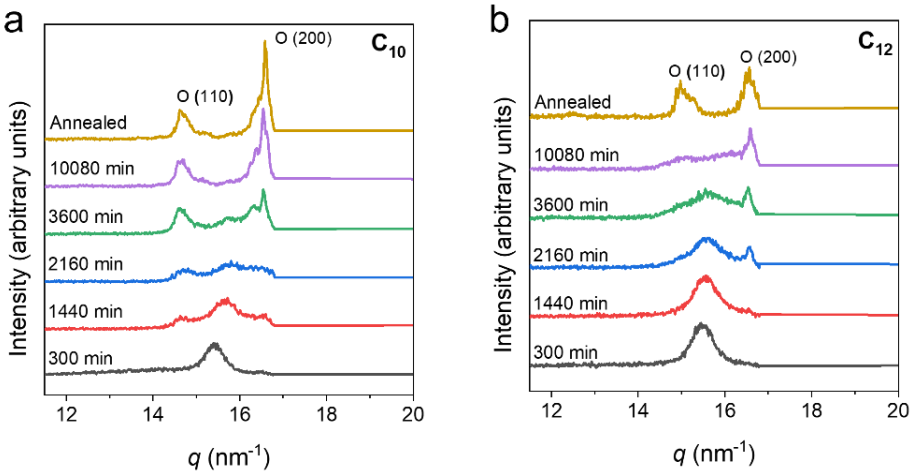

Supplementary Figure 4.6. Benchtop X-ray scttering patterns for C_{10} and C_{12} under ambient conditions. The transition from hexagonal to orthorhombic is preserved in the C_{10} networks, while the C_{12} network partially

Supplementary Figure 4.6. (Continued) transforms to orthorhombic prior to annealing. This is attributed to atmospheric water which can hydrolyse the boronic ester. In contrast, sample in **Figure 5** were crystallized in a glove box and rigorously dried.

Linear polyethylene instantly crystallized into the orthorhombic phase upon cooling to room temperature (**Supplementary Fig. 4.7**).

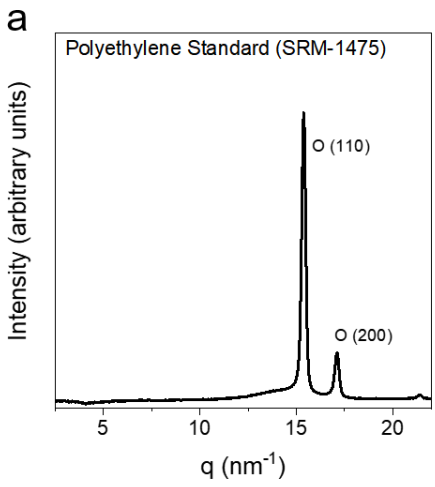

Supplementary Figure 4.7. (a) WAXS for PE standard. The canonical orthorhombic phase is predominant in the linear polyethylene.

Optical microscopy was used to visually track the crystals, and for C_{12} networks was substantially different from the C_{10} crystals (**Supplementary Figure 4.8**).

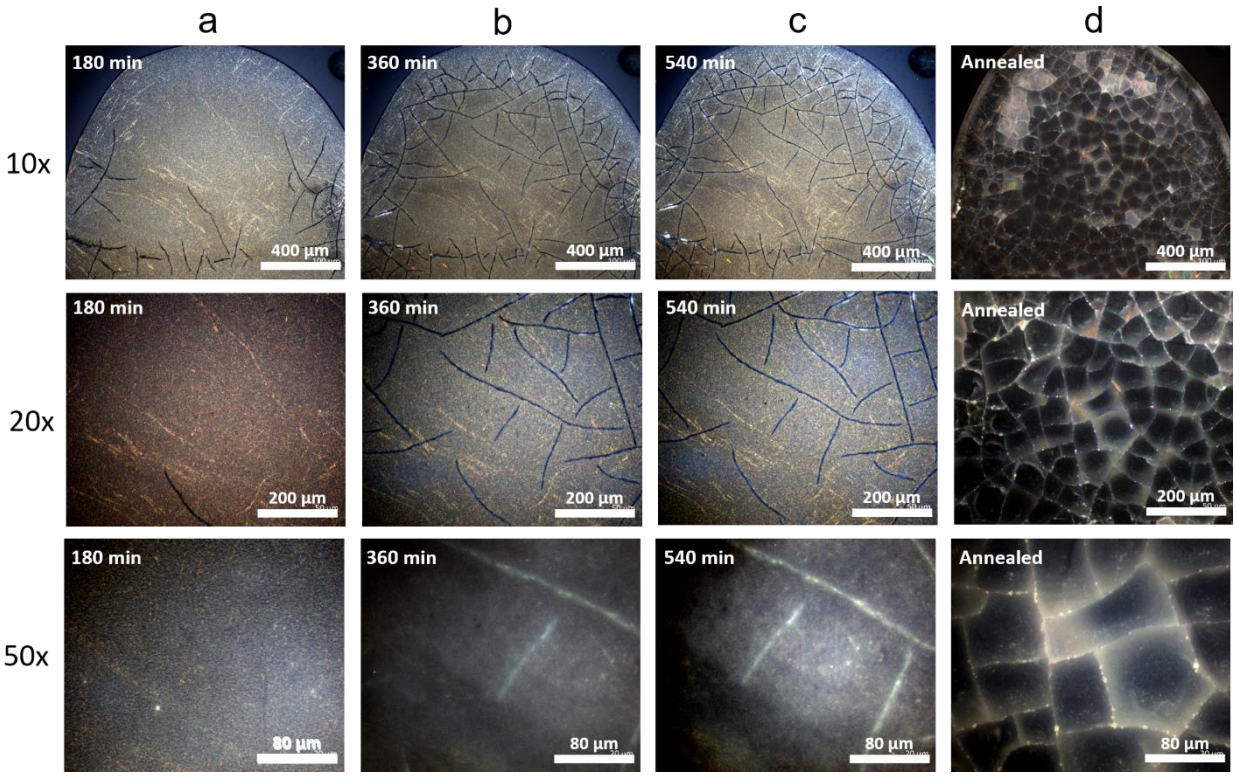

Supplementary Figure 4.8. Optical microscopy of C_{12} vitrimer, crystallization at room temperature after (a) 180, (b) 360 and (c) 540 min of crystallization time, (d) Sample annealed at 65 °C for 2880 min after 10080 min of room temperature crystallization. Over time the grains shrink and collide. No dendritic structures are observed, consistent with the absence of a second melting peak in DSC.

The final vitrimer T_m exceeded that of the alkane diol, and the diffraction patterns are substantially different indicating the diols are not being expelled from the network and independently crystallizing (**Supplementary Fig. 4.9**). The diols peaks were indexed and are a good match with literature.[1-3]

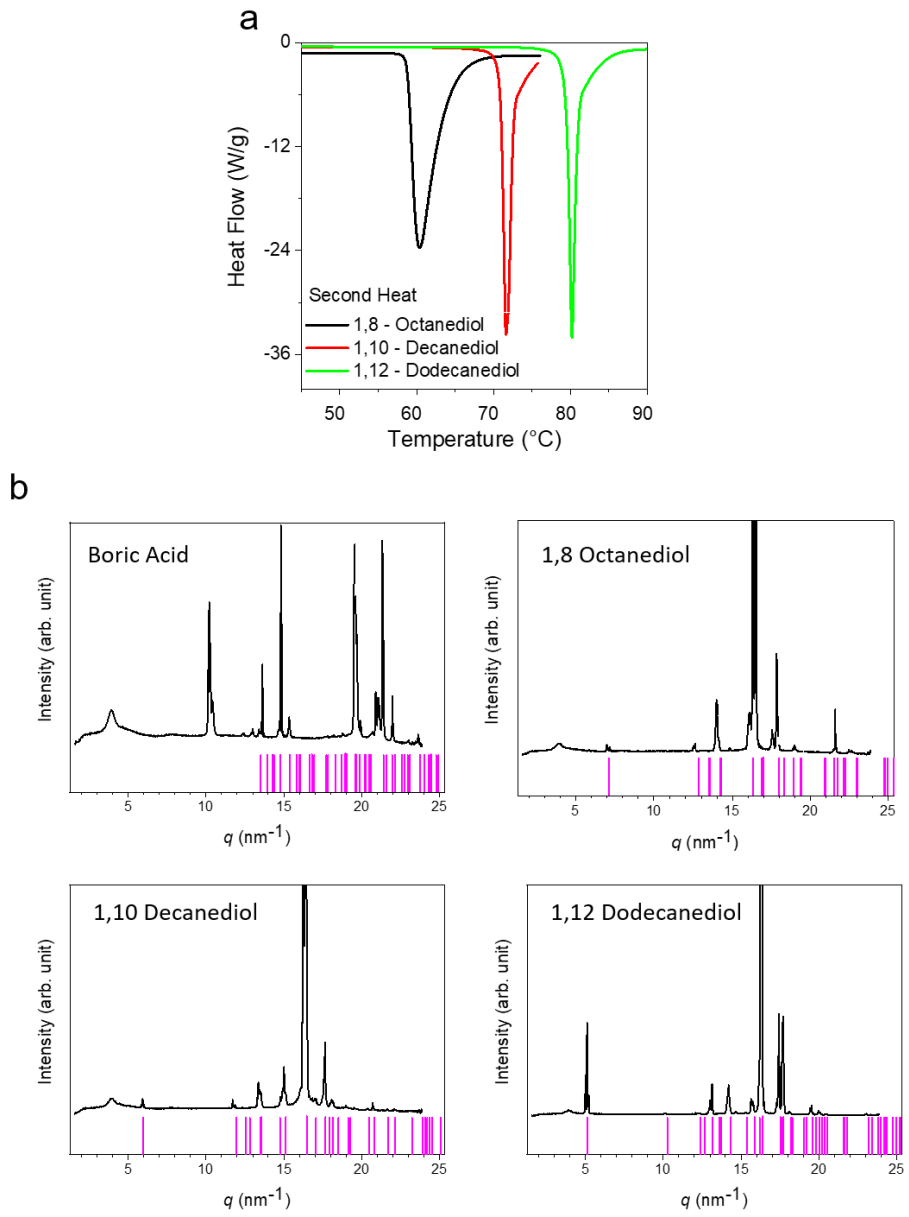

Supplementary Figure 4.9. (a) Melting curves of the diol monomers show a sharp melting transition. (b) WAXS patterns of the diol monomers and boric acid crosslinker overlaid with simulated powder diffraction peaks shown as pink lines (VESTA software was used for the simulation).

4.6. References

1. Geyer, R.; Jambeck, J. R.; Law, K. L., Production, use, and fate of all plastics ever made. *Science Advances* **2017,** *3* (7), e1700782.

2. Lu, Y.-X.; Tournilhac, F.; Leibler, L.; Guan, Z., Making Insoluble Polymer Networks Malleable via Olefin Metathesis. *Journal of the American Chemical Society* **2012,** *134* (20), 8424-8427.

3. Montarnal, D.; Capelot, M.; Tournilhac, F.; Leibler, L., Silica-Like Malleable Materials from Permanent Organic Networks. *Science* **2011,** *334* (6058), 965.

4. Ciarella, S.; Biezemans, R. A.; Janssen, L. M. C., Understanding, predicting, and tuning the fragility of vitrimeric polymers. *Proceedings of the National Academy of Sciences* **2019,** *116* (50), 25013.

5. Lei, Q.-L.; Xia, X.; Yang, J.; Pica Ciamarra, M.; Ni, R., Entropy-controlled cross-linking in linker-mediated vitrimers. *Proceedings of the National Academy of Sciences* **2020,** *117* (44), 27111.

6. Lossada, F.; Jiao, D.; Yao, X.; Walther, A., Waterborne Methacrylate-Based Vitrimers. *ACS Macro Letters* **2020,** *9* (1), 70-76.

7. Self, J. L.; Sample, C. S.; Levi, A. E.; Li, K.; Xie, R.; de Alaniz, J. R.; Bates, C. M., Dynamic Bottlebrush Polymer Networks: Self-Healing in Super-Soft Materials. *Journal of the American Chemical Society* **2020,** *142* (16), 7567-7573.

8. Yang, Y.; Pei, Z.; Li, Z.; Wei, Y.; Ji, Y., Making and Remaking Dynamic 3D Structures by Shining Light on Flat Liquid Crystalline Vitrimer Films without a Mold. *Journal of the American Chemical Society* **2016,** *138* (7), 2118-2121.

9. Jing, B. B.; Evans, C. M., Catalyst-Free Dynamic Networks for Recyclable, Self-Healing Solid Polymer Electrolytes. *Journal of the American Chemical Society* **2019,** *141* (48), 18932-18937.

10. Cash, J. J.; Kubo, T.; Bapat, A. P.; Sumerlin, B. S., Room-Temperature Self-Healing Polymers Based on Dynamic-Covalent Boronic Esters. *Macromolecules* **2015,** *48* (7), 2098-2106.

11. Cromwell, O. R.; Chung, J.; Guan, Z., Malleable and Self-Healing Covalent Polymer Networks through Tunable Dynamic Boronic Ester Bonds. *Journal of the American Chemical Society* **2015,** *137* (20), 6492-6495.

12. Ricarte, R. G.; Tournilhac, F.; Cloître, M.; Leibler, L., Linear Viscoelasticity and Flow of Self-Assembled Vitrimers: The Case of a Polyethylene/Dioxaborolane System. *Macromolecules* **2020,** *53* (5), 1852-1866.

13. Ricarte, R. G.; Tournilhac, F.; Leibler, L., Phase Separation and Self-Assembly in Vitrimers: Hierarchical Morphology of Molten and Semicrystalline Polyethylene/Dioxaborolane Maleimide Systems. *Macromolecules* **2019,** *52* (2), 432-443.

14. Caffy, F.; Nicolaÿ, R., Transformation of polyethylene into a vitrimer by nitroxide radical coupling of a bis-dioxaborolane. *Polymer Chemistry* **2019,** *10* (23), 3107-3115.

15. Saed, M. O.; Gablier, A.; Terentejv, E. M., Liquid Crystalline Vitrimers with Full or Partial Boronic-Ester Bond Exchange. *Advanced Functional Materials* **2020,** *30* (3), 1906458.

16. Röttger, M.; Domenech, T.; van der Weegen, R.; Breuillac, A.; Nicolaÿ, R.; Leibler, L., High-performance vitrimers from commodity thermoplastics through dioxaborolane metathesis. *Science* **2017,** *356* (6333), 62-65.

17. Ogden, W. A.; Guan, Z., Recyclable, Strong, and Highly Malleable Thermosets Based on Boroxine Networks. *Journal of the American Chemical Society* **2018,** *140* (20), 6217-6220.

18. Soman, B.; Evans, C. M., Effect of precise linker length, bond density, and broad temperature window on the rheological properties of ethylene vitrimers. *Soft Matter* **2020**.

19. Fortman, D. J.; Brutman, J. P.; Cramer, C. J.; Hillmyer, M. A.; Dichtel, W. R., Mechanically Activated, Catalyst-Free Polyhydroxyurethane Vitrimers. *Journal of the American Chemical Society* **2015,** *137* (44), 14019-14022.

20. Guerre, M.; Taplan, C.; Nicolaÿ, R.; Winne, J. M.; Du Prez, F. E., Fluorinated Vitrimer Elastomers with a Dual Temperature Response. *Journal of the American Chemical Society* **2018,** *140* (41), 13272-13284.

21. Lessard, J. J.; Scheutz, G. M.; Hughes, R. W.; Sumerlin, B. S., Polystyrene-Based Vitrimers: Inexpensive and Recyclable Thermosets. *ACS Applied Polymer Materials* **2020**.

22. Lessard, J. J.; Scheutz, G. M.; Sung, S. H.; Lantz, K. A.; Epps, T. H.; Sumerlin, B. S., Block Copolymer Vitrimers. *Journal of the American Chemical Society* **2020,** *142* (1), 283-289.

23. Spiesschaert, Y.; Guerre, M.; De Baere, I.; Van Paepegem, W.; Winne, J. M.; Du Prez, F. E., Dynamic Curing Agents for Amine-Hardened Epoxy Vitrimers with Short (Re)processing Times. *Macromolecules* **2020,** *53* (7), 2485-2495.

24. Liu, W.-X.; Zhang, C.; Zhang, H.; Zhao, N.; Yu, Z.-X.; Xu, J., Oxime-Based and Catalyst-Free Dynamic Covalent Polyurethanes. *Journal of the American Chemical Society* **2017,** *139* (25), 8678-8684.

25. He, C.; Shi, S.; Wang, D.; Helms, B. A.; Russell, T. P., Poly(oxime–ester) Vitrimers with Catalyst-Free Bond Exchange. *Journal of the American Chemical Society* **2019,** *141* (35), 13753-13757.

26. Liu, H.; Nelson, A. Z.; Ren, Y.; Yang, K.; Ewoldt, R. H.; Moore, J. S., Dynamic Remodeling of Covalent Networks via Ring-Opening Metathesis Polymerization. *ACS Macro Letters* **2018,** *7* (8), 933-937.

27. Obadia, M. M.; Mudraboyina, B. P.; Serghei, A.; Montarnal, D.; Drockenmuller, E., Reprocessing and Recycling of Highly Cross-Linked Ion-Conducting Networks through Transalkylation Exchanges of C–N Bonds. *Journal of the American Chemical Society* **2015,** *137* (18), 6078-6083.

28. Nishimura, Y.; Chung, J.; Muradyan, H.; Guan, Z., Silyl Ether as a Robust and Thermally Stable Dynamic Covalent Motif for Malleable Polymer Design. *Journal of the American Chemical Society* **2017,** *139* (42), 14881-14884.

29. Tretbar, C. A.; Neal, J. A.; Guan, Z., Direct Silyl Ether Metathesis for Vitrimers with Exceptional Thermal Stability. *Journal of the American Chemical Society* **2019,** *141* (42), 16595-16599.

30. Zych, A.; Pinalli, R.; Soliman, M.; Vachon, J.; Dalcanale, E., Polyethylene vitrimers via silyl ether exchange reaction. *Polymer* **2020,** *199*, 122567.

31. El-Zaatari, B. M.; Ishibashi, J. S. A.; Kalow, J. A., Cross-linker control of vitrimer flow. *Polymer Chemistry* **2020**.

32. Ishibashi, J. S. A.; Kalow, J. A., Vitrimeric Silicone Elastomers Enabled by Dynamic Meldrum's Acid-Derived Cross-Links. *ACS Macro Letters* **2018,** *7* (4), 482-486.

33. Denissen, W.; Winne, J. M.; Du Prez, F. E., Vitrimers: Permanent organic networks with glass-like fluidity. *Chemical Science* **2016,** *7* (1), 30-38.

34. Van Zee, N. J.; Nicolaÿ, R., Vitrimers: Permanently crosslinked polymers with dynamic network topology. *Progress in Polymer Science* **2020,** *104*, 101233-101233.

35. Ziaie, F.; Borhani, M.; Mirjalili, G.; Bolourizadeh, M. A., Effect of crystallinity on electrical properties of electron beam irradiated LDPE and HDPE. *Radiation Physics and Chemistry* **2007,** *76* (11), 1684-1687.

36. Krishnaswamy, R. K.; Yang, Q.; Fernandez-Ballester, L.; Kornfield, J. A., Effect of the Distribution of Short-Chain Branches on Crystallization Kinetics and Mechanical Properties of High-Density Polyethylene. *Macromolecules* **2008,** *41* (5), 1693-1704.

37. Mirabella Jr, F. M.; Westphal, S. P.; Fernando, P. L.; Ford, E. A.; Williams, J. G., Morphological explanation of the extraordinary fracture toughness of linear low density polyethylenes. *Journal of Polymer Science Part B: Polymer Physics* **1988,** *26* (9), 1995-2005.

38. Simis, K. S.; Bistolfi, A.; Bellare, A.; Pruitt, L. A., The combined effects of crosslinking and high crystallinity on the microstructural and mechanical properties of ultra high molecular weight polyethylene. *Biomaterials* **2006,** *27* (9), 1688-1694.

39. Borhani zarandi, M.; Amrollahi Bioki, H.; Mirbagheri, Z.-a.; Tabbakh, F.; Mirjalili, G., Effect of crystallinity and irradiation on thermal properties and specific heat capacity of LDPE & LDPE/EVA. *Applied Radiation and Isotopes* **2012,** *70* (1), 1-5.

40. Son, S. Y.; Kim, Y.; Lee, J.; Lee, G.-Y.; Park, W.-T.; Noh, Y.-Y.; Park, C. E.; Park, T., High-Field-Effect Mobility of Low-Crystallinity Conjugated Polymers with Localized Aggregates. *Journal of the American Chemical Society* **2016,** *138* (26), 8096-8103.

41. Wu, Y.; Schneider, S.; Walter, C.; Chowdhury, A. H.; Bahrami, B.; Wu, H.-C.; Qiao, Q.; Toney, M. F.; Bao, Z., Fine-Tuning Semiconducting Polymer Self-Aggregation and Crystallinity Enables Optimal Morphology and High-Performance Printed All-Polymer Solar Cells. *Journal of the American Chemical Society* **2020,** *142* (1), 392-406.

42. Sun, J.; Liao, X.; Minor, A. M.; Balsara, N. P.; Zuckermann, R. N., Morphology-Conductivity Relationship in Crystalline and Amorphous Sequence-Defined Peptoid Block Copolymer Electrolytes. *Journal of the American Chemical Society* **2014,** *136* (42), 14990-14997.

43. Yan, L.; Rank, C.; Mecking, S.; Winey, K. I., Gyroid and Other Ordered Morphologies in Single-Ion Conducting Polymers and Their Impact on Ion Conductivity. *Journal of the American Chemical Society* **2020,** *142* (2), 857-866.

44. Stoeva, Z.; Martin-Litas, I.; Staunton, E.; Andreev, Y. G.; Bruce, P. G., Ionic Conductivity in the Crystalline Polymer Electrolytes PEO6:LiXF6, X = P, As, Sb. *Journal of the American Chemical Society* **2003,** *125* (15), 4619-4626.

45. Ji, F.; Liu, X.; Lin, C.; Zhou, Y.; Dong, L.; Xu, S.; Sheng, D.; Yang, Y., Reprocessable and Recyclable Crosslinked Polyethylene with Triple Shape Memory Effect. *Macromolecular Materials and Engineering* **2019,** *304* (3), 1800528.

46. Maaz, M.; Riba-Bremerch, A.; Guibert, C.; Van Zee, N. J.; Nicolaÿ, R., Synthesis of Polyethylene Vitrimers in a Single Step: Consequences of Graft Structure, Reactive Extrusion Conditions, and Processing Aids. *Macromolecules* **2021,** *54* (5), 2213-2225.

47. Brutman, J. P.; Delgado, P. A.; Hillmyer, M. A., Polylactide Vitrimers. *ACS Macro Letters* **2014,** *3* (7), 607-610.

48. Yan, L.; Bustillo, K. C.; Panova, O.; Minor, A. M.; Winey, K. I., Solution-grown crystals of precise acid-and ion-containing polyethylenes. *Polymer* **2018,** *135*, 111-119.

49. Yan, L.; Häußler, M.; Bauer, J.; Mecking, S.; Winey, K. I., Monodisperse and telechelic polyethylenes form extended chain crystals with ionic layers. *Macromolecules* **2019,** *52* (13), 4949-4956.

50. Yang, K.; Cai, Z.; Jaiswal, A.; Tyagi, M.; Moore, J. S.; Zhang, Y., Dynamic Odd–Even Effect in Liquid n-Alkanes near Their Melting Points. *Angewandte Chemie International Edition* **2016,** *55* (45), 14090-14095.

51. Badea, E.; Gatta, G. D.; D'Angelo, D.; Brunetti, B.; Rečková, Z., Odd–even effect in melting properties of 12 alkane-α,ω-diamides. *The Journal of Chemical Thermodynamics* **2006,** *38* (12), 1546-1552.

52. Thalladi, V. R.; Nüsse, M.; Boese, R., The Melting Point Alternation in α,ω-Alkanedicarboxylic Acids. *Journal of the American Chemical Society* **2000,** *122* (38), 9227-9236.

53. Yan, L.; Häußler, M.; Bauer, J.; Mecking, S.; Winey, K. I., Monodisperse and Telechelic Polyethylenes Form Extended Chain Crystals with Ionic Layers. *Macromolecules* **2019,** *52* (13), 4949-4956.

54. Zhang, X.; Zuo, X.; Ortmann, P.; Mecking, S.; Alamo, R. G., Crystallization of Long-Spaced Precision Polyacetals I: Melting and Recrystallization of Rapidly Formed Crystallites. *Macromolecules* **2019,** *52* (13), 4934-4948.

55. Trigg, E. B.; Gaines, T. W.; Maréchal, M.; Moed, D. E.; Rannou, P.; Wagener, K. B.; Stevens, M. J.; Winey, K. I., Self-assembled highly ordered acid layers in precisely sulfonated polyethylene produce efficient proton transport. *Nature Materials* **2018,** *17* (8), 725-731.

56. Rank, C.; Yan, L.; Mecking, S.; Winey, K. I., Periodic Polyethylene Sulfonates from Polyesterification: Bulk and Nanoparticle Morphologies and Ionic Conductivities. *Macromolecules* **2019,** *52* (21), 8466-8475.

57. Shen, C.; Zhao, Q.; Evans, C. M., Ion specific, odd–even glass transition temperatures and conductivities in precise network polymerized ionic liquids. *Molecular Systems Design & Engineering* **2019,** *4* (2), 332-341.

58. Bassett, D. C., Chain-extended polyethylene in context: a review. *Polymer* **1976,** *17* (6), 460-470.

59. Wunderlich, B.; Davidson, T., Extended-chain crystals. I. General crystallization conditions and review of pressure crystallization of polyethylene. *Journal of Polymer Science Part A-2: Polymer Physics* **1969,** *7* (12), 2043-2050.

60. Middleton, L. R.; Trigg, E. B.; Schwartz, E.; Opper, K. L.; Baughman, T. W.; Wagener, K. B.; Winey, K. I., Role of periodicity and acid chemistry on the morphological evolution and strength in precise polyethylenes. *Macromolecules* **2016,** *49* (21), 8209-8218.

61. Smith, M. K.; Northrop, B. H., Vibrational Properties of Boroxine Anhydride and Boronate Ester Materials: Model Systems for the Diagnostic Characterization of Covalent Organic Frameworks. *Chemistry of Materials* **2014,** *26* (12), 3781-3795.

62. Springsteen, G.; Wang, B., A detailed examination of boronic acid–diol complexation. *Tetrahedron* **2002,** *58* (26), 5291-5300.

63. Flory, P. J., *Principles of polymer chemistry*. Cornell University Press: 1953.

64. Loo, Y.-L.; Register, R. A.; Ryan, A. J., Polymer Crystallization in 25-nm Spheres. *Physical Review Letters* **2000,** *84* (18), 4120-4123.

65. Mandelkern, L., Crystallization kinetics of homopolymers: overall crystallization: a review. *Biophysical Chemistry* **2004,** *112* (2), 109-116.

66. Alfonso, G. C.; Pedemonte, E.; Ponzetti, L., Mechanism of densification and crystal perfection of poly(ethylene terephthalate). *Polymer* **1979,** *20* (1), 104-112.

67. Zhuravlev, E.; Madhavi, V.; Lustiger, A.; Androsch, R.; Schick, C., Crystallization of Polyethylene at Large Undercooling. *ACS Macro Letters* **2016,** *5* (3), 365-370.

68. Tian, M.; Loos, J., Investigations of morphological changes during annealing of polyethylene single crystals. *Journal of Polymer Science Part B: Polymer Physics* **2001,** *39* (7), 763-770.

69. Moyses, S. C.; Zukermann-Schpector, J., Annealing in Low Density Polyethylene at Several Temperatures. *Polymer Journal* **2004,** *36* (9), 679-683.

70. Holdsworth, P. J.; Turner-Jones, A., The melting behaviour of heat crystallized poly(ethylene terephthalate). *Polymer* **1971,** *12* (3), 195-208.

71. Hiramatsu, N.; Hirakawa, S., Melting Behavior of Poly(ethylene terephthalate) Crystallized and Annealed under Elevated Pressure. *Polymer Journal* **1980,** *12* (2), 105-111.

72. Nealy, D. L.; Davis, T. G.; Kibler, C. J., Thermal history and melting behavior of poly(ethylene terephthalate). *Journal of Polymer Science Part A-2: Polymer Physics* **1970,** *8* (12), 2141-2151.

73. Mehta, A.; Gaur, U.; Wunderlich, B., Equilibrium melting parameters of poly(ethylene terephthalate). *Journal of Polymer Science: Polymer Physics Edition* **1978,** *16* (2), 289-296.

74. Li, Q.; Zhou, J.; Vatankhah-Varnoosfaderani, M.; Nykypanchuk, D.; Gang, O.; Sheiko, S. S., Advancing Reversible Shape Memory by Tuning the Polymer Network Architecture. *Macromolecules* **2016,** *49* (4), 1383-1391.

75. Ingram, P.; Schindler, A., Morphology of as-polymerized polythylene II. Electron microscopy. *Die Makromolekulare Chemie* **1968,** *111* (1), 267-270.

76. Geil, P. H.; Anderson, F. R.; Wunderlich, B.; Arakawa, T., Morphology of polyethylene crystallized from the melt under pressure. *Journal of Polymer Science Part A: General Papers* **1964,** *2* (8), 3707-3720.

77. Atkinson, C. M. L.; Richardson, M. J., Thermodynamic properties of ideally crystalline polyethylene. *Transactions of the Faraday Society* **1969,** *65* (0), 1764-1773.

78. Tsubakihara, S.; Nakamura, A.; Yasuniwa, M., Hexagonal Phase of Polyethylene Fibers under High Pressure. *Polymer Journal* **1991,** *23* (11), 1317-1324.

79. Bassett, D. C.; Block, S.; Piermarini, G. J., A high-pressure phase of polyethylene and chain-extended growth. *Journal of Applied Physics* **1974,** *45* (10), 4146-4150.

80. Bruno, J. A. O.; Allan, N. L.; Barron, T. H. K.; Turner, A. D., Thermal expansion of polymers: Mechanisms in orthorhombic polyethylene. *Physical Review B* **1998,** *58* (13), 8416-8427.

81. Yamada, K.; Hikosaka, M.; Toda, A.; Yamazaki, S.; Tagashira, K., Equilibrium Melting Temperature of Isotactic Polypropylene with High Tacticity: 1. Determination by Differential Scanning Calorimetry. *Macromolecules* **2003,** *36* (13), 4790-4801.

82. Hoffman, J. D.; Lauritzen, J. I., Jr., Crystallization of Bulk Polymers With Chain Folding: Theory of Growth of Lamellar Spherulites. *J Res Natl Bur Stand A Phys Chem* **1961,** *65A* (4), 297-336.

83. Goldenfeld, N., Theory of spherulitic crystallization. *Journal of Crystal Growth* **1987,** *84* (4), 601-608.

84. Campbell, C. T.; Parker, S. C.; Starr, D. E., The Effect of Size-Dependent Nanoparticle Energetics on Catalyst Sintering. *Science* **2002,** *298* (5594), 811.

85. Wang, S.; Ma, S.; Li, Q.; Yuan, W.; Wang, B.; Zhu, J., Robust, Fire-Safe, Monomer-Recovery, Highly Malleable Thermosets from Renewable Bioresources. *Macromolecules* **2018,** *51* (20), 8001-8012.

86. Lossada, F.; Jiao, D.; Hoenders, D.; Walther, A., Recyclable and Light-Adaptive Vitrimer-Based Nacre-Mimetic Nanocomposites. *ACS nano* **2021**.

87. Cheng, L.; Liu, S.; Yu, W., Recyclable ethylene-vinyl acetate copolymer vitrimer foams. *Polymer* **2021**, 123662.

88. Li, G.; Zhang, P.; Huo, S.; Fu, Y.; Chen, L.; Wu, Y.; Zhang, Y.; Chen, M.; Zhao, X.; Song, P., Mechanically Strong, Thermally Healable, and Recyclable Epoxy Vitrimers Enabled by ZnAl-Layer Double Hydroxides. *ACS Sustainable Chemistry & Engineering* **2021,** *9* (6), 2580-2590.

89. Häußler, M.; Eck, M.; Rothauer, D.; Mecking, S., Closed-loop recycling of polyethylene-like materials. *Nature* **2021,** *590* (7846), 423-427.

CHAPTER 5: EFFECT OF DANGLING CHAINS ON THE CRYSTALLIZATION KINETICS, CRYSTAL STRUCTURE, AND RUBBERY MODULUS OF ETHYLENE VITRIMERS

5.1. Abstract

In this report, we investigate the effect of dangling chain defects on the crystallization kinetics, shear modulus, and the crystal structure of precise ethylene vitrimers. Dangling chain defects are incorporated by precise ratios of difunctional and monofunctional alkane chains with alcohol functional groups which undergo step-growth polymerization in the presence of boric acid. Dangling chains lead to a decrease in the shear modulus as anticipated by the Flory-Stockmayer theory up to a critical concentration, beyond which the network percolation is lost and a steep drop in modulus is observed. Isothermal crystallization at room temperature results in the formation of lamellar crystals with a hexagonal unit cell. X-ray scattering patterns reveal that with increasing concentration of dangling chains results in formation of imperfect crystals. The crystallization kinetics are studied using calorimetry and show an unexpected trend that changes with crystallization temperature. The counterintuitive crystallization kinetics are attributed to the increase in entropy due to the dangling chains.

5.2. Introduction

Vitrimers, polymer networks crosslinked by dynamic covalent bonds, have properties that are intermediate to thermosets and thermoplastics.[1-10] Dynamic bonds undergo reversible exchange reactions that impart an additional degree of freedom to the network strand, allowing them to reorganize and relax stresses. Vitrimers have been extensively studied in the past decade

due to their unique self-healing and reprocessability. Depending on the chemistry and the architecture of the networks, some vitrimers can be dissolved in solvents to retrieve their monomer constituents.[11, 12] These properties make vitrimers attractive materials to replace commodity polymers as the need for sustainable plastics continues to grow. In parallel to the need to develop novel polymers, management of plastic waste is a major social and scientific challenge. One of the many approaches used to tackle this problem is to chemically modify waste plastics to make higher-value products[13] and in the last few years, vitrimerization[14-17] has been used to convert thermoset waste to recyclable and reprocessable polymers. Two key issues must be addressed with vitrimer approaches to sustainability. First, many relevant polymers are semi-crystalline and an understanding of how dynamic bonds impact crystallization is lacking. Second, a common drawback with recycling and reprocessing is the incorporation of defects or impurities into the polymer chemistry or architecture that degrade the performance of the plastics compared to their virgin form.[18] If vitrimers are to replace commodity plastics and be used as recyclable and reprocessable materials, understanding the role of defects on crystallinity and material properties will be critical.

Topological defects like dangling chains and loops in polymer networks have been shown to reduce the fracture toughness and fatigue performance.[19, 20] The swelling of polymer networks which influences properties like mass transport and elasticity has also been shown to change due to topological defects,[21] these properties are crucial for drug delivery and tissue engineering application. In semi-crystalline polymer, defects can influence crystal structure,[22] crystallization kinetics, and melting temperatures.[23] Dangling chain defects and loops impact the elasticity of polymer networks and numerous theoretical models have been proposed to

predict how loops modify the modulus in polymer network, including the recent RENT theory.[24]

Precise ethylene vitrimers with an exact number of methyl groups between boronic ester junctions were previously synthesized to study their rheology[25] and crystallization.[26] Here, a series of C12 ethylene vitrimer, dynamically crosslinked networks with exactly 12 carbons between boronic ester junctions with an increasing percentage of dangling chain defects are synthesized. We track the effect of dangling chains on the shear modulus, isothermal crystallization kinetics, and the crystal structure of the networks. Dangling chains are incorporated by replacing alkane diols with mono functional alcohols as shown in **Fig 5.1**, and the synthesis protocol is detailed in our previous work. The shear modulus decreases with increasing defects and follows a predictable trend up to a critical defect concentration beyond which a steep drop is observed. The drop is attributed to a loss in network percolation. At room temperature the crystallization kinetics decrease with increasing defect concentration, this counterintuitive observation is attributed to the higher entropy of dangling chains that retard crystal growth. With decreasing temperature, this trend reverse, and a clear crossover in kinetics is observed. The incorporation of defects does not affect the density of the crystals, as is evident from the consistent peak positions in the wide angle x-ray scattering (WAXS) patterns, but comparing the intensity of the peaks indicates increasing disordered of the ethylene chains.

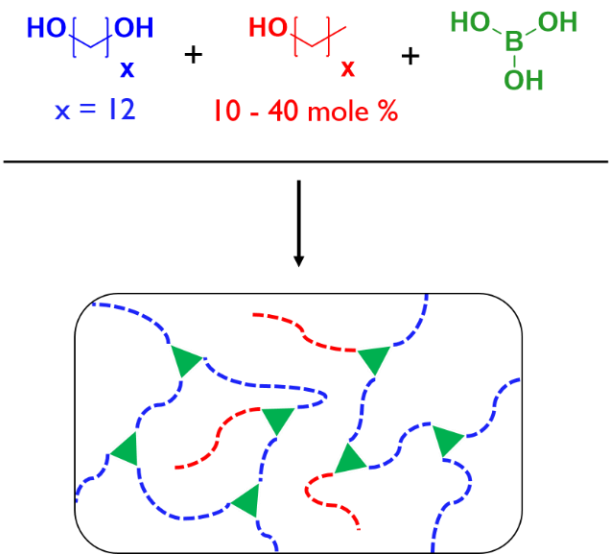

Figure 5.1. Schematic representation of the C12 ethylene vitrimer with dangling chain defects. Using mono and di-functional aliphatic alcohols, a series of precise ethylene vitrimers (C12) with an exact percentage of dangling chain defects were synthesized using a protocol previously shown.[25, 26] Stoichiometric amount of boric acid is added to the mix, such that there are no unreacted diols in the network.

5.3. Results and Discussion

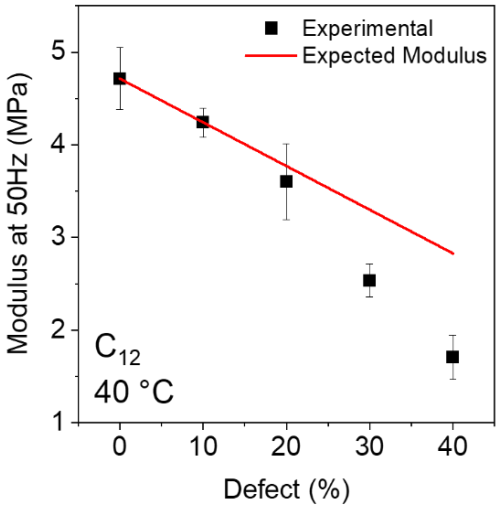

Figure 5.2. The rubbery plateau modulus for the C12 networks is measured from frequency sweeps at 40 °C. The modulus at 50 Hz is plotted as a function of increasing defect percentage. The red line tracks the expected modulus which is based on the theoretical idea that 10% dangling chains should cause the modulus to decrease by 10% from its no defect baseline value. The experimental data track well with the prediction of up to 20% defect concentration, after which a steep drop in the modulus is observed.

5.3.1. Decrease in Shear Modulus with Increasing Defect Concentration

Oscillatory shear rheology was used to measure the shear modulus of the pure C12 and defected C12 networks. All rheological measured were made on amorphous vitrimer samples. Frequency sweeps were performed at 40 ℃ and the plateau modulus in the high frequency range was used to calculate the rubbery plateau modulus. The theoretical modulus of a polymer network with a 12 carbon length linker is estimated using the affine and the phantom networks theory. Using amorphous polyethylene to approximate the density of amorphous C12 vitrimers, we calculate a rubbery modulus of 12.6 MPa and 4.2 MPa for the affine and phantom models respectively.[27] Numerous studies on polymer networks have shown the experimental modulus often lies between these two theoretical predictions. For the C12 network, the experimental modulus is closer to the phantom network prediction with an average value of 4.7 MPa.

With increasing dangling chain concentration, a monotonic decrease in the rubbery plateau modulus is observed (**Fig 5.2**). A dangling chain is an elastically inactive chain, it is connected to the network at only one end and thus cannot transfer strain or store energy, hence a decrease in modulus is expected with the incorporation of these defects. The affine and the phantom network theory have a common underlying assumption, the modulus of a rubbery network is directly proportional to the number of elastically active strands. If the shear modulus of the pure C12 network is taken as the baseline, a simple calculation allows us to predict the effect of dangling chains on the modulus. For example, the incorporation of 10% dangling chains would result in a 10% decrease in the total number of the elastically active strand, which based on the proportionality assumption should decrease the modulus by 10%. When the experimental modulus is plotted vs defect concentration (Figure 2), we see that the experimental values track

well with the prediction up to 20% defect concentration, The modulus of the 30% and 40% defect samples deviate from the prediction line, and show a steep drop. We suspect this is due to the loss of percolation at a critical dangling chain concentration. Using the Flory-Stockmayer percolation theory, the required fractional conversion for percolation in a stoichiometric A_3 (trifunctional *A* units) – B_2 (di-functional *B* units) system is calculated to be approximately 70%.[28, 29] For the ethylene vitrimer which is an $A_3 – B_2$ system, a critical conversion of 70% would indicate percolation would be lost if the dangling chain concentration goes beyond 30%. This matches well with the observed modulus values.

5.3.2. Effect of Defect Concentration on Crystallization Kinetics

Differential scanning calorimetry (DSC) was used to study the crystallization kinetics of the C12 vitrimers. Samples were isothermally crystallized at different crystallization temperatures (T_c) for a specific time (**Fig 5.3a, 5.3c**) and then heated at 20 ℃/min to get the corresponding melting curves (**Fig 5.3b, 5.3d**). The half time of crystallization ($t_{1/2}$) was used as a parameter to compare crystallization kinetics. For the $t_{1/2}$ measurement, samples were allowed to completely crystallize, which we define as the time at which the heat flow curve returns to the baseline after going through the exothermic peak. At T_c = 20 ℃ and 30 ℃, a monotonic decrease in crystallization kinetics with increasing defect concentration is observed. This is a counterintuitive observation as the conventional expectation would be to see an increase in nucleation and growth kinetics due to the higher mobility of dangling chain defects. When crystallization is carried out at a lower temperature of 0 ℃ and 10 ℃, the kinetics trend reverses and follows the expected increase with increasing defect concentration.

A similar observation in crystallization kinetics was reported by Dalnoki-Veress and coworkers. Binary blends of low and high molecular weight polyethylene oxide (PEO) showed non-monotonic crystallization kinetics with an increasing fraction of smaller chains.[30] The authors attribute the decrease in kinetics to the higher entropy of small PEO chains compared to the long chains. Smaller chains have a higher energy barrier to crystallization and thus retards crystal growth. In the ethylene vitrimers, dangling chains are effectively high entropy defects and could have a similar effect as the small chain PEO. This would explain the decrease in kinetics with increasing defect concentration. The Dalnoki-Veress group also argues that as T_c is lowered, crystallization takes place at a higher growth rate that results in the formation of imperfect crystals and imperfect crystals are less sensitive to entropic defects. This can explain why the crystallization trends reverse at lower T_c.

In contrast to crystallization kinetics, the melting temperatures show a monotonic decrease with increasing defect concentration, irrespective of the crystallization temperature. This is expected as crystals with defects should have a higher Gibbs free energy and thus a lower T_m.[31]

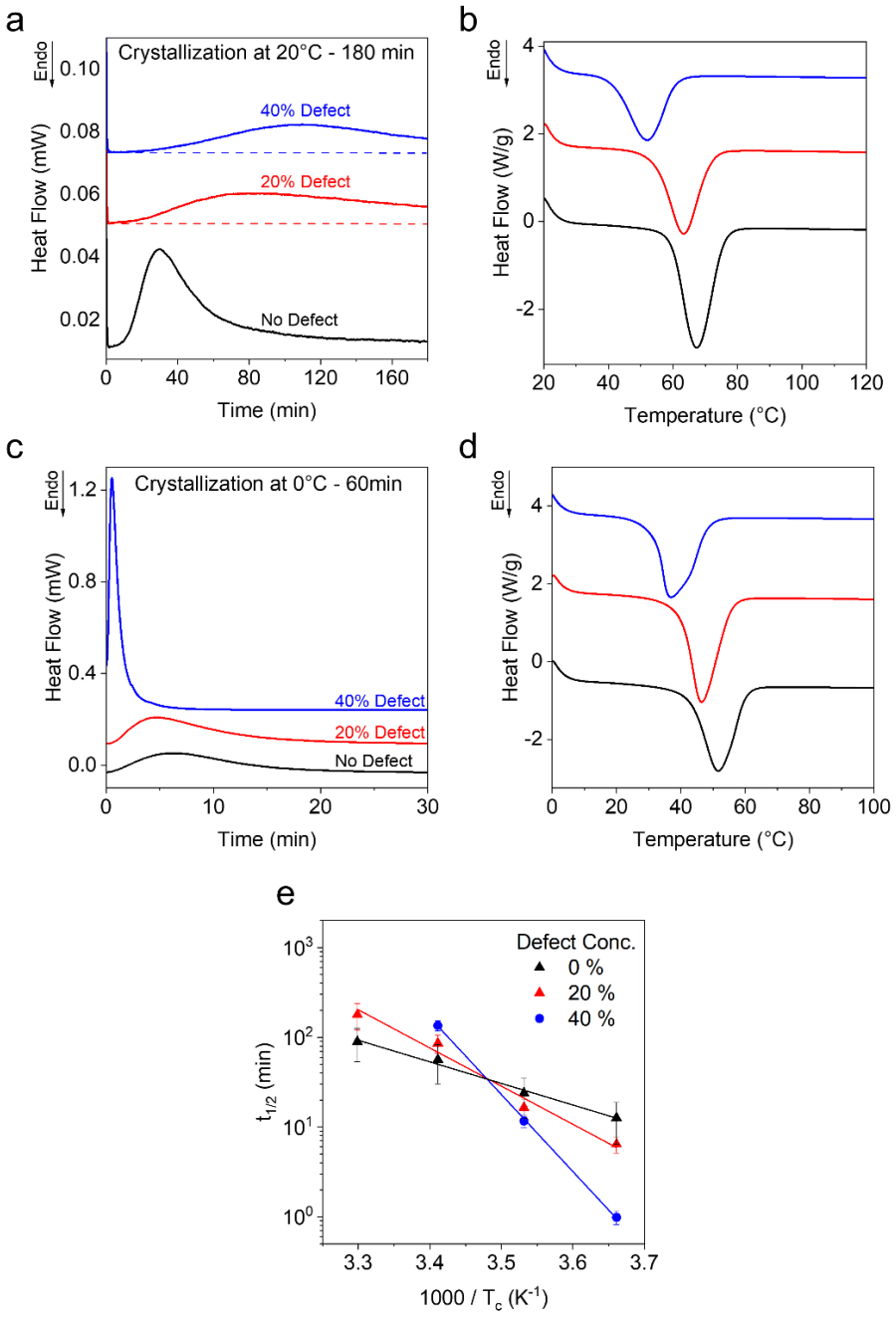

Figure 5.3. (a) Heat flow vs time for isothermal crystallization at 20 °C for 60 min and (b) the corresponding heating curves. (c) Heat flow vs time for isothermal crystallization at 0 °C for 180 min and (d) the corresponding heating curves. (e) Half time of crystallization ($t_{1/2}$) vs inverse crystallization temperature for the 0%, 20%, and 40% defect networks. A clear crossover of the $t_{1/2}$ is seen at ~ 14 °C.

5.3.3. Incorporation of Defects Results in the Formation of Imperfect Crystals

Vitrimer samples were isothermally crystallized for 1 day at room temperature (RT) and wide angle x-ray scatter (WAXS) patterns were collected (**Fig 5.4**). As shown in our previous work[26], ethylene vitrimers show two peaks in the WAXS region. The first at q ~ 3.7 nm^{-1} corresponds to the boron-boron correlation peak which is dependent on the length of the carbon linker and the second at q ~ 15.4 nm^{-1} corresponds to the hexagonal arrangement of the ethylene chains.

When the scattering intensities are normalized by the intensity of the hexagonal peak, a monotonic decrease in the height of the low *q* peak is observed. This decrease is be attributed to two sources. With increasing dangling chains, the concentration of boron in the networks decreases. In the 40% defect network the boron content reduces by ~20%. But at the same defect concentration, the decrease in peak intensity is ~60%. Thus, the lower boron content cannot completely account for the decrease in peak height. We believe that the dangling chains are poorly organized within the hexagonal crystals due to reduced spatial constraint, as these chains are connected to the network at one end. The imperfect organization results in a decrease in scattering intensity. This observation also provides evidence that the networks with defects form imperfect crystals and validates the decrease in T_m with increasing defect concentration as shown in the DSC plots.

The *q* position of both peaks does not change with increasing defect concentration, indicating that the density of the crystals is the same for all samples. The corresponding d spacing was calculated using the simple conversion $d = 2\pi/q$, and the correlation length of the crystals was

calculated using the Scherrer equation $\varepsilon = 2\pi/\Delta q$ where Δq is the full width at half maximum of the peak. Values are reported in Table 2. For the low q peak, the d spacing is slightly shorter than the all-trans configuration of the C12 ethylene. The correlation lengths (ε) corresponding to both peak shows a slight increase with increasing defects concentration and indicates an increase in the size of the lamella stacks and the hexagonal crystals.

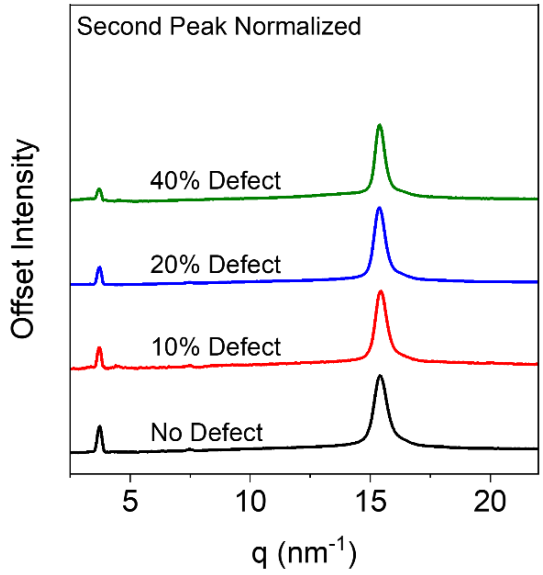

Figure 5.4. WAXS spectra collected after 1 day of isothermal crystallization at room temperature. The overall intensity has been normalized by the intensity of the highest peak. The spectra show a high q peak at ~15.4 nm^{-1} which corresponds to the hexagonal crystal phase and a low q peak at ~3.7 nm^{-1} which corresponds to the boron-boron correlation along the length of the linker. The intensity of the low q peak decreases with increasing defect concentration, indicating a loss of correlation between the boron. This is suspected to be due to the imperfect orientation of the dangling chains within the hexagonal crystals.

Table 5.1. Location of q scattering peak and analysis of d-spacing and peak width using the Scherrer equation.

Sample (C_{12})	Low q			High q		
	q (nm^{-1})	d (nm)	ε (nm)	q (nm^{-1})	d (nm)	ε (nm)
No Defects	3.73	1.68	31.4	15.4	0.4	9.8
10% Defect	3.73	1.68	35.9	15.4	0.4	11.3
20% Defect	3.73	1.68	33.7	15.3	0.4	11.6
40% Defect	3.69	1.70	33.9	15.4	0.4	13.5

5.4. Conclusions

We synthesized a series of precise ethylene vitrimer with an exact percentage of dangling chain defects. Oscillatory shear measurements show a monotonic decrease in the rubbery plateau modulus with increasing defect concentration, the decrease is predicted well from theory but deviates when the network percolation is lost. Calorimetry reveals an unexpected trend in the crystallization kinetics which reverses at lower temperatures and is explained based on the higher entropy and a higher energy barrier for crystallization of the dangling chains. X-ray scattering reveals that the boron correlation that is coupled with the orientation of the ethylene backbone decrease with increasing dangling chains, which indicates an imperfect organization of the ethylene linkers in the hexagonal crystals. Our results show that defects can dramatically change the properties of vitrimer and understanding how defects affect vitrimer properties will be critical to the design, processing, and use of vitrimers as sustainable alternatives to commodity plastics.

5.5. References

1. Luo, J.; Demchuk, Z.; Zhao, X.; Saito, T.; Tian, M.; Sokolov, A. P.; Cao, P.-F., Elastic vitrimers: Beyond thermoplastic and thermoset elastomers. *Matter* **2022,** *5* (5), 1391-1422.

2. Porath, L.; Soman, B.; Jing, B. B.; Evans, C. M., Vitrimers: Using Dynamic Associative Bonds to Control Viscoelasticity, Assembly, and Functionality in Polymer Networks. *ACS Macro Letters* **2022,** *11* (4), 475-483.

3. Denissen, W.; Winne, J. M.; Du Prez, F. E., Vitrimers: permanent organic networks with glass-like fluidity. *Chemical science* **2016,** *7* (1), 30-38.

4. Brutman, J. P.; Delgado, P. A.; Hillmyer, M. A., Polylactide vitrimers. *ACS Macro letters* **2014,** *3* (7), 607-610.

5. Röttger, M.; Domenech, T.; van der Weegen, R.; Breuillac, A.; Nicolaÿ, R.; Leibler, L., High-performance vitrimers from commodity thermoplastics through dioxaborolane metathesis. *Science* **2017,** *356* (6333), 62-65.

6. Montarnal, D.; Capelot, M.; Tournilhac, F.; Leibler, L., Silica-like malleable materials from permanent organic networks. *Science* **2011,** *334* (6058), 965-968.

7. Van Lijsebetten, F.; De Bruycker, K.; Spiesschaert, Y.; Winne, J. M.; Du Prez, F. E., Suppressing Creep and Promoting Fast Reprocessing of Vitrimers with Reversibly Trapped Amines. *Angewandte Chemie International Edition* **2022,** *61* (9), e202113872.

8. Li, L.; Chen, X.; Jin, K.; Torkelson, J. M., Vitrimers designed both to strongly suppress creep and to recover original cross-link density after reprocessing: Quantitative theory and experiments. *Macromolecules* **2018,** *51* (15), 5537-5546.

9. Guerre, M.; Taplan, C.; Winne, J. M.; Du Prez, F. E., Vitrimers: directing chemical reactivity to control material properties. *Chemical science* **2020,** *11* (19), 4855-4870.

10. Alabiso, W.; Schlögl, S., The impact of vitrimers on the industry of the future: Chemistry, properties and sustainable forward-looking applications. *Polymers* **2020,** *12* (8), 1660.

11. Zhang, X.; Eichen, Y.; Miao, Z.; Zhang, S.; Cai, Q.; Liu, W.; Zhao, J.; Wu, Z., Novel Phosphazene-Based flame retardant polyimine vitrimers with Monomer-Recovery and high performances. *Chemical Engineering Journal* **2022,** *440*, 135806.

12. Jing, B. B.; Evans, C. M., Catalyst-free dynamic networks for recyclable, self-healing solid polymer electrolytes. *Journal of the American Chemical Society* **2019,** *141* (48), 18932-18937.

13. Chen, X.; Wang, Y.; Zhang, L., Recent progress in the chemical upcycling of plastic wastes. *ChemSusChem* **2021,** *14* (19), 4137-4151.

14. Kar, G. P.; Saed, M. O.; Terentjev, E. M., Scalable upcycling of thermoplastic polyolefins into vitrimers through transesterification. *Journal of Materials Chemistry A* **2020,** *8* (45), 24137-24147.

15. Yue, L.; Bonab, V. S.; Yuan, D.; Patel, A.; Karimkhani, V.; Manas-Zloczower, I., Vitrimerization: A novel concept to reprocess and recycle thermoset waste via dynamic chemistry. *Global Challenges* **2019,** *3* (7), 1800076.

16. Nicolas, S.; Richard, T.; Dourdan, J.; Lemiegre, L.; Audic, J. L., Shape memory epoxy vitrimers based on waste frying sunflower oil. *Journal of Applied Polymer Science* **2021,** *138* (36), 50904.

17. Imbernon, L.; Norvez, S., From landfilling to vitrimer chemistry in rubber life cycle. *European Polymer Journal* **2016,** *82*, 347-376.

18. La Mantia, F. P., Polymer mechanical recycling: Downcycling or upcycling? *Progress in Rubber Plastics and Recycling Technology* **2004,** *20* (1), 11-24.

19. Alamé, G.; Brassart, L., Effect of topological defects on the elasticity of near-ideal polymer networks. *Journal of Applied Mechanics* **2020,** *87* (12).

20. Lin, S.; Ni, J.; Zheng, D.; Zhao, X., Fracture and fatigue of ideal polymer networks. *Extreme Mechanics Letters* **2021,** *48*, 101399.

21. Rebello, N. J.; Beech, H. K.; Olsen, B. D., Adding the Effect of Topological Defects to the Flory–Rehner and Bray–Merrill Swelling Theories. *ACS Macro Letters* **2021,** *10* (5), 531-537.

22. De Rosa, C.; Auriemma, F.; Malafronte, A.; Scoti, M., Crystal structures and polymorphism of polymers: Influence of defects and disorder. *Polymer Crystallization* **2018,** *1* (4), e10015.

23. Wunderlich, B., The melting of defect polymer crystals. *Polymer* **1964,** *5*, 611-624.

24. Zhong, M.; Wang, R.; Kawamoto, K.; Olsen, B. D.; Johnson, J. A., Quantifying the impact of molecular defects on polymer network elasticity. *Science* **2016,** *353* (6305), 1264-1268.

25. Soman, B.; Evans, C. M., Effect of precise linker length, bond density, and broad temperature window on the rheological properties of ethylene vitrimers. *Soft Matter* **2021,** *17* (13), 3569-3577.

26. Soman, B.; Go, Y. K.; Shen, C.; Leal, C.; Evans, C. M., Impact of dynamic covalent chemistry and precise linker length on crystallization kinetics and morphology in ethylene vitrimers. *Soft Matter* **2022,** *18* (2), 293-303.

27. Flory, P. J., Molecular theory of rubber elasticity. *Polymer journal* **1985,** *17* (1), 1-12.

28. Flory, P. J., Molecular size distribution in three dimensional polymers. I. Gelation1. *Journal of the American Chemical Society* **1941,** *63* (11), 3083-3090.

29. Stauffer, D.; Coniglio, A.; Adam, M., Gelation and critical phenomena. In *Polymer networks*, Springer: 1982; pp 103-158.

30. Carvalho, J. L.; Cormier, S. L.; Lin, N.; Dalnoki-Veress, K., Crystal growth rate in a blend of long and short polymer chains. *Macromolecules* **2012,** *45* (3), 1688-1691.

31. Martuscelli, E., A review of the properties of polymer single crystals with defects within the macromolecular chain. *Journal of Macromolecular Science, Part B: Physics* **1975,** *11* (1), 1-20.

CHAPTER 6: FUTURE DIRECTIONS AND OUTLOOK

6.1. Viscoelasticity in Vitrimers

The past decade has seen a large variety of dynamic bonds incorporated into a range of polymer matrices including commodity polymers like ethylene,[31] and Arrhenius behavior of stress relaxation times or viscosities has been observed with activation energies typically spanning ~ 30 – 160 kJ/mol,[32-36] although values greater than 300 kJ/mol have been reported.[37] Adding a catalyst decreases the relaxation time and can also change the activation energy (**Figure 2b**). [32, 35, 38-48] The Arrhenius dependence of viscosity or macroscopic stress relaxation time has also been observed in networks with dissociative bonds,[32, 49-55] raising the question of how the mechanism of bond exchange gives rise to the temperature-dependent viscosity.

In addition to bulk relaxation, dynamic processes can impact polymer networks over a broad range of time and length scales. The quantitative relationship between the macroscopic timescale for self-healing or reprocessing of vitrimers and the timescale for bond exchange is not well understood. For example, Guan and coworkers examined two crosslinkers for boronic ester networks that differed by the presence of a neighboring group which destabilized the dynamic bond and led to faster exchange reactions.

An unresolved question for dynamic network classification is if they all sit on some spectrum ranging from linear stiffening with temperature ($G \sim \nu kT$, where G is the storage modulus (G), ν is the network strands per volume, k is the Boltzmann constant, and T is temperature) to decreasing modulus when network crosslinks dissociate. More investigations into the rheological properties of associative and dissociative networks are needed, with an emphasis on temperature-dependent moduli and viscosity profiles. A systematic study between networks of identical

polymer linkers crosslinked using either dissociative or associative crosslinkers (with similar kinetics and activation energies) would provide much needed results on how their viscoelastic properties differ with temperature and time. Investigating the placement of dynamic bonds within the network, for example in telechelic linkers or in strands with multiple crosslinks per chain, will also be crucial to developing molecular-scale structure property relationships.

Control of the relaxation spectrum and tan δ peaks has been demonstrated in soft hydrogels using a combination of metal ions which lead to different exchange rates with organic ligands.[57] Two tan δ peaks were observed in these metallogels (a dissociative dynamic network) when two different metal ions were used, but not in boronic ester hydrogels with two kinetically distinct dynamic bonds.[58] Dry vitrimers have also used kinetically different bonds[59] and showed either one or three modes depending on the difference between the bond relaxation timescales. Mixed networks with both associative and dissociative bonds have also been explored recently with mixed systems tending to have faster network relaxation times than the corresponding pure systems.[60-63] Our understanding of how multiple dynamic bonds give rise to multiple peaks in a damping spectrum is still limited. Some work has implicated dynamic bonds as an efficient route to shockwave energy dissipation (~1 GPa peak pressure in ~10 ns),[64] where the dissipation increased as more dynamic bonds were incorporated into the network. More work is needed to make quantitative comparisons between bond exchange rates and the timescale of the input pressure wave. Precise selection of the dynamic bonds, polymer chemistry, and presence of multiple dynamic moieties could be utilized to design materials for a range of damping applications, in addition to the aforementioned T_g and copolymerization strategies, which will ultimately provide even greater tunability.

6.2. Self-Assembly in Vitrimers

Much of the work to date on vitrimers has focused on their dynamic properties (such as stress relaxation times or viscosities) as well as the mechanical properties before and after recycling. Most vitrimers are studied in the amorphous state, but recent investigations have probed how dynamic bonds impact the nanostructure, including phase separation [1-7] and crystallization [8-12]. If vitrimers are slated to be replacements for commodity plastics, an improved understanding of assembly, crystallization, and phase separation is needed for the broad range of polymer applications. One of the earliest examples of was in polyethylene vitrimers which have been shown to form nanoscale clusters of the dioxaborolane crosslinking moieties within the incompatible matrix which provides additional crosslinking and impacts the stress relaxation of the network.[1, 7] Understanding when the dynamic bonds will phase separate from the matrix is critical for the interpretation of stress relaxation and self-healing investigations.

While the crystallization of polymers has been heavily investigated for decades, melting temperatures (T_m) have only been reported in a limited number of vitrimers based on PE, [8, 9] PDMS,[10] poly(butylene terephthalate),[11] and poly(butylene succinate).[12] It has recently been reported that the presence of dynamic bonds in vitrimers allows for crystallization which is not possible in a permanent network with the same linker.[8] The concomitant increases in percent crystallinity and enthalpy of fusion (relative to the permanent network) will lead to large effects on other properties such as thermal conductivity.[13] Quantitatively relating the bond exchange processes to the kinetics of crystallization and T_m evolution is an outstanding challenge.

The linking of two immiscible polymers to form a block copolymer (BCP) can lead to microphase separation in a wide array of nanostructures depending on the composition, architecture, and incompatibility of the blocks. [14, 15] This thermodynamically driven polymer self-assembly is a critical aspect of many current and emerging technologies including nanolithography, [16, 17] toughened rubbers and epoxies,[18] battery electrolytes, [19, 20] and photonic materials. [21] Block copolymers containing one block which can participate in associative dynamic bonding have recently been investigated and can self-assemble at the nanoscale.[22] The resulting self-assembled structures have been shown to reduce macroscopic flow (creep) in vitrimer block copolymer relative to a statistical copolymer with the same monomers and dynamic bond densities. Such studies build upon the work of block polymers containing permanently crosslinked blocks which display rich physics distinct from linear AB type diblocks.[23-25] It will be important to understand how bond exchange impacts the kinetics of assembly and alignment in these systems relative to permanently crosslinked diblocks, as well as linear block polymers, which can be investigated via shear alignment[26] solvent annealing, [27] use of magnetic or electric fields,[28] and graphoepitaxy.[29, 30]

One of the open questions for vitrimers is how phase separated domains and crystallites will impact dynamic bond exchange if they sit within or at the interface of the crystalline regions. The local environment of the bond may impact the stress relaxation and may lead to a reduction in creep of the network. An understanding of how the distribution of amorphous and crystalline regions impacts vitrimer static and dynamic properties is also currently lacking. Most vitrimers are comprised of distributions in linker lengths, and the role of precise lengths may give rise to odd-even effects on T_m and crystallinity. Key scientific questions for dynamic diblocks center around the role of bond exchange on the assembly and alignment processes. In

addition to the aforementioned crosslinked blocks, another iteration where a single dynamic bond is placed at the junction may lead to large effects on the kinetics of phase separation. Depending on the choice of dynamic bond, diblocks could be forced to only form AB linkages or to sample a combination of AA, AB, and BB in a binary system. Diblocks with a single dynamic junction may always favor macrophase separation, and a judicious combination of permanent and dynamic junctions may be required to stabilize the microphases. Understanding self-assembly in block copolymers with dynamic junctions could also inform the design of multistrand vitrimers leading to greater control and tunability of the static and dynamic properties. Knowledge of how to elicit or suppress macrophase separation in dynamic networks will be critical in these cases.

6.3. Conclusion

Vitrimers open a vast rheological design space, with tunability not present in linear polymers, permanently crosslinked networks, or even dissociative dynamic networks that could be essential for unprecedented control of polymer modulus and viscosity. Key open questions remain, including the role of associative versus dissociative bonding on a broad range of macroscopic properties. The dynamic nature of vitrimers is also important for tuning and understanding self-assembly in crystallizable or multicomponent systems where heterogeneity may play a major role in structural and dynamic phenomena. For adoption into real-world applications, the interplay between polymer chemistry and dynamic bonds should be leveraged to design next generation functional materials including electrolytes, damping materials, and stimuli-responsive systems.

6.4. References

1. Ricarte, R. G.; Tournilhac, F.; Leibler, L., Phase Separation and Self-Assembly in Vitrimers: Hierarchical Morphology of Molten and Semicrystalline Polyethylene/Dioxaborolane Maleimide Systems. *Macromolecules* **2019,** *52* (2), 432-443.

2. Breuillac, A.; Caffy, F.; Vialon, T.; Nicolaÿ, R., Functionalization of polyisoprene and polystyrene via reactive processing using azidoformate grafting agents, and its application to the synthesis of dioxaborolane-based polyisoprene vitrimers. *Polymer Chemistry* **2020,** *11* (40), 6479-6491.

3. Ling, F.; Liu, Z.; Chen, M.; Wang, H.; Zhu, Y.; Ma, C.; Wu, J.; Huang, G., Compatibility driven self-strengthening during the radical-responsive remolding process of poly-isoprene vitrimers. *Journal of Materials Chemistry A* **2019,** *7* (44), 25324-25332.

4. Maaz, M.; Riba-Bremerch, A.; Guibert, C.; Van Zee, N. J.; Nicolaÿ, R., Synthesis of Polyethylene Vitrimers in a Single Step: Consequences of Graft Structure, Reactive Extrusion Conditions, and Processing Aids. *Macromolecules* **2021,** *54* (5), 2213-2225.

5. Niu, W.; Zhang, Z.; Chen, Q.; Cao, P.-F.; Advincula, R. C., Highly Recyclable, Mechanically Isotropic and Healable 3D-Printed Elastomers via Polyurea Vitrimers. *ACS Materials Letters* **2021,** *3* (8), 1095-1103.

6. Peng, L.-M.; Xu, Z.; Wang, W.-Y.; Zhao, X.; Bao, R.-Y.; Bai, L.; Ke, K.; Liu, Z.-Y.; Yang, M.-B.; Yang, W., Leakage-Proof and Malleable Polyethylene Wax Vitrimer Phase Change Materials for Thermal Interface Management. *ACS Applied Energy Materials* **2021,** *4* (10), 11173-11182.

7. Ricarte, R. G.; Tournilhac, F.; Cloître, M.; Leibler, L., Linear viscoelasticity and flow of self-assembled vitrimers: the case of a polyethylene/dioxaborolane system. *Macromolecules* **2020,** *53* (5), 1852-1866.

8. Soman, B.; Go, Y. K.; Shen, C. T.; Leal, C.; Evans, C. M., Impact of dynamic covalent chemistry and precise linker length on crystallization kinetics and morphology in ethylene vitrimers. *Soft Matter* **2021**.

9. Caffy, F.; Nicolay, R., Transformation of polyethylene into a vitrimer by nitroxide radical coupling of a bis-dioxaborolane. *Polymer Chemistry* **2019,** *10* (23), 3107-3115.

10. Porath, L. E.; Evans, C. M., Importance of Broad Temperature Windows and Multiple Rheological Approaches for Probing Viscoelasticity and Entropic Elasticity in Vitrimers. *Macromolecules* **2021,** *54* (10), 4782-4791.

11. Demongeot, A.; Groote, R.; Goossens, H.; Hoeks, T.; Tournilhac, F.; Leibler, L., Cross-Linking of Poly(butylene terephthalate) by Reactive Extrusion Using Zn(II) Epoxy-Vitrimer Chemistry. *Macromolecules* **2017,** *50* (16), 6117-6127.

12. Yin, Y.; Yang, J.; Meng, L. H., Preparation of poly(butylene succinate) vitrimer with thermal shape stability via transesterification reaction. *J Appl Polym Sci* **2021,** *138* (39).

13. Lv, G. X.; Soman, B.; Shan, N. S.; Evans, C. M.; Cahill, D. G., Effect of Linker Length and Temperature on the Thermal Conductivity of Ethylene Dynamic Networks. *Acs Macro Letters* **2021,** *10* (9), 1088-1093.

14. Lodge, T. P., Block Copolymers: Long-Term Growth with Added Value. *Macromolecules* **2020,** *53* (1), 2-4.

15. Bates, F. S.; Hillmyer, M. A.; Lodge, T. P.; Bates, C. M.; Delaney, K. T.; Fredrickson, G. H., Multiblock Polymers: Panacea or Pandora's Box? *Science* **2012,** *336* (6080), 434-440.

16. Bates, C. M.; Seshimo, T.; Maher, M. J.; Durand, W. J.; Cushen, J. D.; Dean, L. M.; Blachut, G.; Ellison, C. J.; Willson, C. G., Polarity-Switching Top Coats Enable Orientation of Sub-10-nm Block Copolymer Domains. *Science* **2012,** *338* (6108), 775-779.

17. Bang, J.; Jeong, U.; Ryu, D. Y.; Russell, T. P.; Hawker, C. J., Block Copolymer Nanolithography: Translation of Molecular Level Control to Nanoscale Patterns. *Advanced Materials* **2009,** *21* (47), 4769-4792.

18. Thompson, Z. J.; Hillmyer, M. A.; Liu, J.; Sue, H. J.; Dettloff, M.; Bates, F. S., Block Copolymer Toughened Epoxy: Role of Cross-Link Density. *Macromolecules* **2009,** *42* (7), 2333-2335.

19. Singh, M.; Odusanya, O.; Wilmes, G. M.; Eitouni, H. B.; Gomez, E. D.; Patel, A. J.; Chen, V. L.; Park, M. J.; Fragouli, P.; Iatrou, H.; Hadjichristidis, N.; Cookson, D.; Balsara, N. P., Effect of molecular weight on the mechanical and electrical properties of block copolymer electrolytes. *Macromolecules* **2007,** *40* (13), 4578-4585.

20. Bouchet, R.; Maria, S.; Meziane, R.; Aboulaich, A.; Lienafa, L.; Bonnet, J. P.; Phan, T. N. T.; Bertin, D.; Gigmes, D.; Devaux, D.; Denoyel, R.; Armand, M., Single-ion BAB triblock copolymers as highly efficient electrolytes for lithium-metal batteries. *Nature Materials* **2013,** *12* (5), 452-457.

21. Kang, Y.; Walish, J. J.; Gorishnyy, T.; Thomas, E. L., Broad-wavelength-range chemically tunable block-copolymer photonic gels. *Nature Materials* **2007,** *6* (12), 957-960.

22. Lessard, J. J.; Scheutz, G. M.; Sung, S. H.; Lantz, K. A.; Epps III, T. H.; Sumerlin, B. S., Block copolymer vitrimers. *Journal of the American Chemical Society* **2019,** *142* (1), 283-289.

23. Hahn, H.; Chakraborty, A. K.; Das, J.; Pople, J. A.; Balsara, N. P., Order-disorder transitions in cross-linked block copolymer solids. *Macromolecules* **2005,** *38* (4), 1277-1285.

24. Gomez, E. D.; Das, J.; Chakraborty, A. K.; Pople, J. A.; Balsara, N. P., Effect of cross-linking on the structure and thermodynamics of lamellar block copolymers. *Macromolecules* **2006,** *39* (14), 4848-4859.

25. Hahn, H.; Eitouni, H. B.; Balsara, N. P.; Pople, J. A., Responsive solids from cross-linked block copolymers. *Phys Rev Lett* **2003,** *90* (15).

26. Newby, G. E.; Hamley, I. W.; King, S. M.; Martin, C. M.; Terrill, N. J., Structure, rheology and shear alignment of Pluronic block copolymer mixtures. *J Colloid Interf Sci* **2009,** *329* (1), 54-61.

27. Li, X.; Peng, J.; Wen, Y.; Kim, D. H.; Knoll, W., Morphology change of asymmetric diblock copolymer micellar films during solvent annealing. *Polymer* **2007,** *48* (8), 2434-2443.

28. Thurn-Albrecht, T.; DeRouchey, J.; Russell, T. P.; Kolb, R., Pathways toward electric field induced alignment of block copolymers. *Macromolecules* **2002,** *35* (21), 8106-8110.

29. Segalman, R. A.; Yokoyama, H.; Kramer, E. J., Graphoepitaxy of spherical domain block copolymer films. *Advanced Materials* **2001,** *13* (15), 1152-+.

30. Bita, I.; Yang, J. K. W.; Jung, Y. S.; Ross, C. A.; Thomas, E. L.; Berggren, K. K., Graphoepitaxy of self-assembled block copolymers on two-dimensional periodic patterned templates. *Science* **2008,** *321* (5891), 939-943.

31. Röttger, M.; Domenech, T.; van der Weegen, R.; Breuillac, A.; Nicolaÿ, R.; Leibler, L., High-performance vitrimers from commodity thermoplastics through dioxaborolane metathesis. *Science* **2017,** *356* (6333), 62-65.

32. Jourdain, A.; Asbai, R.; Anaya, O.; Chehimi, M. M.; Drockenmuller, E.; Montarnal, D., Rheological Properties of Covalent Adaptable Networks with 1,2,3-Triazolium Cross-Links: The Missing Link between Vitrimers and Dissociative Networks. *Macromolecules* **2020,** *53* (6), 1884-1900.

33. Han, J.; Liu, T.; Hao, C.; Zhang, S.; Guo, B.; Zhang, J., A Catalyst-Free Epoxy Vitrimer System Based on Multifunctional Hyperbranched Polymer. *Macromolecules* **2018,** *51* (17), 6789-6799.

34. Lessard, J. J.; Scheutz, G. M.; Hughes, R. W.; Sumerlin, B. S., Polystyrene-Based Vitrimers: Inexpensive and Recyclable Thermosets. *ACS Applied Polymer Materials* **2020,** *2* (8), 3044-3048.

35. Chen, X.; Li, L.; Wei, T.; Venerus, D. C.; Torkelson, J. M., Reprocessable Polyhydroxyurethane Network Composites: Effect of Filler Surface Functionality on Cross-link Density Recovery and Stress Relaxation. *ACS Applied Materials & Interfaces* **2019,** *11* (2), 2398-2407.

36. Brutman, J. P.; Delgado, P. A.; Hillmyer, M. A., Polylactide Vitrimers. *ACS Macro Letters* **2014,** *3* (7), 607-610.

37. Ruiz de Luzuriaga, A.; Solera, G.; Azcarate-Ascasua, I.; Boucher, V.; Grande, H.-J.; Rekondo, A., Chemical control of the aromatic disulfide exchange kinetics for tailor-made epoxy vitrimers. *Polymer* **2022,** *239*, 124457.

38. Zheng, N.; Fang, Z.; Zou, W.; Zhao, Q.; Xie, T., Thermoset Shape-Memory Polyurethane with Intrinsic Plasticity Enabled by Transcarbamoylation. *Angewandte Chemie International Edition* **2016,** *55* (38), 11421-11425.

39. Fortman, D. J.; Brutman, J. P.; Cramer, C. J.; Hillmyer, M. A.; Dichtel, W. R., Mechanically Activated, Catalyst-Free Polyhydroxyurethane Vitrimers. *Journal of the American Chemical Society* **2015,** *137* (44), 14019-14022.

40. Zheng, H.; Liu, Q.; Lei, X.; Chen, Y.; Zhang, B.; Zhang, Q., A conjugation polyimine vitrimer: Fabrication and performance. *Journal of Polymer Science Part A: Polymer Chemistry* **2018,** *56* (22), 2531-2538.

41. Denissen, W.; Rivero, G.; Nicolaÿ, R.; Leibler, L.; Winne, J. M.; Du Prez, F. E., Vinylogous Urethane Vitrimers. *Advanced Functional Materials* **2015,** *25* (16), 2451-2457.

42. Ishibashi, J. S. A.; Kalow, J. A., Vitrimeric Silicone Elastomers Enabled by Dynamic Meldrum's Acid-Derived Cross-Links. *ACS Macro Letters* **2018,** *7* (4), 482-486.

43. Christensen, P. R.; Scheuermann, A. M.; Loeffler, K. E.; Helms, B. A., Closed-loop recycling of plastics enabled by dynamic covalent diketoenamine bonds. *Nature Chemistry* **2019,** *11* (5), 442-448.

44. He, C.; Shi, S.; Wang, D.; Helms, B. A.; Russell, T. P., Poly(oxime–ester) Vitrimers with Catalyst-Free Bond Exchange. *Journal of the American Chemical Society* **2019,** *141* (35), 13753-13757.

45. Cromwell, O. R.; Chung, J.; Guan, Z., Malleable and Self-Healing Covalent Polymer Networks through Tunable Dynamic Boronic Ester Bonds. *Journal of the American Chemical Society* **2015,** *137* (20), 6492-6495.

46. Lu, Y.-X.; Tournilhac, F.; Leibler, L.; Guan, Z., Making Insoluble Polymer Networks Malleable via Olefin Metathesis. *Journal of the American Chemical Society* **2012,** *134* (20), 8424-8427.

47. Self, J. L.; Dolinski, N. D.; Zayas, M. S.; Read de Alaniz, J.; Bates, C. M., Brønsted-Acid-Catalyzed Exchange in Polyester Dynamic Covalent Networks. *ACS Macro Letters* **2018,** *7* (7), 817-821.

48. Capelot, M.; Unterlass, M. M.; Tournilhac, F.; Leibler, L., Catalytic Control of the Vitrimer Glass Transition. *ACS Macro Letters* **2012,** *1* (7), 789-792.

49. Diaz, M. M.; Van Assche, G.; Maurer, F. H. J.; Van Mele, B., Thermophysical characterization of a reversible dynamic polymer network based on kinetics and equilibrium of an amorphous furan-maleimide Diels-Alder cycloaddition. *Polymer* **2017,** *120*, 176-188.

50. Polgar, L. M.; Kingma, A.; Roelfs, M.; van Essen, M.; van Duin, M.; Picchioni, F., Kinetics of cross-linking and de-cross-linking of EPM rubber with thermoreversible Diels-Alder chemistry. *Eur Polym J* **2017,** *90*, 150-161.

51. Sheridan, R. J.; Bowman, C. N., A Simple Relationship Relating Linear Viscoelastic Properties and Chemical Structure in a Model Diels-Alder Polymer Network. *Macromolecules* **2012,** *45* (18), 7634-7641.

52. Kloxin, C. J.; Scott, T. F.; Bowman, C. N., Stress Relaxation via Addition-Fragmentation Chain Transfer in a Thiol-ene Photopolymerization. *Macromolecules* **2009,** *42* (7), 2551-2556.

53. Zhang, Y.; Broekhuis, A. A.; Picchioni, F., Thermally Self-Healing Polymeric Materials: The Next Step to Recycling Thermoset Polymers? *Macromolecules* **2009,** *42* (6), 1906-1912.

54. Adzima, B. J.; Aguirre, H. A.; Kloxin, C. J.; Scott, T. F.; Bowman, C. N., Rheological and Chemical Analysis of Reverse Gelation in a Covalently Cross-Linked Diels-Alder Polymer Network. *Macromolecules* **2008,** *41* (23), 9112-9117.

55. Elling, B. R.; Dichtel, W. R., Reprocessable Cross-Linked Polymer Networks: Are Associative Exchange Mechanisms Desirable? *ACS Central Science* **2020,** *6* (9), 1488-1496.

56. Sperling, L. H., Sound and Vibration Damping with Polymers. In *Sound and Vibration Damping with Polymers*, American Chemical Society: 1990; Vol. 424, pp 5-22.

57. Grindy, S. C.; Learsch, R.; Mozhdehi, D.; Cheng, J.; Barrett, D. G.; Guan, Z.; Messersmith, P. B.; Holten-Andersen, N., Control of hierarchical polymer mechanics with bioinspired metal-coordination dynamics. *Nature Materials* **2015,** *14* (12), 1210-1216.

58. Yesilyurt, V.; Ayoob, A. M.; Appel, E. A.; Borenstein, J. T.; Langer, R.; Anderson, D. G., Mixed Reversible Covalent Crosslink Kinetics Enable Precise, Hierarchical Mechanical Tuning of Hydrogel Networks. *Advanced Materials* **2017,** *29* (19).

59. El-Zaatari, B. M.; Ishibashi, J. S. A.; Kalow, J. A., Cross-linker control of vitrimer flow. *Polymer Chemistry* **2020,** *11* (33), 5339-5345.

60. Zhang, H.; Wang, D.; Wu, N. N.; Li, C. H.; Zhu, C. Z.; Zhao, N.; Xu, J., Recyclable, Self-Healing, Thermadapt Triple-Shape Memory Polymers Based on Dual Dynamic Bonds. *Acs Applied Materials & Interfaces* **2020,** *12* (8), 9833-9841.

61. Chen, Y.; Tang, Z. H.; Liu, Y. J.; Wu, S. W.; Guo, B. C., Mechanically Robust, Self-Healable, and Reprocessable Elastomers Enabled by Dynamic Dual Cross-Links. *Macromolecules* **2019,** *52* (10), 3805-3812.

62. Chen, M.; Zhou, L.; Wu, Y. P.; Zhao, X. L.; Zhang, Y. J., Rapid Stress Relaxation and Moderate Temperature of Malleability Enabled by the Synergy of Disulfide Metathesis and Carboxylate Transesterification in Epoxy Vitrimers. *Acs Macro Letters* **2019,** *8* (3), 255-260.

63. Fortman, D. J.; Snyder, R. L.; Sheppard, D. T.; Dichtel, W. R., Rapidly Reprocessable Cross-Linked Polyhydroxyurethanes Based on Disulfide Exchange. *Acs Macro Letters* **2018,** *7* (10), 1226-+.

64. Lee, J.; Jing, B. B.; Porath, L. E.; Sottos, N. R.; Evans, C. M., Shock Wave Energy Dissipation in Catalyst-Free Poly(dimethylsiloxane) Vitrimers. *Macromolecules* **2020,** *53* (12), 4741-4747.

SUMMARY

Vitrimers have emerged as a promising platform for sustainable and reprocessable materials. Their dynamic crosslinks junctions which undergo reversible exchange reactions give them properties that are intermediate to thermosets and thermoplastics. They have opened a vast rheological design space, that could be essential for unprecedented control of polymer properties. This report investigated material properties that will be critical to the design, processing, and use of vitrimers as sustainable commodity polymers and functional materials. A series of precise ethylene based vitrimers were synthesized and investigated for their (i) rheological response, (ii) dielectric relaxation behavior, and (iii) the effect of dynamic bonds and topological defects on modulus crystal structure and crystallization kinetics. The ethylene vitrimers can also be dissolved in water and alcohol-based solvents and recovered by repolymerization while preserving their material properties.

Over a broad temperature window, the viscosity of the vitrimer shows a positive deviation from its characteristic Arrhenius trend, indicating an increasing role of segmental dynamics on flow. From dielectric spectroscopy, three distinct relaxation modes are identified - the alpha process, the beta process, and a normal mode relaxation that is interpreted as the time taken for the exchange of network strands between crosslink junctions. At high temperatures, a strong correlation between the rheological flow timescale and the normal mode relaxation shows that flow is controlled by bond exchange, while at lower temperatures a steep increase in alpha relaxation time correlates with the positive deviation from Arrhenius behavior in the networks. A comparison between permanent and dynamic networks with the same linker length, suggests that the incorporation of dynamic junctions allows for local rearrangement of the network structure

which facilitates crystallization. In addition, an unexpected evolution in melting temperature, crystal structure, and morphology is observed over time and is attributed to the dynamic bond exchange. The incorporation of dangling chain defects in the networks results in a decrease in shear modulus. X-ray scattering patterns reveal that networks with dangling chain defects form imperfect crystals and have a lower melting temperature. Topological defects also impact the crystallization kinetics, a counterintuitive trend in the kinetics is observed and explained based on entropic contributions from the dangling chain defects.